Investigation of Wind Turbine Fatigue Loads under Wind Farm Control: Analysis of Field Measurements

by

FEDERICO TAGLIATTI

in partial fulfillment of the requirements for the degrees

Master of Science
in Engineering (European Wind Energy)

at The Technical University of Denmark,

Master of Science
in Aerospace Engineering

at the Delft University of Technology,

to be defended publicly on Tuesday August 13th, 2019 at 13:00.

Supervisors:	Søren Juhl Andersen	DTU
	Gregor Giebel	DTU
	Tühfe Göçmen	DTU
	Wim Bierbooms	TU Delft
	Thomas Duc	Engie Green
	Lucas Alloin	Engie Green
Thesis committee:	Søren Juhl Andersen	DTU
	Gregor Giebel	DTU
	Tühfe Göçmen	DTU
	Wim Bierbooms	TU Delft
	Simon Watson	TU Delft
	Thomas Duc	Engie Green
	Lucas Alloin	Engie Green

Abstract

Wind energy is one of the most promising sources of renewable energy and has experienced a very rapid growth in the last 15 years. In order to maintain and sustain this growth wind energy needs to be competitive with the other sources of energy, especially with fossil fuels. A major factor keeping the competitiveness of wind energy is the sustained investment made on research and innovation. Active wake wind farm control is part of the research effort that aims to reduce the cost of producing wind energy; these new control strategies have the goal of reducing wind turbine wakes interactions in order to increase the power production and to minimize loads and fatigue.

Literature shows good potential for these control strategies; however most of the studies have been made in a virtual environment through the use of computer simulations and as a consequence there is a lack of real field measurement data analysis that could confirm the potential of these strategies. The French National Research Agency SMARTEOLE project implemented two wind farm control strategies in an operating wind farm called La Sole du Moulin Vieux and owned by Engie Green in order to assess the effects that the applied innovative wind farm control strategies have on the blade loads, particularly in terms of blade fatigue. The two wind farm control strategies applied are the curtailment strategy and the yaw-control strategy.

It needs to be noted that due to the high sensitivity of loads and fatigue to inflow conditions and due to the limited amount of data available the results observed should be considered as general trends very specific for this particular wind turbine set up and location.

In the curtailment strategy the upstream turbine SMV6 loads decreased up to 33% (at 9 m/s) in the flapwise direction and up to 67% (at 8 m/s) in the edgewise direction. Fatigue loads decreased up to 22% (at 9 m/s) in the flapwise direction and up to 2% (at 9 m/s) in the edgewise direction. In the downstream turbine no clear trend has been detected due to the high uncertainty in the results. Most likely low amount of data and increased turbulence in the downstream turbine led to this uncertainty in the trends.

In the yaw-control strategy loads showed a decrease up to 8% (at 9 m/s) in the flapwise direction loads and up to 72% (at 9 m/s) in the edgewise direction loads for the upstream turbine SMV6. Fatigue also decreased up to 19% (at 11 m/s) in the flapwise direction loads and up to 1.3% (at 10 m/s) in the edgewise direction for the upstream turbine. The downstream turbine SMV5 showed no significant reductions in the flapwise loads and fatigue when the whole wake was analyzed but, when the full-wake only was analyzed, a significant increase in loads and power produced, without any significant increase in fatigue loads have been observed. This underlines the potential of the yaw-controlled strategy to increase power production without significantly increasing fatigue.

Acknowledgement

This master thesis has been possible thanks to many people that followed the work from ENGIE Green side, DTU side and TU Delft side. I would like to thank Thomas Duc and Lucas Alloin for their guidance, ideas and help throughout the 6 month I spent in France. I would like also to thank all the Engie Green colleagues that made me feel a part of the company every day of the internship.

On the DTU side I would like to thank Tuhfe Göçmen, Gregor Giebel, Søren Juhl Andersen and Albert Meseguer for many suggestions, corrections and great feedbacks given weekly through Skype meetings.

On the TU Delft side I would like to thank Wim Bierbooms for accepting to supervise this thesis and also for the great feedbacks provided.

Finally I would like to thank my parents that made it possible for me to undertake this great study path!

Lists of Abbreviations/Symbols

CP	Compression
C_t	Thrust Coefficient
d	Inner diameter of the blade
d_i	Damage in the ith class of the fatigue load spectrum
D	Wind turbine diameter
D_{total}	Total Damage
DEL	Damage equivalent load
E	Blade young modulus
EG	ENGIE Green
EU	European Union
IEC	International Electrotechnical Commission
IQR	Interquartile range
LE	Leading edge
M_t	Instantaneous strain
N	Total number of cycles that leads to failure
n_{eq}	Equivalent number of cycles
n_i	Number of cycles in the ith class of the fatigue load spectrum
OD	Outer diameter of the blade
S	Load range
S_0	Intersection between the S-N curve and the y-axis
S_{eq}	Equivalent loads
SCADA	Supervisory Control and Data Acquisition
SU	Suction
SMV	La Sole du Moulin Vieux
TE	Trailing edge
TI	Turbulence intensity
TNO	The Netherlands Organization of Applied Scientific Research
TSR	Tip speed ratio
U_0	Wind velocity at the rotor disk
β	Wake expansion coefficient
ρ	Air density
χ	Wake angle / Skew angle
γ	Yaw angle
$\overline{\lambda_S}$	Mean wavelength of the strain sensor
$\widehat{\lambda_S}$	Peak to peak wavelength of the strain sensor
λ_S^t	Instantaneous strain measurement
$\overline{\lambda_T}$	Mean wavelength of the temperature sensor
λ_T^t	Instantaneous temperature measurement
λ_{TD}^t	Displacement of central wavelength
λ_{TS}^t	Sensitivity of the strain sensor
ΔM_0	Peak to peak variation of the gravity loads

Contents

1 Introduction

The demand in energy production is rising globally as a consequence of increasing population and emerging nations that are going through the process of economic development. The energy production sector is one of the major greenhouse gases emitters due to the major use of fossil fuels throughout the globe, which are increasing in demand and are becoming increasingly depleted [1]. In order to limit the global temperature increase and to secure energy independence, many European countries have invested strongly on renewable sources of energy [1].

Out of the many different possible ways of producing renewable energy, wind energy is the most promising and fast growing sector in Europe in 2018 with an additional installed capacity of 11.7GW reaching 189GW of total installed wind power capacity, with a growth of 6% compared to 2017 [2]. This rising trend has been constant during the last years supplying up to 14% of the total electricity produced in the European Union (EU) in 2018; by 2030 wind energy is expected to supply almost 30% of the total EU power demand, increasing employed people up to 570,000 [2]. European Union goals are to make wind power production the first source of energy production by 2027. These plans are very ambitious and can be achieved only if the wind power generating technology is competitive with the other energy sources [2]. Currently the bidding electricity price at onshore wind auctions is about 40 euros/MWh while in 2013 it was 100 euros/MWh. This is an example that shows the constant and fast decline in LCOE (Levelized Cost of Energy) that makes wind energy one of the cheapest sources of energy production as seen in Figure 1.1. LCOE of offshore wind is expected to have the biggest fall between 40 and 70 euros/MWh by 2030 with a reduction of almost 50% between 2015 and 2030 [3]

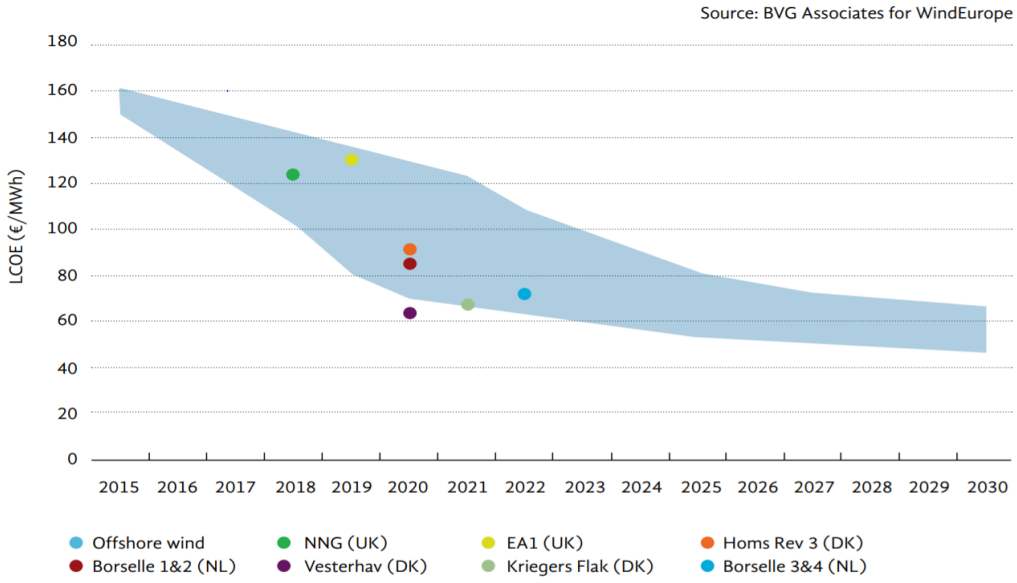

Figure 1.1: Offshore wind energy predicted LCOE. Retrieved from [1].

One of the major factors leading to the present competitiveness of wind energy is the sustained investment made by the public and private sectors on research and innovation [3]. Every year European wind energy companies and governments invest more than 1 billion euros in the research and development of new technologies and equipment. Innovation and research in the sector of wind energy is divided in 4 major categories:

- future technologies;
- grid and system integration;
- operation and maintenance;

- floating wind.

Inside the category of operation and maintenance, a very recent and new field of research is the smart wind farm operations. Smart wind farm operations include advanced control of the whole wind farm in order to increase the power production and to minimize loads and fatigue. They also include the introduction and integration of new sensors that are able to predict the incoming flow with the wind farm control, making it possible to optimize the flow of air inside the wind farm [3].

The company ENGIE Green, where this master thesis has been developed, is a major partner of the French National Research Agency research project SMARTEOLE. One of the main focuses of this smart wind farm operations project is the development and the analysis of innovative active control strategies, like yaw-control and curtailment, that would be able to increase the lifetime of the turbines inside a wind farm by reducing the loads and as a consequence decreasing the LCOE and increasing the profitability of wind energy generation in farms. This project will be analyzed more in depth in chapter 3.

Projects like SMARTEOLE are the state of the art of research and innovation that will be keen to increase the competitiveness of wind energy in the power production sector is what is needed in order to achieve the European Union wind energy goals.

Contents and Aim of the Thesis

This master thesis has been based on the data collected during the second measurement campaign (June 2017- March 2018) done by the company Engie Green in the context of the SMARTEOLE project. During this period wind farm active control strategies like yaw-control and curtailment have been applied. These strategies are called innovative because they do not rely any more on the optimization of the controls of each single turbine individually but they take into consideration the presence of other turbines around them. There has been little research on this very recent concept so it is an area that strongly needs and welcomes research.

The goal of this master thesis (done in cooperation with ENGIE Green) is to analyze and study the data collected at the Engie Green wind farm and to assess the effects that the applied innovative wind farm control strategies have on the blade loads, particularly in terms of blade fatigue. As previously stated in the introduction, this research field is extremely important in order to increase the competitiveness of wind energy in a busy energy market that is more and more pushed toward renewable energy for environmental reasons but at the same time needs to generate profit in order to be appealing to investors. This project aims to increase the knowledge on the application of new innovative wind farm active wake control that, in the future, is going to be keen in decreasing the LCoE so making wind energy cheaper and more competitive. Due to time constraints the parts of the turbine analyzed are going to be only the rotor blades. They have been chosen because they represent the region where most of the loads of a wind turbine originate.

Initially, the fundamentals on wind turbines wakes and the fundamentals on wind turbine loads are reported at the beginning of chapter 2. A description of the principles behind the wind farm active wake control strategies analyzed in this thesis, followed by the most significant results of similar wake control strategies found in literature, will end chapter 2. Chapter 3 describes the SMARTEOLE project and the main instrumentation used for the collection of the data for this thesis.

Chapter 4 describes the strain gauges calibration method that has been used in this thesis (developed by Engie Green) followed by the calculation of the loads from the strain signals. The loads are then be validated in chapter 5. Once the loads signals have been validated, fatigue loads (DEL) are calculated using rain-flow counting in chapter 5 and have been validated in chapter 6.

In chapter 7 the impact on wind turbine loads and fatigue of different inflow condition parameters is assessed; finally the impact of the innovative control strategies on the turbines loads and fatigue is analyzed in chapter 8 and chapter 9.

2 Theoretical Background and Literature Review

2.1 Wind Turbine Wake

When the air approaches the wind turbine, the pressure starts to increase and as a consequence its velocity stars to decrease. Immediately after crossing the wind turbine, the air pressure falls creating irregular pressure and axial velocity drops [4]. Sheets of trailing vortices are shed because of the pressure difference that is present between the lower and upper sides of the blades that deflects the streamlines of air passing under (outwards) and over (inwards) the wing. This is what extracting kinetic energy with a wind turbine does to the air flow, it creates a wake where the mean wind speed of the air mass is decreased and where the turbulence intensity is increased [4].

Wind turbine wakes are composed of two main regions with different characteristics: the near wake and the far wake. The near wake is generally up to 5 rotor diameter following the wind turbine and is mainly characterized by the geometry of the blade that interacts with the flow defining the aerodynamic yield of the the blade [5]. In this region a shear flow is created due to the pressure and velocity gap between the free stream and the wake; the presence of turbulence mixing enable the growth of the shear as it proceeds downstream as illustrated in Figure 2.1 [4]. The higher the thrust impressed by the wind turbine, the higher the velocity deficit between the free flow and the wake; this leads to a steeper shear characterized by higher turbulence derived by the increased momentum transfer to the wake [5]. As previously mentioned the wake expansion depends mostly on the ambient turbulence; when this expansion of the shear layer arrives to the wake axis, so that all the wake is turbulent, it begins the far wake region [5].

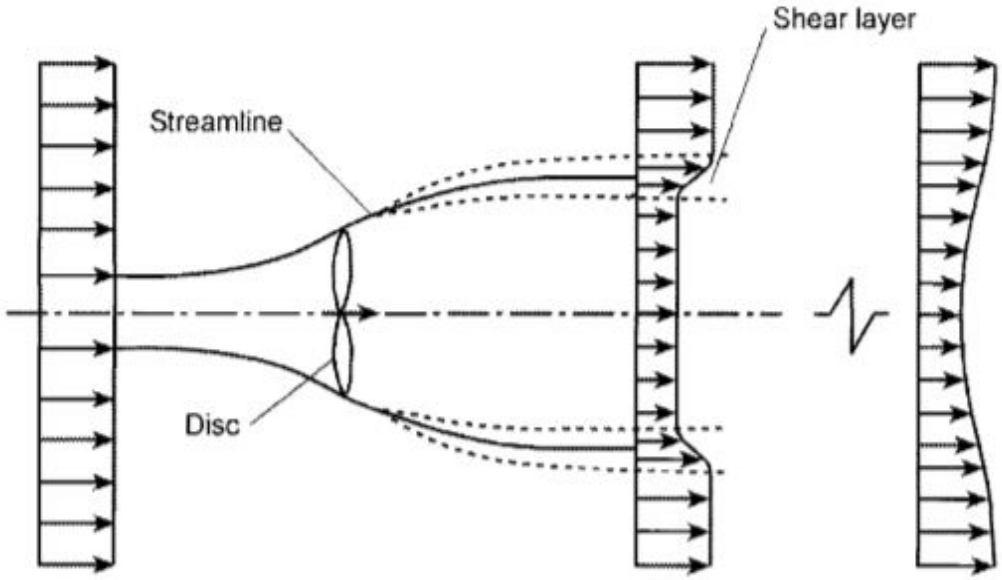

Figure 2.1: Wind turbine wake expansion sketch. Retrieved from [4].

In the far wake region the wake is fully developed and is assumed that the turbulence and velocity profiles are Gaussian, self similar and axisymmetric [5]. In this region pressure gradients decrease so as a consequence the velocity deficit also decreases enhancing the importance of turbulence. This theory has been shown by J. Højstrup [6], where wake turbulence intensity is said to be still relevant after 15D while wake velocity deficit is negligible after 10D.

Wind energy is usually produced in wind farms generally made up of multiple rows of wind turbines. In these wind farms there is inevitably interaction between the wakes and the turbines due to the close proximity, that increases the loading and decreases the power produced [5]. In order to decrease these effects in parks wind turbines are spaced usually 6 to 10 diameters in the prevalent wind direction and

1.5 to 3 diameters in the same row perpendicular to the prevalent wind direction [5]. These distances are considered a good trade-off between power produced, capital and operating costs of wind farms. The maximum distance where the wake effects are still noticeable varies significantly with ambient turbulence and thrust coefficient; high ambient turbulence facilitates turbulence mixing between the wake and the free flow, decreasing the recovery distance of the wake while high thrust coefficients increase the velocity deficit and so the turbulence of the wake with the effect of increasing the recovery distance [5]. In offshore wind the wakes are very relevant due to the low ambient turbulence that favors more persistent wakes.

Another important consideration inside a wind farm is that the wake of a down stream wind turbine recovers much quickly compared to the upwind turbine; this is explained by the fact that the turbulence created by the upstream turbine allows a quick recovery of the wake of the downstream turbine [5]. This means that the decrease in power and increase in loads experienced by the turbines coming after the upstream turbine is very similar as seen in Figure 2.2 taken from [7]. This could be explained by the saturation of the turbulence that after few turbines reaches a stable level.

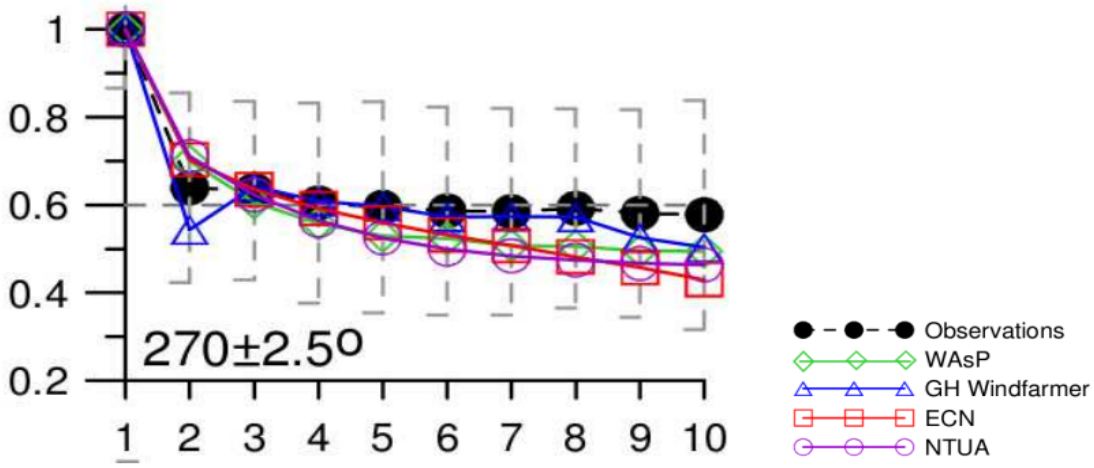

Figure 2.2: Normalized observed and simulated power output as a function of wind turbine number. Retrieved from [7].

2.2 Loads on a Wind Turbine

Wind turbines are becoming very large machines designed to withstand between 10^7 and 10^8 cycles during a lifetime of around 20 to 30 years and are exposed usually to rough ambient conditions. In order to fulfill these design requirements, the analysis of the wind turbine loads is a necessary step and it is performed widely in both industry and research. Despite major improvements in the materials used in the realization of a modern wind turbine, the scale of such system is so important that it can be considered as an elastic structure significantly interacting with the airflow; this creates very unique and specific aeroelastic interactions that induce important dynamic loads, vibrations and damping on the components of the wind turbine [8]. Most of the loads on a wind turbine originates from the loads action on the rotor because this is the region where the kinetic energy of the wind is converted into mechanical energy using a very large area (air density is low) [8]. From this region then they are transmitted to all the other components of the wind turbine. As a consequence the loads acting on the rotor are the most studied and thus the ones analyzed in the following thesis.

The two main categories of forces acting on the rotor of a wind turbine are the aerodynamic forces and the gravitational/inertial forces [8]. As a consequence, these forces create the aerodynamic loads and gravitational/inertial loads; both these loads families are divided into steady loads and unsteady loads. Steady loads assume that the time dependency, given a constant rotor speed, is constant in time. Unsteady loads on the other end are time dependent: this time dependency can be periodic in case it

happens every revolution (these are called cyclic loads) or it can be more random in the case it happens at irregular intervals (these are called non-cyclic loads)[8].

When forces and loads are analyzed the coordinate systems used need to be specified so that the direction of the forces and loads with respect to the wind turbine and the environment around is clear. In wind turbine loads analysis usually two coordinate systems are used as seen in Figure 2.3. One is used for the forces acting on the blade of the rotor: it is a coordinate system that rotates with the blade where the direction of the forces/loads components acting in the chord direction is called edgewise (or chordwise) and the direction of the components acting on the direction perpendicular to the chord is called flapwise. The other is used when the system is taken with respect to the rotor plane instead of the blades; in this case forces and loads are decomposed in the plane of rotation direction (also called tangential components) and perpendicularly to the plane of rotation (also called thrust components) [8].

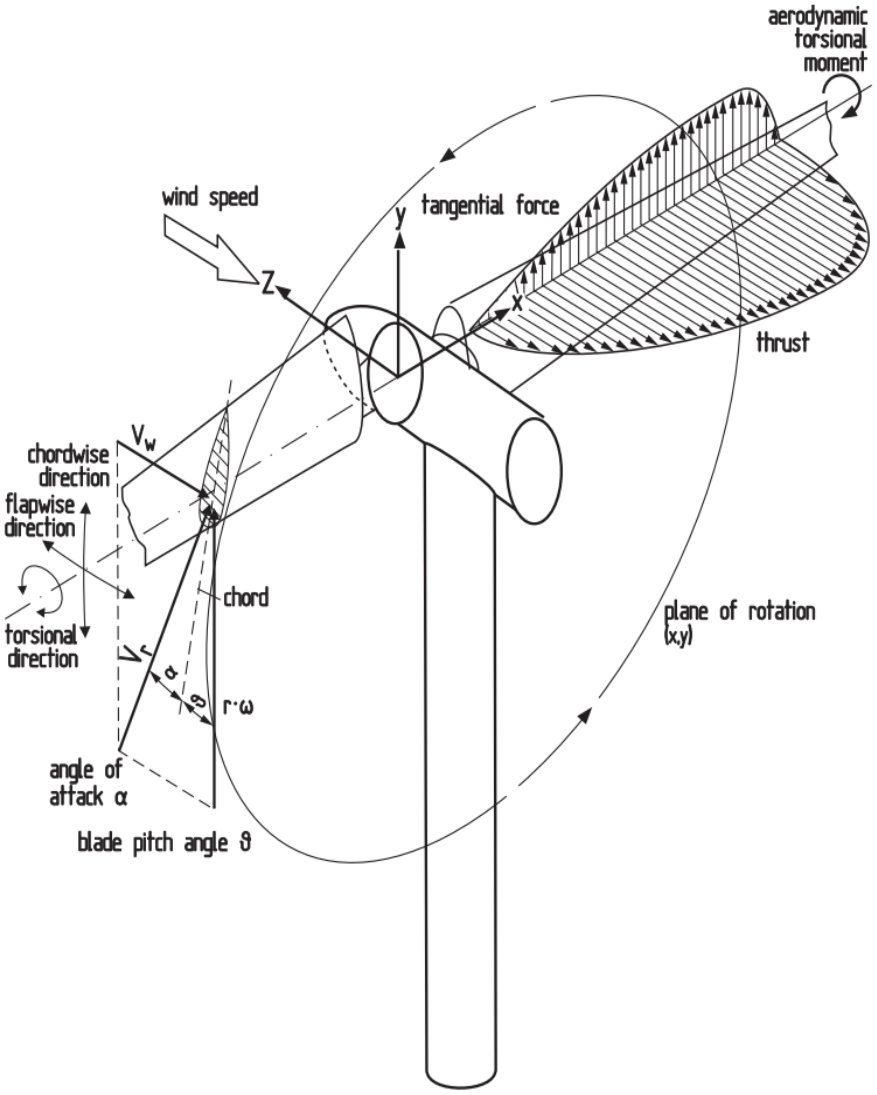

Figure 2.3: Wind turbine coordinate systems used for load assessment. Retrieved from [8].

A wind rotor has 7 main sources of loads:

- Uniform and steady flow of air
- Wind shear and Veer

- Cross winds
- Tower shadow effect
- Wind gusts and turbulence
- Gravity and Inertia
- Wind turbine wakes

2.2.1 Uniform and Steady Flow of Air

When a steady and uniform flow of air goes through the rotor area, it exerts a steady aerodynamic force on the blades. This force is time independent and is dependent on the mean wind speed of the air mass [9]. The distribution of the loads on the blade mainly depends on the geometry and on the position relative to the tip where the perceived velocity is the highest and so the steady aerodynamic loads [8]. The force acting on the rotor, due to the specific design of the blade, creates a tangential force that exerts an edgewise bending moment on the blade while thrust force created exerts a flapwise bending moment on the blade [8]. It can be concluded that the static load level is characterized by the total thrust of the rotor and by the rotor torque. In pitch controlled wind turbines total thrust reaches the highest value at rated power and then decreases due to the pitching of the blade while the rotor torque reaches the maximum at rated power and keep this value up to cut-out wind speed (this is thanks to the pitching of the blade) [9]. Load distributions are present also over the chord of the blade but they are usually of less importance [8] and so they are not going to be analyzed in the present thesis.

2.2.2 Wind Shear and Wind Veer

The variation of average wind speed and direction with increasing altitude is known as wind shear as well as wind gradient and wind veer. The wind shear is very dependent on the stability of the atmosphere, it generally shows a daily trend with more stable conditions during the night, when the warming action of the sun on the ground is absent, with a consequent stratification of the atmospheric boundary layer developing strong shear. During the day the sun warms the ground increasing instability and the mixing of the atmospheric boundary layer [9]. In the more recent and bigger wind turbines the difference between the mean wind speed present in the low part of the rotor and the one in the higher part can be very significant especially with high atmospheric stability [9]. When the the rotor is crossed by an asymmetric wind flow, unsteady fluctuating loads are produced [8]. In the case of wind shear the part of the rotor located further away from the ground experiences higher loads that will be cyclical (every one revolution) for the blades. The main affected loads are the flapwise blade bending moment and fatigue on the components of the yaw drive systems [9].

2.2.3 Cross Winds

Another source of asymmetry is when the wind direction changes rapidly so that the yawing system is not able to promptly follow the direction of the wind creating a crosswind effect on the rotor [8]. Crosswind also creates a periodic increasing and decreasing on the loads of the blades in a similar way discussed in the wind shear and veer section affecting as well the flapwise blade bending moment and fatigue on the components of the yaw drive system [8].

2.2.4 Tower Dam Effect

In order to keep the cost of the wind turbine low, the nacelle is made as short as possible with just the safe tip clearance between the blade and the tower. For this reason the blades of the rotor operate relatively close to the tower and as a consequence, they are affected by the distortion of the flow around the tower. On an up-wind rotor the blades feel the so called “tower dam effect”; the flow of air that approaches the tower is slightly slowed down right in front of it, decreasing the mean wind speed and as so creating periodical loads on the blade [8]. These loads are less important compared to the rest but, due to the periodic nature, if they approach the natural bending frequency of the tower at specific rotational speeds, they could cause excitation that could lead to increase structural fatigue with eventual

damages [8]. Down-wind rotors are much more influenced by the tower presence but will not be analyzed in this thesis.

2.2.5 Wind Gusts and Turbulence

Random fluctuations of the wind are the most challenging source of loads for wind turbine rotors. These fluctuations are non-periodic and time dependent and they are generally referred as turbulence [9]. Turbulence is determinant in the blades fatigue stress. Turbulence is characterized by the fluctuation of the air flow in three dimensions but the most important component for loads analysis is the longitudinal turbulence [8]. Wind turbulence is described by the presence of gusts; gusts are significant increases or decreases (negative gust) of the mean wind speed that last usually up to 20 seconds. In the loads calculations turbulence is treated deterministically, meaning that every single gust is considered as an independent load event characterized by a shape, duration and intensity [8]. Multiples gust shapes have been used for the calculation of loads and more extensively for the calculation of extreme loads; the three main shapes used for idealized wind gust, have been based on meteorological data and are the rectangular shape, the trapezoidal shape and the one dimension cosine function shape $(1 - cos(2\pi/\tau))$[8]. Beside shape, gusts are also described by a gust factor. This factor is dependent on the length of the gust, on the value of the mean wind speed and on the probability of occurrence [8]. The lower is the mean wind speed the higher the value of the gust factor, the gust factor is also inversely proportional to the length of the gust [8]. In Figure 2.4 shows the effects induced by the presence of turbulence on the flapwise bending deflection of the wind turbine HWP-300 compared to the only presence of cyclic disturbances like wind shear. It can be seen that the deflection in the presence of turbulence is increased of almost 100% and as a consequence dynamic loads in the flapwise direction are expected to increase noticeably [8]. Extreme gusts are the main sources of extreme loads but they will not be considered in this thesis due to time constraints.

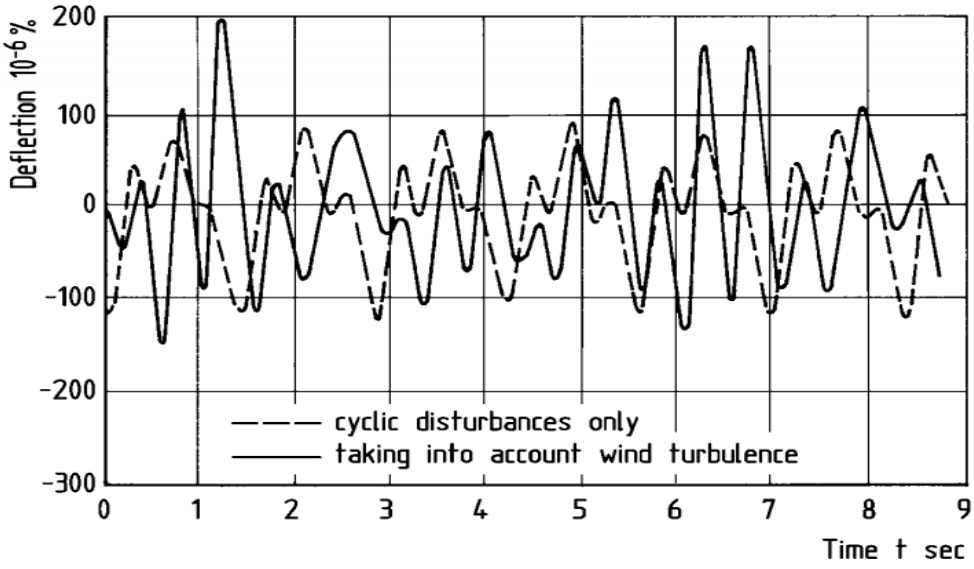

Figure 2.4: Example of blade flapwise deflection with and without turbulence. Retrieved from [8].

2.2.6 Gravity and Inertia

Gravitational loading is with turbulence the main driver for fatigue stress due to loading on a wind turbine [8]. The weight of the wind turbine components, especially the one of the rotor blades, needs to be taken into account as a major source of loading and fatigue; the blades are subjected to sinusoidal edgewise loading due to the gravitational Earth force acting on the center of gravity of the blades [10]. The main positions where the blade is subjected to the highest loading are shown in Figure 2.5

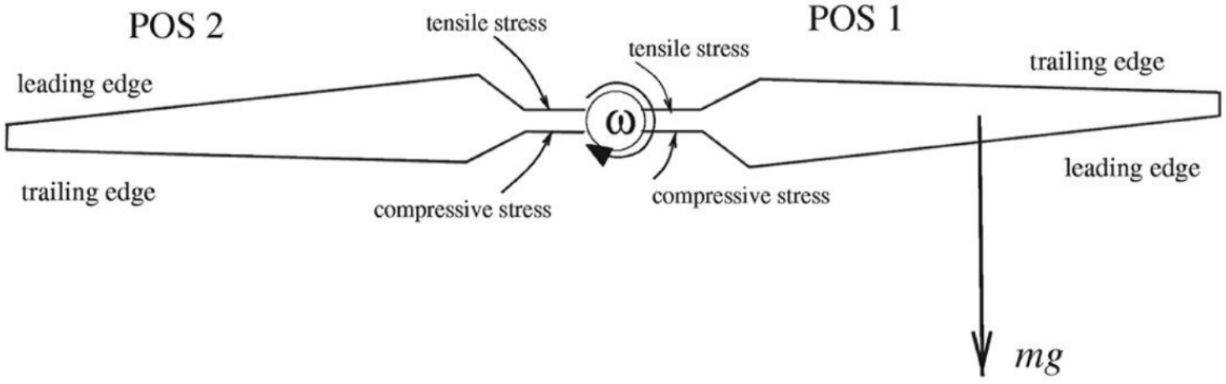

Figure 2.5: Gravitational load on a wind turbine rotor. Retrieved from [10].

In POS 1 the blade is rotating in the downward direction with the leading edge of the root subjected to compressive stress and the trailing edge of the root subjected to tensile stress, while in POS 2 the blade is rotating in the upward direction with the leading edge of the root subjected to tensile stress and the trailing edge of the root subjected to compressive stress [10]. POS 2 is encountering the highest loads since it is moving against the force of gravity. The periodic gravitational loading on the blade is caused by the fluctuating edgewise and flapwise bending moments and are characterized by a frequency of once per revolution, also called 1P: since wind turbines are designed to withstand between 10^7 and 10^8 cycles during their lifetime [10], blades are exposed to very large fatigue due to gravitational loading [10]. The larger the wind turbine is the more prominent this source of loading and fatigue is going to be [8].

The first loading due to inertia that is going to be analyzed is centrifugal loading. Centrifugal loading is not considered a main source of loading for wind turbines because they do operate at relatively low rotational speeds but it can be used to alleviate the loads on the flapwise direction of the blade [10]. This alleviation can be done by inserting a cone angle on the design of the rotor; this angle does split the centrifugal force into the spanwise and normal direction. The normal component of the centrifugal force, with this angle, creates a moment in the opposite direction of the total flapwise bending moment that alleviates it [10].

Another inertia loading is the gyroscopic loading. These loads are experienced by the rotor when there is a yaw angle with the air inflow and they produce pitching moments on the axis of the rotor [8]. These moments are the higher the faster the yawing is; usually yawing rates are low, so the moments induced are considered low and not concerning [8]. It can be a serious source of loads for passive yawing wind turbines but this type of machines is not going to be analyzed in this thesis.

2.2.7 Wind Turbine Wakes

As previously stated in the wind turbine wake section, wakes from upwind turbines do increase aerodynamics loads and, as a consequence, fatigue on the downwind turbines [9]. Being in the path of a wind turbine wake changes the characteristics of the flow of air due to the increased levels of turbulence, reduced wind speed and changes in the wind shear affecting the loading on the rotor of the wind turbine mainly in the flapwise direction [11]. Measurement campaigns have been done in the past decade in order to assess the extent of this increase. Volund and Stiesdal found an increase in the flapwise bending moment standard deviation of about 100% when in the wake of turbines placed between 2-3 D (the highest values where obtained in half-wake exposition) [12] [13]. Dahlberg JA, Poppen M, Thor SE have done measurements inside Alsvik wind farm in Sweden where the turbines are spaced 5D, 7D and 9.5D in a very low turbulence environment. Equivalent loads were calculated and they showed an increase between 10% (9.5D) and 45% (4.5D) depending on the spacing [14]. Another measurement campaign was done by Frandsen S and Thomsen K. in the off-shore environment of Vindeby wind farm; fatigue

was calculated and it showed an increase of fatigue loads of about 80% when in wake conditions even if the distance between the turbines was high [15].

2.3 Wind Farm Active Wake Control Strategies

Wind turbines are generally put into wind farms in order to fulfill specific economic and logistic constraints. Common practice is the power maximization of each wind turbine without taking into consideration that the air inflow may be influenced by the presence of upwind turbines. The interaction between the wakes formed and the turbines, as explained in section 2.1, can be detrimental for power production and for the loading distribution of the whole wind farm. With the presence of aerodynamic interactions, the power maximization of the single turbines doesn't coincide with the power maximization of the whole wind farm, so in the past two decades researchers have increased the focus in control strategies for the whole wind farm to maximize power production and simultaneously decrease dynamic loading and fatigue on the wind turbines so increasing their lifespan [16][17]. These control strategies are called "active wake control" because their goal is to actively decrease the effect of the wakes present in the whole wind farm. In this thesis only the two most important are analyzed: the axial induction control strategy (curtailment strategy) and the wake redirection strategy, mainly achieved by yaw misalignment (yaw-control strategy) [17].

2.3.1 Curtailment Strategy

The main idea behind this active wake control strategy is that, by decreasing the axial induction factor of the first upwind turbine (generally done by changing the pitch angle and in some cases also the rotational speed), the wind speed deficit, the turbulence intensity and the velocity shear of the generated wake decrease, leaving the possibility to increase the power produced as well as to decrease the dynamic loads on all the downwind turbines. Curtailing the turbine by modifying the pitch angle and or the rotational speed, affects the blade aerodynamics (like thrust, lift and drag) affecting the creation of the wake that results weaker. This leads to a higher power produced by the wind farm possibly achieving higher lifetime [17]. Up to now there has been major interest in the power maximization while there has been limited research on the effects of curtailment strategies on the loads of turbines especially the downwind one [18]. The major part of the studies done on the loads used aeroelastic simulation with very simplified wake models focusing mainly on the optimization method [17].

A recent paper (2018) from Christos Galinos et al. [18] studies the effects of the loads on the downwind turbine for three different curtailment strategies applied on the upwind turbine: minimum rotational speed (minRS), maximum rotational speed (maxRS) and minimum thrust (minT). The wind farm layout is very simple: two turbines (2 MW) with two different inter spaces of 4D and 7D used, the available power is derated by 20% and 40% for different wind directions of ± 15 degrees. The simulations are done using the high fidelity aero-servo-elastic code HAWC2 coupled with the Dynamic Wake Meandering Model and they show that the blade root fatigue loads can decrease significantly up to around 30% (compared to the case where no curtailment is applied) when the right curtailment strategy is chosen leading to an increase of the lifetime of the wind turbine parts. This paper also showed that the fatigue loads on the blade roots are the smallest when minRS and minT curtailment strategies are applied.

Another paper by S.K. Kanev et al. [17] used a trade-off between computational power and model fidelity in order to asses the benefits of active wake control on the lifetime power production and on the fatigue loading on a wide variety of existing wind farms with different characteristics. The tool used to calculate the effects of wind farm wakes is the TNO's 3D parabolized Navier-Stokes FarmFlow software; this code uses a k-ϵ turbulence model to account for turbulence in the wake. Additionally, to develop a database the aeroelastic tool Focus/Phatas has been used to perform simulations on a 5 MW turbine. This paper states that the curtailment strategy is mostly interesting in wind farms with turbine with average inter spaces lower than 7D. It also shows that this specific active wake control is not able to reduce loads significantly (compared to no curtailment): for example blade flap loads do not decrease more than 0.1% in most of the wind farms.

Only one paper from K. Boorsma [19] was found with full-scale analysis of field measurements. These fields measurements have been taken by the Wind Energy Research Center of the Netherlands at the TNO Wind Turbine Test Site Wieringermeer (from December 2004 until April 2009) within the Active Wake Control project FLOW. The wind farm consists of a row of five 2500 kW turbines placed at equal distances of 3.8 rotor diameters. The downwind turbine has been instrumented with blade root strain gauges and hence is used for the loads analysis. The curtailment strategy adopted in this measurement campaign is to compare 3 different pitch-control curtailment strategies and compare them with no curtailment; unfortunately, after measurement filtering, due to insufficient data, only the 2° and 4° pitching strategies have been used in the loads analysis. Reduction of flapwise fatigue loading in the range of 10% is observed in the downwind turbine when a 2° pitch is applied to the upwind turbine. A larger reduction, only restricted to the wake sector, of the flapwise fatigue loading is observed in the downwind turbine when a 4° pitch is applied to the upwind turbine. Reductions of the edgewise fatigue loading are very small and confined to the range of 1% due to predominant gravitational nature of the loads.

2.3.2 Yaw-control Strategy

A flow of air going through a yawed wind turbine creates an asymmetric distorted wake characterized by an angle χ (called wake angle or skew angle) with the rotor axis that, as shown in figure 2.6, is bigger compared to the yaw-angle γ and the upwind side of the rotor is farther away from the center line of the wake compared to the downwind side [5]. The deviation angle θ is the difference between the skew angle χ and the yaw angle γ. The reason of this distortion of the wake is that, due to the yaw angle, a lateral force is imposed on the flow making it turn [23].

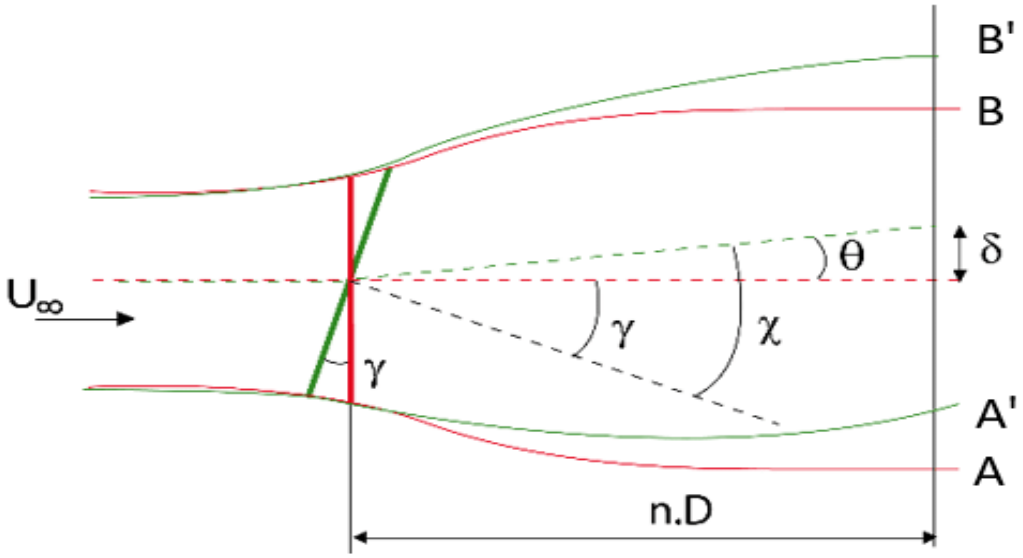

Figure 2.6: Representation of the skew angle χ, the yaw angle γ and and the deviation angle θ. Retrieved from [24].

Yaw-control strategy principle is to apply a voluntary yaw misalignment to redirect the wake away from the downwind turbines and so, as a consequence, increase overall power production and ideally decrease dynamic loads [17]. In some particular inflow conditions this control strategy has the potential to also increase the dynamic loads of some components like drive-train and tower [17][20]. Generally there has been discrepancies between industry research suggesting not to use yaw-control operations and scholar research recommending to use it in order to increase the overall wind farm power production so, as a consequence, owners of wind farms do not have a clear idea of the extent and certainty of the benefits (increase overall power production) compared to the risks (increase in loads and so decrease in

lifetime of some components) [16]. As for the curtailment strategy, up to now there has been major interest in the power maximization but limited research on the effects on turbines loads, especially the downwind one [18].

K.A. Krag and M.H. Hansen [21] demonstrate that the yaw-control blade fatigue alleviation under yaw-control strategy is dependent on the turbulence level. Simulations with the aero-servo-elastic tool HAWC2 have been used in order to find the yaw angles that give the highest load reduction through a wide range of wind speeds. It is stated that blade loads can be diminished by 20% compared to no yawing, only under a flow with low turbulence; as the turbulence level increase, loads reduction decreases significantly.

In R. Damiani et al.[20] the results of damage equivalent loads (DEL) from aeroelastic simulations done using FASTv8 have been compared with data collected from a 1.5MW GE turbine (upwind) located near Boulder Colorado. The original aeroelastic model from GE has been modified in order to be used in the aero-servo-elastic tool FASTv8. The yaw-offset applied to the turbine has been 0, $\pm$12.5, $\pm$18, $\pm$25 using the convention showed in figure 2.7. The paper shows good agreement between the predicted DEL (damage equivalent loads) using FASTv8 and the measurements; the flapwise DEL have a minimum when the flow is aligned: as the yaw angle increases in both positive and negative directions, the DEL also increase with higher values in the negative direction. The edgewise DEL are characterized by less variation with a decreasing trend for positive yaw-offsets due to the major influence of gravitational loading.

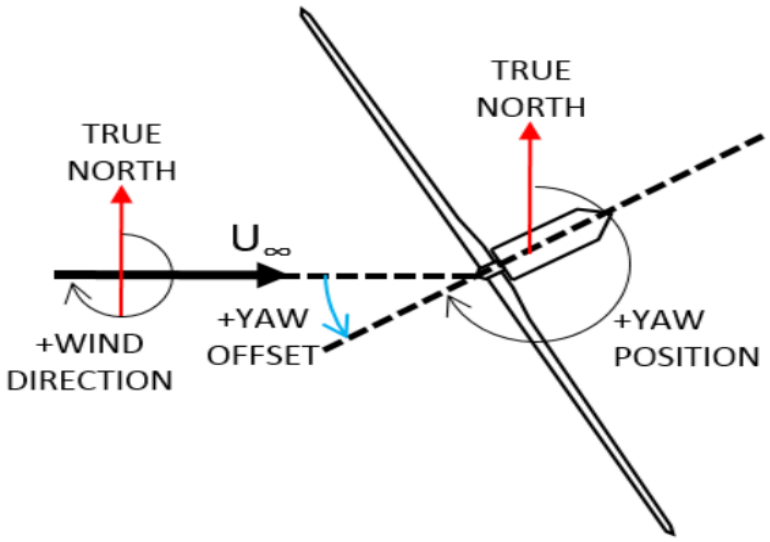

Figure 2.7: Yaw-angle convention used in [20]. Retrieved from [20].

The same paper described in the curtailment strategy section by S.K. Kanev et al. [17] also analyzes the benefits of yaw-control strategy on the lifetime power production and on the fatigue loading on a wide variety of existing wind farms with different characteristics. Here is underlined how not only the yaw-control strategy leads to an increase in the average power production of a wind farm without increasing the loads on the considered components but it is also able to reduce the loading, compared to no-yaw-control: for example blade flap loads decrease in some wind farms by more than 2%.

Another really interesting paper by Albert M. Urbán et al. [22] focuses on the optimal yaw-control strategy that enables loads reduction in the downwind turbine using the concept of wake redirection. The simulations are done using the high fidelity aero-servo-elastic tool HAWC2 coupled with the Dynamic Wake Meander Model on a 2.3MW wind turbine. Blade and tower DEL have been calculated with: a wind

speed range from 4m/s to 25m/s (1m/s steps); turbulence intensities range from 5% to 25% (5% steps) and a yaw-angle range from -30° to +30° (2.5° steps). The results from this paper are very promising and show that "for full wake at 3D inter-spacing and turbulence intensity of 5%, around 35% of load reduction on the 1 Hz Damage Equivalent Loads can be achieved at high wind speeds. Smaller reductions are achieved for higher atmospheric turbulence; the analogue case with 15% turbulence intensity shows 17% potential alleviation" [22]. This means that the loads reduction potential is high with a low turbulence and high mean wind speed flow.

2.4 Summary

It can be concluded that wind turbines are subjected to important loads; most of the loads on a wind turbine are a consequence of the forces acting on the rotor. This is why this thesis is focused on the loads acting on the rotor. There are 7 main sources of loads on a wind turbine: uniform and steady flow of air, wind shear and veer, cross winds, tower shadow effect, wind gusts and turbulence, gravity and inertia and wind turbine wakes.

The last source mentioned is of great interest in this thesis due to the study of the application of active wake wind farm control strategies that are trying to decrease the negative effects of turbine wakes. Wind turbine wakes are created by the extraction of kinetic energy from the wind flow and they are characterized by a decrease in mean wind speed and by an increase in turbulence intensity. This wakes, inside a wind farm, can lead to a decrease in the total power production of the farm and to an increase in the loads and fatigue experienced by the turbines.

Wind farm control strategies have been investigated only in the past few years with the goal of attenuate the aerodynamic wake interactions inside a wind farm. Minimizing these interactions is expected to increase the overall power production of the wind farm and to decrease loads and fatigue faced by the turbines. The two main strategies are: the curtailment strategy and the yaw-control strategy. Most of the previous work has been focused on the power production; regarding loads most of the research done is based on simulations showing that decreases in loads and fatigue are possible, however results are very inconsistent and sensible to inflow parameters.

3 SMARTEOLE Project

In this chapter, the thesis is put into the context of the French National Research Agency (ANR) SMARTEOLE project. A brief description of the members and the objective of the project will be given followed by the description of the experimental setup with all the main instrumentation used.

3.1 Project Abstract and Partners

With the global goal of decreasing the Levelized Cost of Energy of wind energy, research institutions have been trying to increase the focus on innovative solutions with the aim of increasing the competitiveness of wind produced energy in the energy market. To achieve this global goal, the French National Research Agency accepted on January 2015 a 42-months long project called SMARTEOLE intended to end in June 2018. This project has been embraced by six major institutions well known for their knowledge in wind energy conversion systems and in lidar technology:

- ENGIE Green: it was created by the merging of 3 smaller companies MAIA Eolis, La Compagnie du Vent and Futures Energies that were specialized in wind, solar and marine energy. ENGIE Green is a subsidary, specialized in renewable energy, of the major French company ENGIE operating in the field of energy generation and distribution. It has a wind power generation capacity of 1480 MW coming from more than 700 wind turbines located in more than 100 wind farms. This is also the company where this master thesis project is developed.
- Avent Lidar Technology: it is a French company owned by the LEOSPHERE group that designs and builds lidars that can be placed on top of the nacelle of the wind turbine.
- IFP Energies nouvelles: is a public institute of research with the goal of implementing technological innovation.
- LAAS: is a French laboratory of the National Center of Scientific Research located in Toulouse specialized in information sciences and technology.
- LHEEA: is a French laboratory of the National Center of Scientific Research partnering with Ecole Centrale de Nantes and it is specialized in free surface flow, atmosphere flow dynamics and fluid-structure aerodynamics.
- PRISME: is a laboratory of the University of Orléans specialized in Mechanics, System Engineering and Energetics.

The project objective is to optimize the wind turbine efficiency through the development of innovative control techniques that are going to affect and improve the operating conditions of the wind turbine, increasing the power production and/or the lifetime of the wind turbine [25]. The main feature of these innovative control strategies is the presence of an integrated LIDAR sensor system that is able to accurately anticipate the incoming wind flow conditions enabling a more precise real time implementation of the controls systems for nacelle direction and for blade pitching [26]. Being able to optimally predict the characteristics of the incoming flow decreases the real-time load fluctuations felt by the wind turbine, eventually lowering the costs of maintenance and increasing the lifetime of the wind turbine [25]. These innovative control strategies will be developed and applied on three different scales and they will be based on real time measurements of the inflow conditions. The real time measurements have been either full scale experiments of control strategies developed by IFPEN on one ENGIE Green (EG) owned wind farm (also the case for the data acquired for this thesis) or, small scale experiments of control strategies developed by both PRISME and LHEEA inside their own wind tunnels [26]. The three scales are:

- Blade: the objective is to control the aerodynamic performance of the blade by modifying the distribution of pressure, and as a consequence the circulation, with fluidic or plasma actuators distributed along the blade profile. The control of Closed-loop circulation capability to reduce aerodynamic load fluctuations for wind power applications will be demonstrated experimentally in the laboratories [22].

- Wind turbine: the blade scale control strategy will be tested in a wind tunnel on the rotating blades of a wind turbine thanks to an existing wind rotor bench. On the full scale, a new "feed-forward" control strategies for blade pitching is designed for load reduction, including the anticipated measurement of incoming wind using a LIDAR sensor mounted on the wind turbine nacelle. The innovative strategies is then compared to the already existing strategies for pitch control implemented on the wind turbines operated by EG [22].
- Wind farm: innovative wind farm generation strategies taking into consideration each wind turbine incoming flow conditions (wake interactions, for example) will be proposed and applied during full-scale test campaigns. The performance of these global control strategies on overall wind farm power production and on wind turbine loading are analyzed [26]. This is the scale analyzed in this thesis project.

3.2 Experimental Set-up

3.2.1 Wind Farm Choice

The experimental data needed for the SMARTEOLE project have been collected in three major field tests on the Engie Green owned wind farm La Sole du Moulin Vieux (SMV); it is located between Vermandovillers and Ablaincourt-Pressoir, two small towns immersed in the North France countryside. This wind farm is composed by 7 Senvion REpower MM82 2MW wind turbines that have been installed in two different moments with the wind farm completed as it stands in 2013. The current layout of the wind farm can be seen in Figure 3.1 where the names and the inter-distances between the turbines is also shown.

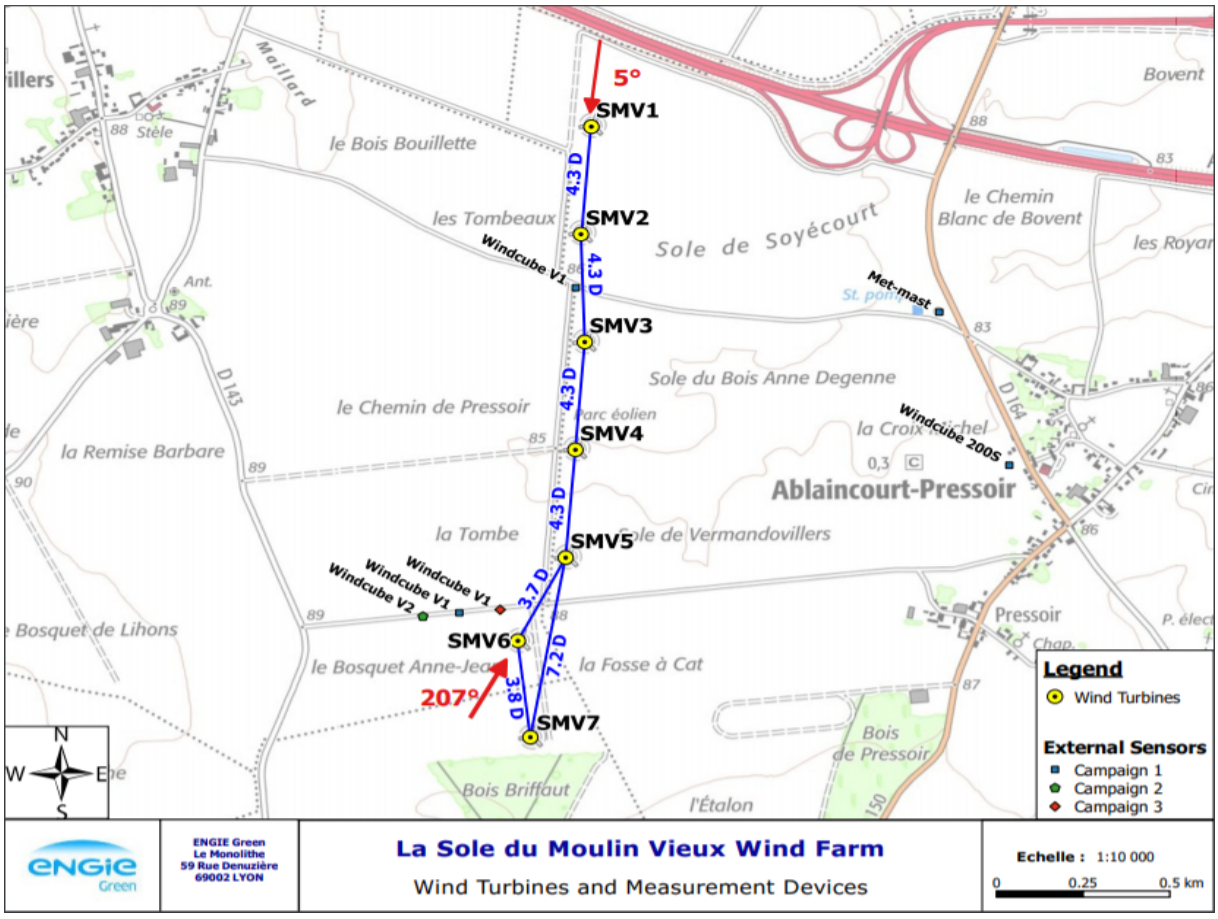

Figure 3.1: Layout of the wind farm La Sole du Moulin Vieux (SMV) owned by ENGIE Green. In red are shown the wind directions that creates wake interaction. Picture made by ENGIE Green

From the layout it can be seen that this specific wind farm was chosen because of the unique alignment between wind turbine SMV6 and SMV5. These two wind turbines are placed very close one to another, with a distance of only 3.7 turbine diameters meaning around 305 m, and they are aligned at 207° that is very close with the main wind direction that in this location is South-West. As a consequence, the turbine SMV5 operates with a strong and predominant wake effect caused by turbine SMV6 creating an optimal set-up for analyzing active wake control strategies. The wind farm is surrounded by fields with only a small forest located south of the wind farm in close proximity to SMV7; this could increase turbulence when wind is from South-West.

3.2.2 Wind Turbine Senvion REpower MM82 2MW

This section describes the wind turbine operational parameters behaviour as a function of wind speed. Figure 3.2 shows the Senvion REpower MM82 2MW characteristic curves given by Senvion and from these curves the 3 control regions of the wind turbine can be seen.

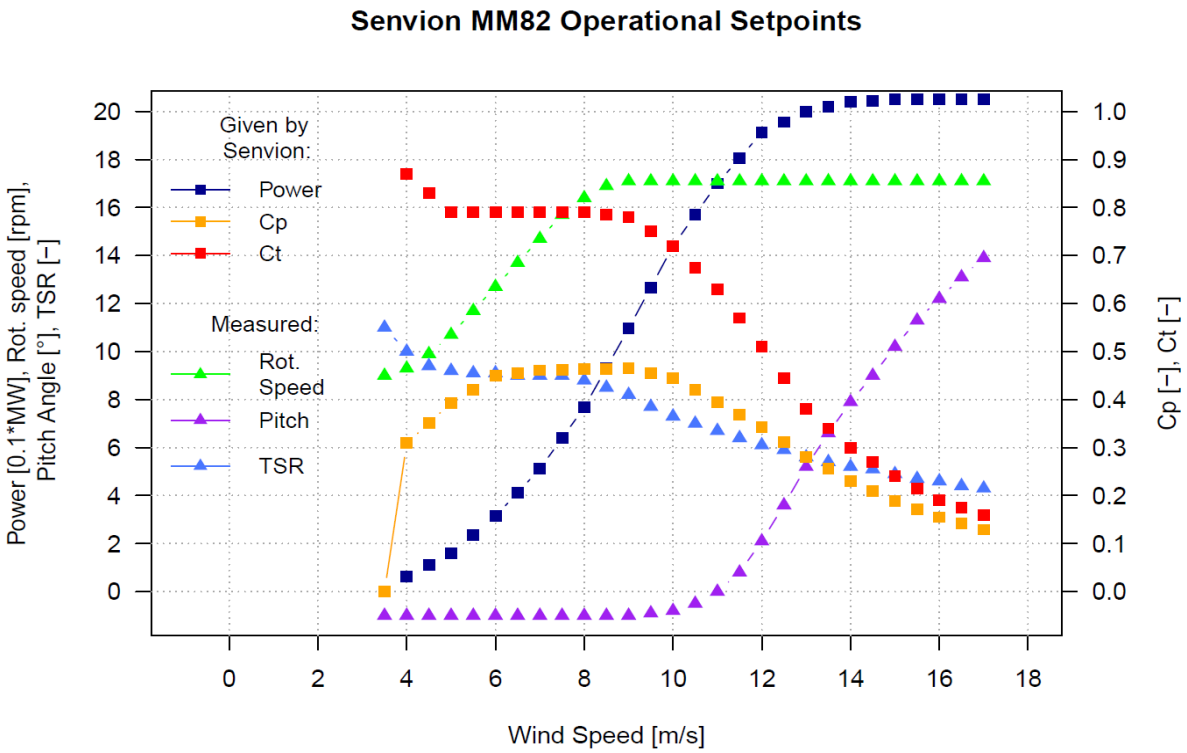

Figure 3.2: Senvion REpower MM82 2MW characteristic curves. Retrieved from [35].

Region 1 is called variable speed region and in this case is between 4 m/s and 9 m/s. In this region the tip speed ratio (TSR) and the pitch angle are kept at the optimal values in order to ensure the best aerodynamic properties of the blade and thus the maximum energy extraction from the wind. As a consequence as the wind speed increases also the rotor speed increases.

Region 2 is called constant rotor speed region and in this case is between 9 m/s and 12.5 m/s. In this region the rortor speed has reached its allowed maximum of 17.1 rpm so the optimal TSR cannot be achieved anymore. The power has not still reached nominal value yet so the pitch angle is kept at optimum and the generator torque is used to regulate rotor speed to the rated speed while still increasing power.

Region 3 is the region after the maximum (nominal) power of 2050 kW has been reached, in this case after 12.5 m/s up to the cut-out wind speed of 25 m/s. In this region the rotor speed is regulated by

pitching (decreasing the aerodynamic efficiency of the blade) and the power is regulated to its nominal value using the generator torque.

3.2.3 Measurements Sensor Set-up

In order for the SMARTEOLE project to be possible, the chosen wind farm has been equipped with external sensors both on the ground and on the wind turbines. As previously mentioned, the main interest is around turbine SMV5 and SMV6 so the sensors are placed taking in consideration this preference. The main sensors installed in the wind farm are listed below with a focus on the ones used for the collection of data considered in this thesis that are the lidars data, the strain gauges data and the SCADA data. This master thesis focuses only on the second field campaign of the SMARTEOLE project that occurred between June 2017 and March 2018.

The sensor installed are:

- Met mast: a lattice met mast with the height of 80 meters has been installed East of the wind farm with a distance of 1.6 km from SMV6 and of 1 km from SMV2; this met mast is shown in Figure 3.1 close to Albaincourt-Pressoir with the name of Albaincourt80. This sensor is not used for this thesis because it was not operating at the time of the strain gauges measurement campaign.
- 2 ground lidars used to measure the vertical profile of the wind flow through the use of laser light:
    1. A scanning lidar placed 1.2 km East of the turbine SMV4 (Shown in Figure 3.3). This sensor is not used in this thesis because it was not operating at the time of the second measurement campaign.
    2. A Windcube V1 lidar measuring the 3 speed components of the wind flow from the height of 40 meters to the height of 200 m was placed initially close to turbine SMV2 and SMV3 as seen in Figure 3.1 (labelled as Windcube V1). In May 2016 however, it was moved closer to SMV5 and SMV6 (Shown in Figure 3.4) with a distance respectively of 4D and 2D. The main reason behind this change in position, was to perform a IEC-confirmed power performance assessment of these two turbines and also to compare the wind measurement of the ground lidar with the nacelle lidars installed on the two turbines. Due to a stolen cable, the availability of this sensor in the first field measurement campaign (November 2015-November 2016) is not extensive. This problem was solved, for the second campaign (June 2017-March 2018), with the installation of a Windcube V2 differentiated by the presence of a solar panel and by a battery that ensure autonomous power supply. The battery failed in January 2018 so, for the third measurement field campaign (October 2018-ongoing), the Windcube V1 has been installed back.

Figure 3.3: The Scanning Lidar 200S. Picture taken by ENGIE Green

Figure 3.4: The Windcube V1 lidar with SMV6 in the background. Picture taken by ENGIE Green

- 2 nacelle based lidar installed in the 2 wind turbines of highest interest SMV5 and SMV6 in order to detect the incoming wind flow conditions that are then used to choose the most adequate control actions:

    1. A Wind Iris lidar was placed on top of the nacelle of SMV5 to measure the incoming inflow conditions during the first field measurement test, the lidar can be seen in Figure 3.5.This sensor is not used in this thesis because it was not operating at the time of the second measurement campaign .
    2. A 5-beam demontrator Wind Orion lidar (prototype) was placed on top of the nacelle of SMV6 to measure the incoming wind inflow conditions during all 3 field measurement campaign of the project. The lidar can be seen in Figure 3.6. This specific lidar sensor is characterized by the presence of 5-beams (4 during the last field test) that are able to collect measurements in 5 (or 4) different points on the rotor, gaining lots of information about the incoming wind flow. Another characteristic of this lidar is that it is also able to measure the vertical and horizontal wind shear at 10 different upstream distances, between 80 meters and 400 meters making easier to build the incoming flow characteristics for the whole area swept by the rotor. This allowed to implement more precisely the control strategies applied to this upwind turbine. This sensor unfortunately encountered some issues during the first measurement campaign losing several months of measurements. During the second campaign no major issues were detected until half way to March 2018 when it stopped working. In the third campaign a problem occurred between October and November 2018 with loss of data. Unfortunately due to time constraints it was not possible to use data from this lidar in the thesis.

Figure 3.5: The Wind Iris nacelle lidar positioned on the turbine SMV5. Picture taken by ENGIE Green

Figure 3.6: The Wind Orion nacelle lidar positioned on the turbine SMV6. Picture taken by ENGIE Green

- A supervisory control and data acquisition system (SCADA) has been installed in each turbine of the wind farm used in the project SMARTEOLE. This system is used to gather information about the weather conditions on top of the nacelle (Wind Speed, wind direction and temperature) and also information about the wind turbine operation (Yaw, pitch, generator speed, active and reactive power, rotor speed etc.). These information have been then synchronized with other sensors (e.g. strain gauges) to analyze the mechanical response of the turbine with respect to the conditions in which it is operating. Usually these SCADA sensors have an acquisition of the 10-min average statistic values but for SMV5 and SMV6 the sampling rate was increased to 1Hz.
- 4 Fiber Bragg strain gauges sensors were installed inside each blade of SMV5 and SMV6. The main function of these sensors is to detect the changes in blade root bending moment and, as a consequence, in fatigue loads on the blades when applying active wake control strategies. These specific sensors are optical strain gauges so light is reflected differently as a function of the strain. These sensors are also dependent on temperature so, for each blade six sensors have been installed as seen in Figure 3.7; two of them are temperature sensors to correct the temperature dependence and the other four are strain gauges sensors placed every 90°. Next chapter will address the optical strain gauges functioning and the calibration process in more details. The sampling rate of these sensor is set to 100Hz; this value was chosen so that it is possible to connect strain modes to their frequencies. As previously stated, the strain gauges data are synchronized to the SCADA data. Strain gauges are very delicate and indeed throughout the 3 field measurement campaigns there have been problems, with consequent loss of data, on multiples strain sensors particularly in the turbine SMV6; however at least one blade with all the sensor working have been confirmed in each of the 3 field campaigns. A picture of an installed optical fiber string can be seen in Figure 3.8

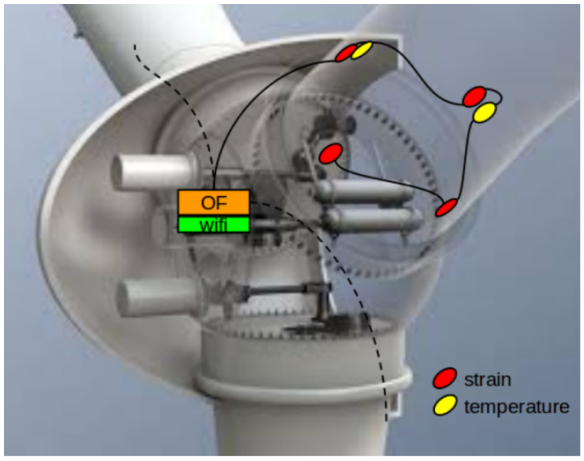

Figure 3.7: Illustration of the positioning of the 6 sensors inside a blade at the root

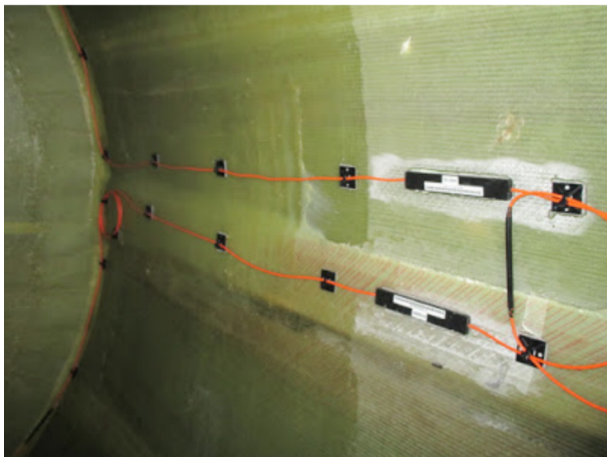

Figure 3.8: Photo of the blade root and of one optical fiber string. Picture taken by ENGIE Green

4 Strain Gauge System and Calibration Procedure

4.1 System description

The strain gauges measure the strain exerted on the blade root due to the loads faced by the wind turbine. In the scope of the SMARTEOLE project, the strain gauges installed are Fiber Bragg Grating based sensors, developed by HBM FiberSensing. They are optical fibers that are fixed on the inner side of the blade, on which several Bragg sensors are disposed. A Bragg sensor reflects the light that is sent through the optical fiber around a certain central wavelength λ_0, as shown on figure 4.1a.

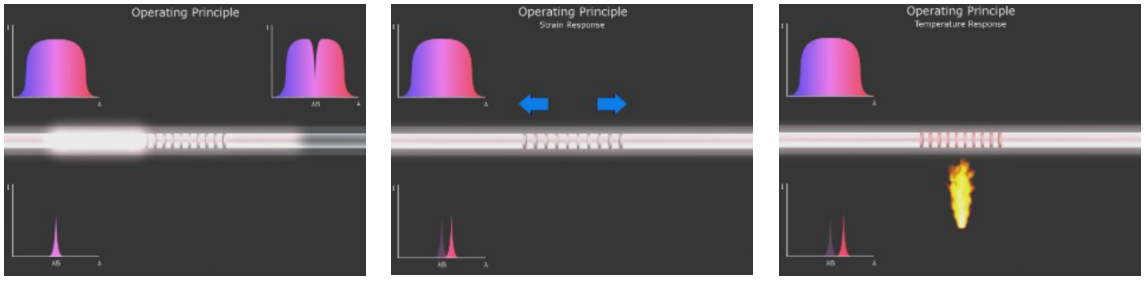

(a) **(b)** **(c)**

Figure 4.1: Principle of a Fiber Bragg Grating sensor. (a) The light goes through the optical fiber and is reflected at a certain wavelength λ_0. (b) The optical fiber faces a strain, consequently the reflected wavelength is changed. (c) The optical fiber faces an increase in temperature, the reflected wavelength is also changed. Pictures taken from the HMB website [27].

When the blade is deformed, the optical fiber also faces a strain and the layout of the Bragg system is changed. Consequently the reflected wavelength λ is also changed by a value $\Delta\lambda = \lambda - \lambda_0$. When the system is properly calibrated, the change in wavelength $\Delta\lambda$ can then be related to the displacement ϵ of the optical fiber and thus the strain faced by the blade (see figure 4.1b). However, these sensors are very sensitive to temperature, which is also influencing the value of $\Delta\lambda$ (see figure 4.1c). The temperature law must therefore be corrected in temperature to make sure that the change in wavelength observed is really caused by a stress on the blade and not a change in temperature. More details can be found on the HBM website [27][28].

4.2 Experimental Setup Configuration in SMARTEOLE

In the SMARTEOLE projects, strain gauges sensors were installed in each blade of wind turbine SMV5 and SMV6. For a particular blade, six sensors were located at the root of the blade: 4 strain gauges sensors (at every 90° approximately) and 2 temperature sensors. All these sensors are available on the same optical fiber, so that only one array by blade is installed. Figures 3.7 and 4.2 display this particular layout.

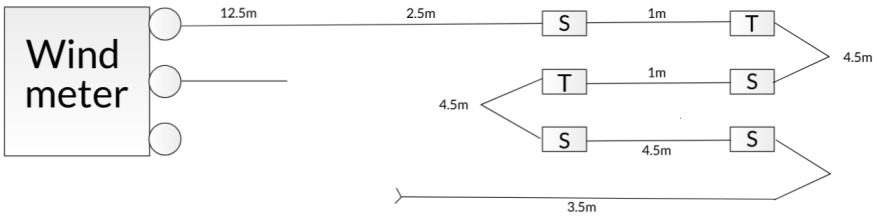

Figure 4.2: Layout of one strain gauge array.

Data acquisition is monitored at 100 Hz, allowing to associate the blade modes with their frequencies. These measurement are synchronized with SCADA 1 Hz values in order to realize the calibration.

Details of the setup:

- Wind turbine: Senvion MM82, hub height = 80 m
- Type of blade: LM40, mass = 6350 kg;
- Location of the sensors: at about 1 m from the blade root;
- Outer diameter of the blade at the sensor location: OD = 2.21 m;
- Inner diameter of the blade at the sensor location: d = 2.01 m;
- Blade Young Modulus: E = 33 GPa;
- Nacelle tilt angle = +5° ;
- Gravity center position = 13m.

4.3 General Calibration Methodology

The calibration of the strain gauges data is realized in two steps (developed by ENGIE Green):

1. Determination of the temperature law: in this first step, measurements when the wind turbine is idling are selected, i.e. when the rotor is slowly turning and the loads faced by the turbine are driven by gravity only. In this case generator speed is below 200 rpm (with a gearbox ratio of 105) and blade pitch angle is 45°. The temperature law is deduced by estimating the theoretical gravity loads from blade characteristics and the analysis of changes in strain as a function of temperature.
2. Calibration of measurements: in this second step, the temperature law calculated in step 1 is applied to the set of data, and the effect of temperature is also taken into account. From the values of strain measured at each sensor, moments at blade root in edge and flap wise are then computed.

4.4 Determination of the temperature Law

To determine the temperature law, the following procedure is used:

1. Selection of idling periods: a routine analyses 1Hz SCADA data file to select the 10-min periods with the relevant generator speed (when it is between -5 and 200 rpm). Associated Fiber Sensing (FS) data files are identified. Then for each selected idling 10-min period the following step 2 to 6 are realized.
2. Filtering: strain and temperature measurements are passed through a low-pass filter (cutoff frequency = 0.2 Hz) in order to smooth out the signal and remove high frequency perturbations.
3. Truncation of signals: the first and last minute of the signal are removed because they are disturbed by the filtering realized in step 3.
4. Making sure that the signal is sinusoidal: this is done in order to make sure that the signal have the expected shape, i.e. a sinus whose frequency is the rotor speed on the low-speed shaft. Knowing that the kurtosis of a sinus is 1.5, the selected period is rejected if the calculated kurtosis of the signal is not between 1.4 and 1.6. An example of valid and rejected measurement are shown on Figure 4.3.

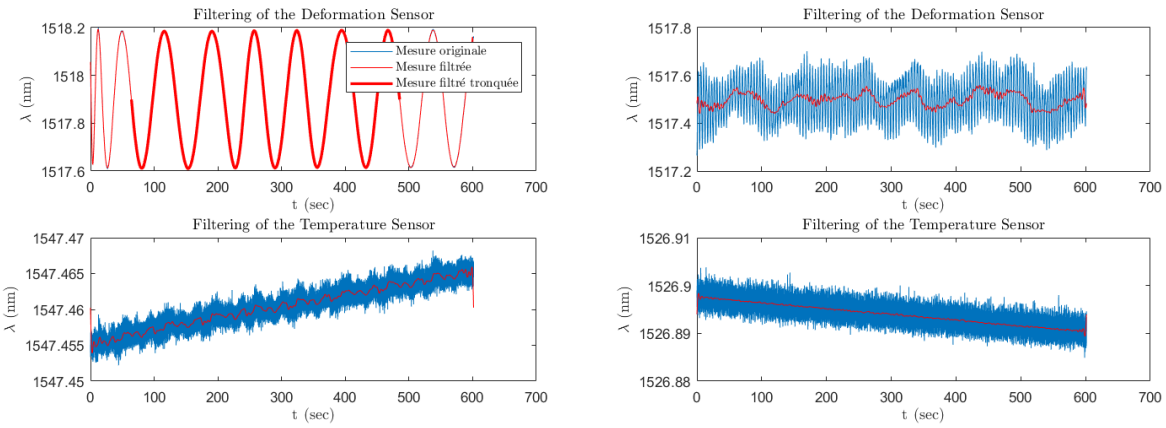

(a) **(b)**

Figure 4.3: Example of a valid (left) and rejected (right) 10-min period. The top graph represents the strain wavelength signal against time step and the bottom graph the associated temperature wavelength signal.

5. Statistics calculation: For all strain and temperature sensors of the array, local minima and maxima are identified and statistics on the 10-min period are computed. The useful values used later in the temperature law are the following: the mean wavelength of the strain sensor $\overline{\lambda_S}$, the peak to peak wavelength of the strain sensor $\widehat{\lambda_S}$ and the mean wavelength of the associated temperature sensor $\overline{\lambda_T}$. $\overline{\lambda_S}$ represents the value which is returned by the sensor when no loads are exerted on the blade (i.e. when the blade is vertical, neglecting compression and traction effects), while $\widehat{\lambda_S}$ is the peak to peak variation of the gravity loads exerted on the blade (i.e. when the blade is horizontal, from one side to another). These two values are expected to vary with temperature, which is why there is the need of calculating a temperature law for gain and offset.

6. Estimation of the temperature law: for each strain sensor, a temperature law, representing the sensitivity of the strain sensor with respect to the temperature (calculated through its associated temperature sensor), is calculated using the statistics data from all the selected 10-min periods. This is done in the following way, also represented on Figure 4.4:

   - Variation of mean strain wavelength $\overline{\lambda_S}$ is represented against variation of the mean temperature wavelength $\overline{\lambda_T}$ (top graph) to model how the central wavelength of the strain sensor is varying with respect to the temperature. This value correspond more ore less to the offset as a function of temperature in the general calibration formula. The obtained behavior is generally almost linear and is fitted with a second order polynomial.
   - Variation of peak to peak strain wavelength $\widehat{\lambda_S}$ is represented against variation of the mean temperature wavelength $\overline{\lambda_T}$ (middle-left graph) to model how the measured (gravity) loads by the strain sensor are being affected by the change of temperature. In general the behavior observed is a practically constant value as seen in the peak to peak amplitude graph in Figure 4.4. This value correspond more ore less to the gain as a function of temperature in the general calibration formula. A first order polynomial is used to fit the data.
   - Residuals of these two fittings are also plotted against $\overline{\lambda_T}$ (middle-right graph) and time (bottom graphs) to detect sensor drifts.

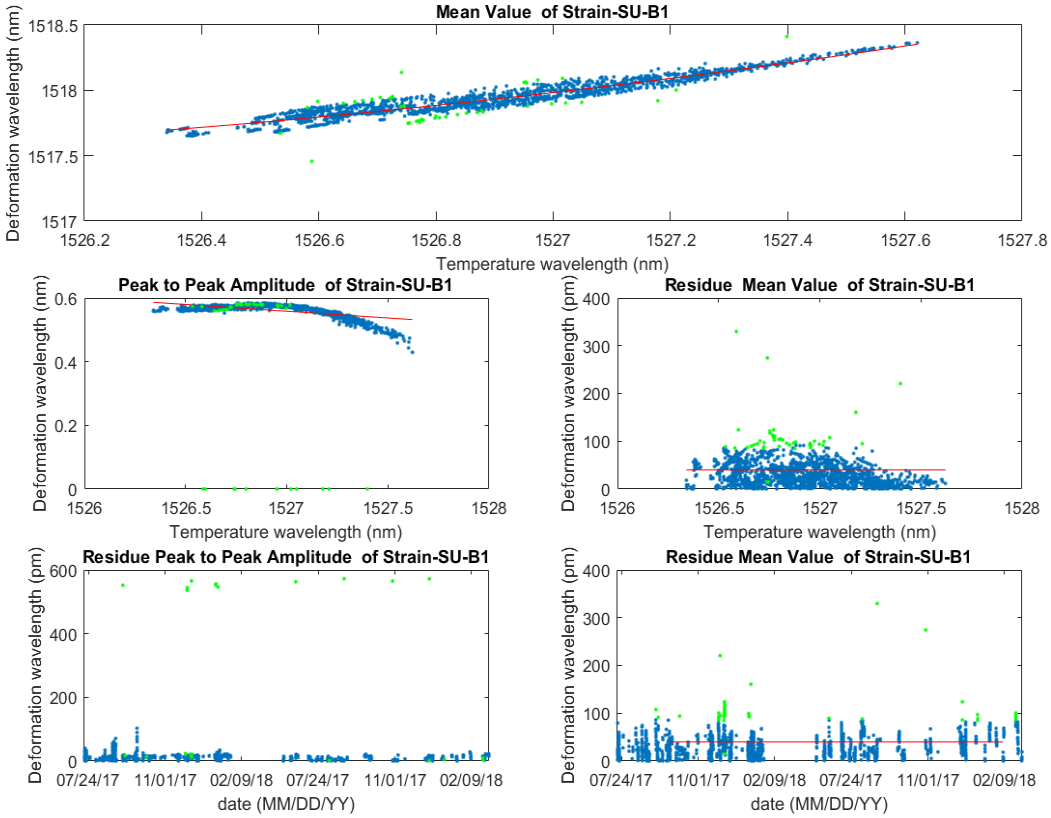

Figure 4.4: Temperature calibration of one strain sensor. One blue point represents one calculated statistic of selected and valid idling 10-min period, red curves are polynomial fitting and green points are detected outliers (calculated as all the residues above 2 standard deviations) that are not included in the fitting of the data. Top: variation of $\overline{\lambda_S}$ with $\overline{\lambda_T}$. Middle: variation of $\widehat{\lambda_S}$ with $\overline{\lambda_T}$ (left) and residual of the fitting of $\overline{\lambda_S}$ against $\overline{\lambda_T}$ (right)(note different scale pm instead of nm). Bottom: residual of the fitting of $\widehat{\lambda_S}$ (left) and $\overline{\lambda_S}$ (right) against time (note different scale pm instead of nm).

At the end of this procedure the calibration allows the user to correct the effect of the temperature on the wavelength deformation, both in terms of mean value and peak to peak value. This temperature law can be applied on all instantaneous measurements and is supposed to be valid on all the second measurement campaign during which idling 10-min periods have been extracted to derive the law.

4.5 Calibration of Measurements and Instantaneous Strain Calculation

Now that the temperature law has been calculated, all 100 Hz measurements need to be calibrated. Generally in strain gauges, the resulting instantaneous strain M^t from the loads can be computed with the following equation where λ_0 is the instantaneous wavelength recorded by the sensor:

$$M^t = Gain * \lambda_0 + Offset \tag{4.1}$$

Unfortunately in optical Fiber Bragg strain gauges, both the gain and the offset are temperature dependent:

$$M^t = Gain(T) * \lambda_0 + Offset(T) \tag{4.2}$$

$$\longrightarrow Gain(T) = \frac{\Delta M_0}{\lambda^t_{TS}} \tag{4.3}$$

$$\longrightarrow Offset(T) = -\frac{\Delta M_0}{\lambda_{TS}^t}\lambda_{TD}^t \tag{4.4}$$

where ΔM_0 is the peak to peak variation of the gravity loads and the λ_{TD}^t and λ_{TS}^t are the temperature dependent values that needs to be calculated for each sensor through the following steps:

1. For each sensor file the corresponding temperature sensors are associated to the strain sensors.
2. From the instantaneous temperature measurement λ_T^t, and using the temperature law derived above, the values λ_{TD}^t and λ_{TS}^t are calculated using the following formulas where a, b, c, d, e represent the fitting parameters calculated in the temperature law:

$$\lambda_{TD}^t = a(\lambda_T^t)^2 + b\lambda_T^t + c \tag{4.5}$$

$$\lambda_{TS}^t = d(\lambda_T^t) + e \tag{4.6}$$

λ_{TD}^t represents the displacement of the central wavelength that would be expected at the temperature λ_T^t if no other loads (other than gravity) were exerted on the wind turbine blade.

λ_{TS}^t represents the expected sensitivity of the strain sensor with respect to loads at the temperature λ_T^t.

Then, by comparing the instantaneous strain measurement of the sensor λ_S^t with these calculated values, the resulting instantaneous strain M^t from the loads can be computed with the equation 4.2 that can be rewritten as:

$$M^t = (\lambda_S^t - \lambda_{TD}^t)\frac{\Delta M_0}{\lambda_{TS}^t} \tag{4.7}$$

where ΔM_0 is the peak to peak variation of the gravity loads and is calculated using the following formula, that is obtained after some trigonometric calculations and taking into consideration only when the turbine is idling with a pitch angle of 45°:

$$\Delta M_0 = M_g * \sqrt(2) * cos(tilt) \tag{4.8}$$

where M_g is the gravity moment obtained by the product of the mass of the blade times gravity times the distance between the blade root and the center of gravity.

In Equation A.8, the first term of the right side $(\lambda_S^t - \lambda_{TD}^t)$ can be seen as the offset of the sensor which is a function of the temperature, while the right term $\frac{\Delta M_0}{\lambda_{TS}^t}$ would be its gain (also dependent on the temperature).

A practical example of the calibration of the measurements and of the instantaneous strain calculation is provided in Appendix A.

From the loads calculated for each signal, it is possible to calculate edgewise and flapwise loads combining respectively LE (leading edge) sensors with TE (trailing edge) sensors and SU (suction) sensors with CP (compression) sensors using the following formulas:

$$M_{Edge} = 0.5(M_{LE} - M_{TE}) \tag{4.9}$$

$$M_{Flap} = 0.5(M_{SU} - M_{CP}) \tag{4.10}$$

The moments in this thesis are expressed in the blade coordinate system (Figure 4.5). It can be noted that the flapwise loads are expected to be negative due to the wind force acting on the blade in this direction while the edgewise loads are expected to be positive due to the higher loads faced in this direction when the blade rises against the force of gravity.

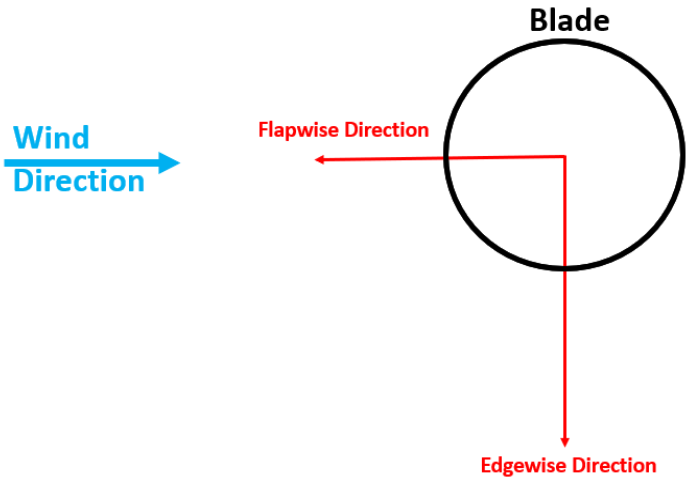

Figure 4.5: Blade coordinate system used in this master thesis. Assuming no pitch angle .

4.6 Summary

The strain gauges used in the SMARTEOLE project are Fiber Bragg Grating based sensors, developed by HBM FiberSensing. They are called optical strain gauges because they consist of optical fibers that are fixed on the inner side of the blade, on which several Bragg sensors are disposed. Unlike normal strain sensors, the optical strain gauges are very sensitive to temperature changes; as a consequence the temperature dependency needs to be investigated and a temperature law determined.

For the determination of the temperature law, only measurements when the wind turbine is idling have been selected (so that the loads faced by the turbine are driven by gravity only). The temperature law is deduced by estimating the theoretical gravity loads from the blade characteristics and the analysis of changes in strain as a function of temperature.

Then the temperature law calculated is applied to the set of data to correct the temperature effect on the strain. From the values of strain measured at each sensor, moments at blade root in the edgewise and in the flapwise directions are then computed.

5 Load Measurements Validation

The edgewise and flapwise loads have been calculated from the strain gauges signals that have been calibrated following the procedure shown in the previous section for both wind turbines.To show that the data acquired by the strain gauges sensors are valid and that they can trustfully be used and analyzed in this thesis, a validation of the load signals needs to be done. The validation has to make sure that the loads detected in the field measurements behave in the expected way and are representative of the actual loads encountered by the turbine blades.

5.1 Single 10-min Time-series Validation

In order to validate the load measurements, firstly individual 10-minutes sensors loads time series have been analyzed during different operating conditions of the wind turbine SMV5 and SMV6 to see if each sensor signal behaved as expected. In the Figure 5.1 below an example of a 10-minutes sensors loads time series analysis is shown for SMV5 during above rated operating conditions.

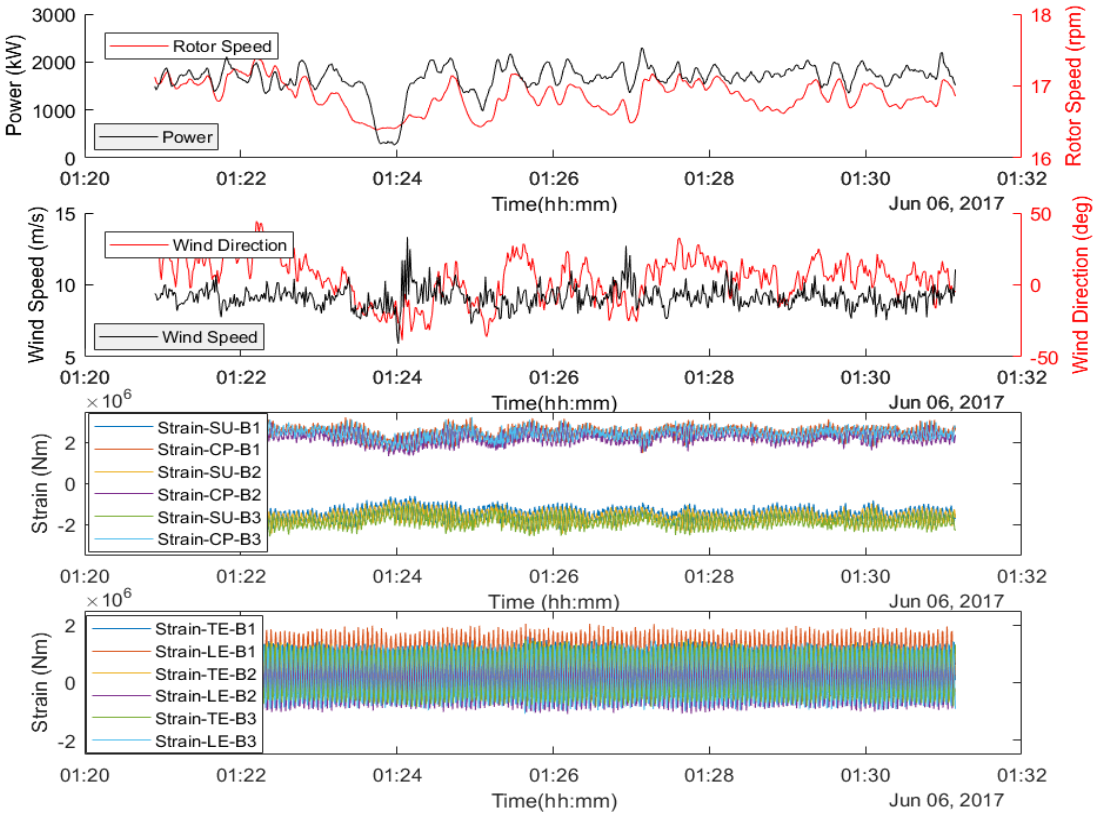

Figure 5.1: Example of a 10-minutes sensors loads time series for SMV5

The first graph of Figure 5.1 shows the power and the rotor speed signals while the second graph shows the wind direction and the wind speed signals. The third graph of Figure 5.1 shows the loads signals of the suction (SU) and compression (CP) sensors placed in the flapwise direction of blade 1 (B1), blade 2 (B2) and blade 3 (B3), whether the forth graph shows the loads signals of the leading-edge (LE) and trailing-edge (TE) sensors placed in the edgewise direction of the same blades. The signals have been compared with wind speed and they show a generally expected behaviour; the signs of the compression sensors loads are positive and the signs of the suction sensors loads are negative due to the permanent force exerted by the wind on the flapwise direction of the blade, while the LE and TE loads fluctuate around zero because they are mostly driven by gravity. As expected the magnitudes are really

similar with a slight higher loads in the compression sensors, also TE loads of blade 2 are shifted towards more positive loads (this could be the result of a misplaced strain gauge sensor). High consistency in the shape and magnitude of the loads from the same sensor in two different blades is observed. Due to the high sampling frequency the loads signals are noisy.

The time series have also been converted to angular series and plotted as a function of one revolution to make sure that there is consistency in the positions where the blade will encounter higher loads, an example is shown in Figure 5.2(a); this to check for synchronization problems. Corresponding flapwise (SU, CP) and edgewise (LE, TE) load signals have also been plotted against each others to check the consistency of these coupled sensors; an example is shown in Figure 5.2(b)

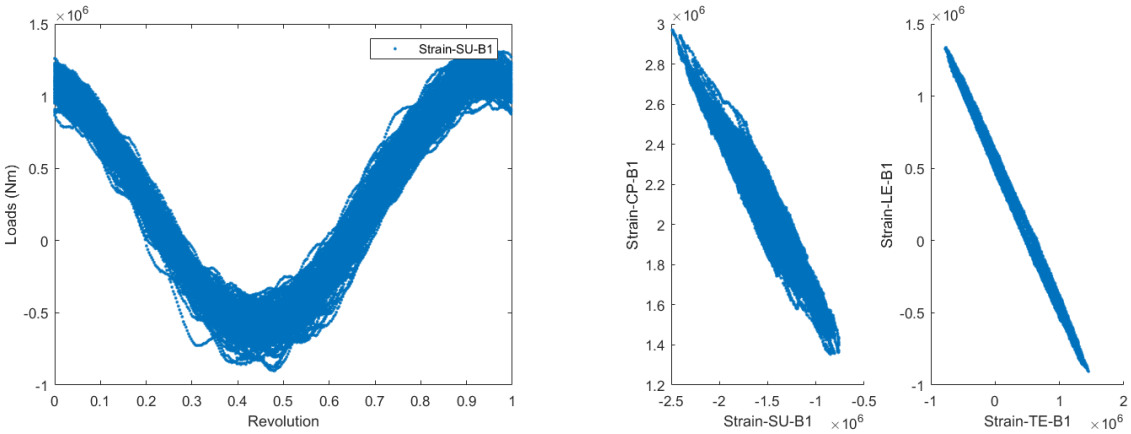

(a) **(b)**

Figure 5.2: Example of SU sensor loads distribution as a function of revolution (a). Example of coupled sensors relationship for both CP-SU and LE-TE.

Figure 5.2 graphs show good consistency for both the load distribution as a function of revolution and for loads from coupled sensors that, as expected, show a negative linear relationship. When one of the sensors (e.g. TE) is positive because it is compressed, then its coupled sensor (LE) is tensed (explained in section 2.2.6). This linearity is less pronounced in the flapwise direction where data are more scattered between the 2 sensors. The difference is probably due to the more sensitivity of SU and CP sensors to wind turbulence. The FFT showing the presence of the main rotational speed frequencies 1P, 2P and 3P is seen in Figure 5.3. This adds validity to the load signal demonstrating a good placement and functioning of the sensors in this specific period. The characteristic blade frequency is not seen.

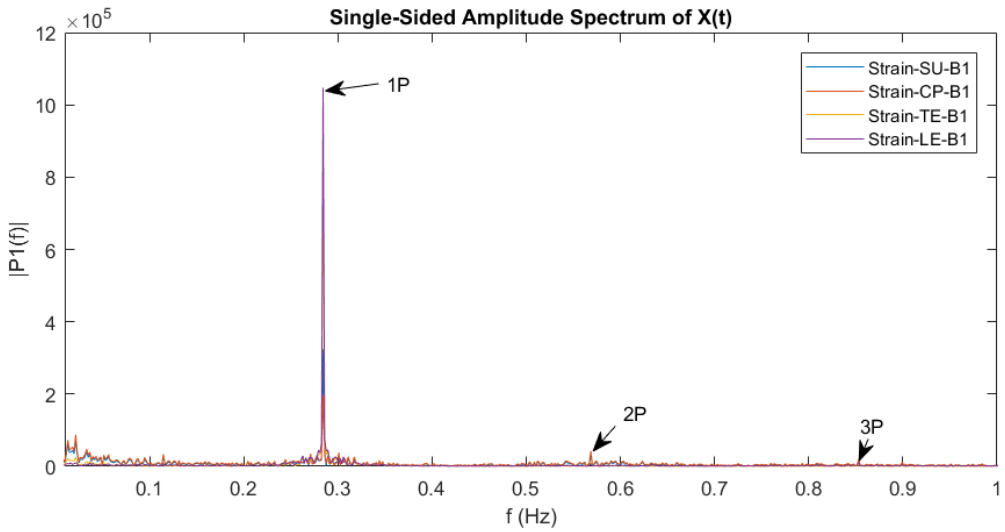

Figure 5.3: Layout of one strain gauge array.

From this single time series analysis the sensors seem to behave well with the except of blade 3 that was not available in this period but, in order to have a more comprehensive view of all the time-series available, the statistics (mean, max, min, std, median and kurtosis) of each time-series have been calculated and analyzed.

5.2 10-min Loads Time-series Statistical Validation

Before the analysis of the loads time-series statistics, some basic filters have been applied to the load data set in order to filter out the erroneous measurements that were more than one order of magnitude higher than the majority of the data; more filters have been applied to the operating conditions of the wind turbine in order to select only the time-series where the wind turbine was operating. The filters are listed below:

- Wind turbine power above 10 kW;
- Rotor speed above 7 rpm;
- Pitch below 40° for all 3 the blades;
- Wind speed above 4 m/s;

After these filters have been applied, with the goals of analyzing and deciding the sensors that could be used, each single statistics (mean, max, min, std, median and kurtosis) of the sensors of the 3 blades in both wind turbines has been analyzed using box plot graphs. Box plot representation is very convenient when dealing with 3 groups of datasets (blade 1, blade 2 and blade 3) with large amounts of data because they are able to display data distribution through their quartiles within small space. Box pots display 5 values: the minimum (Q1 -1.5*IQR)(IQR=interquartile range), the first quartile (Q1), the median, the third quartile (Q3) and the maximum (Q3 + 1.5*IQR). Values that are outside the maximum and minimum limits are shown as outsiders (usually with red dots).

In this analysis the wind flow characteristics have been taken from the data of WindCube V2.

5.2.1 Wind Turbine SMV5

In Figure 5.4 SMV5 boxplots of the mean of the load signal of each filtered 10-min time series is shown for both the flapwise and the edgewise directions and for all 3 blades.

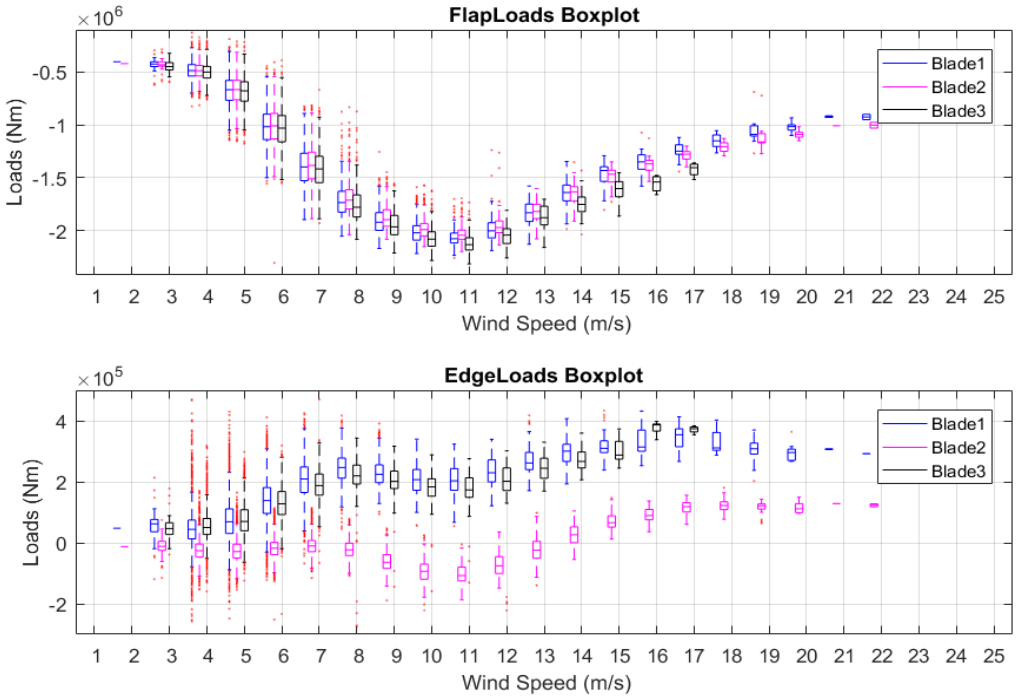

Figure 5.4: Boxplot of the flapwise and edgewise loads signals for SMV5

The boxplot shows distribution of the the flapwise loads of the three blades as a function of wind speed; it presents an increasing trend (more negative) before the turbine starts pitching (∼11 m/s) as well as a less steep decreasing trend of the loads after the turbine started pitching. This trend is present because thrust is the dominating loads resource for blade root flap moment and so for the flapwise loads; it is known that thrust climbs up to rated where it peaks, then it goes down with increasing wind speed due to the pitching of the blades in order to keep constant power. The same trend is seen in Meseguer et al. report [29]. Comparing the flapwise signal of the 3 different blades it can be seen a very consistent trend up to around 10 m/s for all 3 blades with very similar median and interquartile range (IQR); after around 10 m/s blade 3 trend starts to be higher than blade 1 and 2 up to 19% at 17 m/s and then disappear. This trend is explained by a malfunctioning and consequent breaking of the sensors in blade 3 during the winter months (usually where high wind speeds are reached) that might have distorted some measurement right before breaking. Due to the regular behaviour, the SU and CP sensors of the 3 blades plotted against each other are not shown here (see section 5.2.3).

The second boxplot shows distribution of the the edgewise loads of the three blades as a function of wind speed; it presents a slightly increasing trend with loads values around an order of magnitude lower compared to the flapwise loads. The mean edgewise loads are predominately affected by the gravity forces acting on the blades and it is rarely disturbed by wind speed. These loads are much smaller compared to the flapwise ones because loads of the same sensor are positive in one side of the cycle and negative on the other side. Consequently the 10-min mean value of the signal computed is much closer to zero compared to the flapwise signal (since the two sides of the cycle are compensating each other). A similar trend is seen in [29]. Comparing the edgewise signal of the 3 different blades it can be seen a very consistent trend for blade 1 and 3, while blade 2 has much lower loads throughout the whole wind speed spectrum and in some cases the loads have the opposite signal. A more in depth analysis of the LE and TE signals of blade 2 that are used to calculate the edgewise signal is needed.

Figure 5.5 shows the TE and LE sensors of the 3 blades plotted against each other.

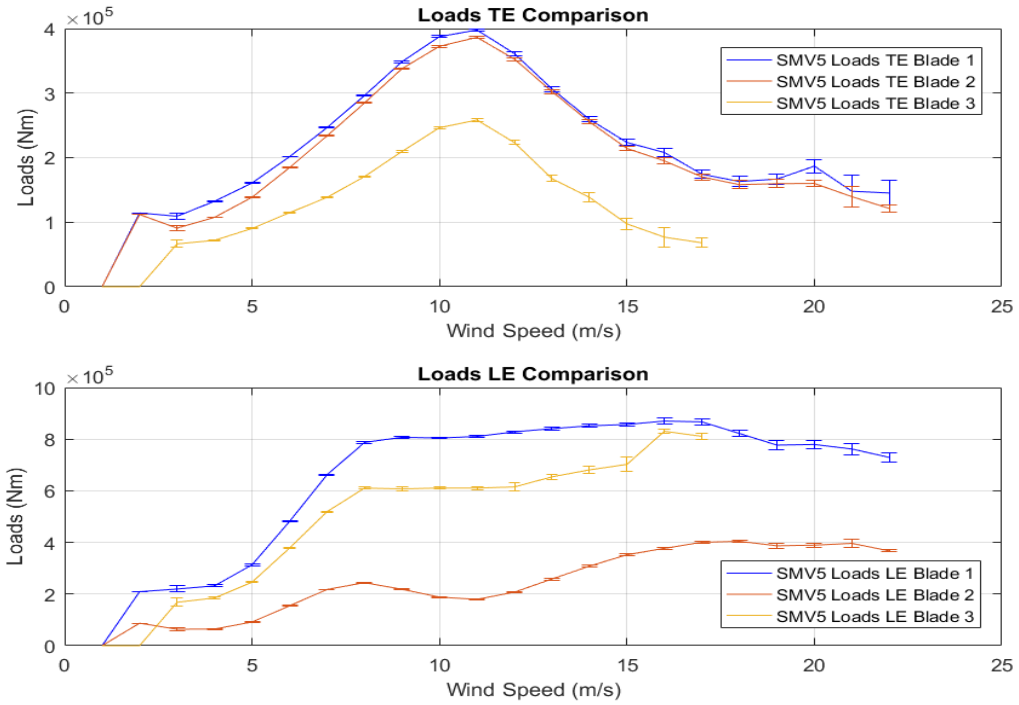

Figure 5.5: Comparison of the 3 blades TE and LE sensors in SMV5. The error bars represent the 95% confidence interval.

The TE sensors show very similar loads trends for all 3 blades; blade 3 shows lower loads throughout the wind speeds range. Here blade 2 seems to behave regularly. The LE sensors however shows more differences in the trends. Blade 1 and blade 3 have similar trends that generally show an increase up to 8 m/s followed by constant loads; as in the TE graph blade 3 shows lower loads throughout the wind speeds range. Blade 2 shows a more fluctuating trend with loads much lower compared to blade 1 and blade 3 (in some parts lower than 70%); these much lower loads in the LE sensor of blade 2 affect the edgewise signal significantly making it behave unexpectedly. The differences shown in the TE and LE signals of blade 3 do not affect the edgewise signal when combined.

5.2.2 Wind Turbine SMV6

In Figure 5.6 SMV6 boxplot of the mean of the loads signal of each filetered 10-min time series is shown for both the flapwise and the edgewise directions for the 3 blades.

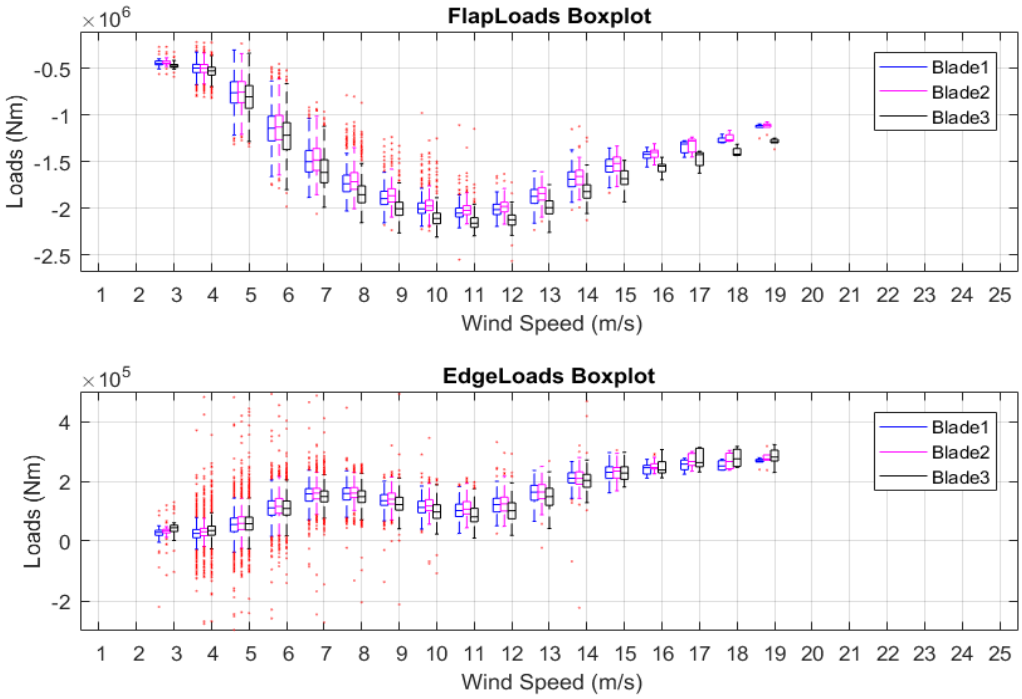

Figure 5.6: Boxplot of the flapwise and edgewise loads signals for SMV6

The boxplot shows distribution of the the flapwise loads of the three blades as a function of wind speed; it presents an increasing trend (more negative) before the turbine starts pitching (∼11 m/s) as well as a less steep decreasing trend of the loads after the turbine started pitching. This trend is explained in SMV5. The same trend is seen in [29]. Comparing the flapwise signal of the 3 different blades it can be seen a very consistent trend for blade 1 and 2 with very similar median and interquartile range (IQR); blade 3 trend is always slightly higher than blade 1 and 2 up arriving up to 11% at 17 m/s. Due to the regular behaviour, the SU and CP sensors of the 3 blades plotted against each other are not shown here (see section 5.2.3)

The second boxplot shows distribution of the the edgewise loads of the three blades as a function of wind speed; it presents a slightly increasing trend with loads values around an order of magnitude lower compared to the flapwise loads (this is due to the higher loads experienced by the blade when it is going upward against gravity). A similar trend is seen in [29]. Comparing the edgewise signal of the 3 different blades it can be seen a very consistent trend from all 3 the blades with almost identical median, first and third quartile statistics. It can be said that the edgewise signal of all 3 the blades is reliable and can be used for the in depth analysis of loads and DEL calculations. However, when the TE and LE sensors (from where the edgewise signal is calculated) of the 3 blades are plotted against each other in Figure 5.7, some unexpected behaviours are seen.

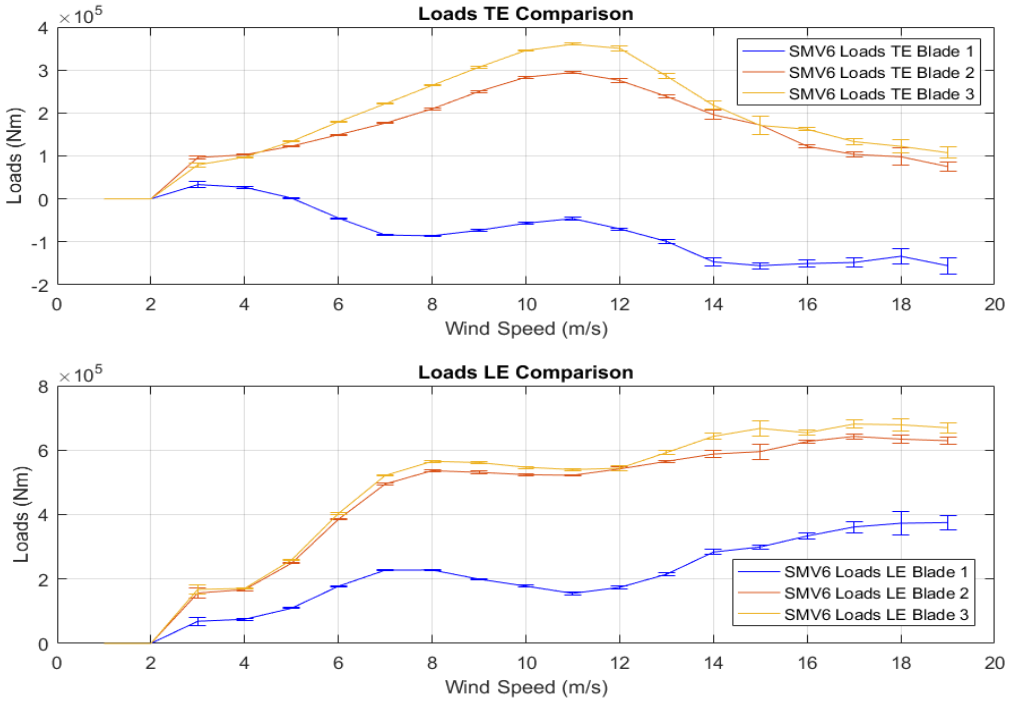

Figure 5.7: Comparison of the 3 blades TE and LE sensors in SMV6. The error bars represent the 95% confidence interval.

While the LE and TE load signals of blade 2 and blade 3 follow similar trends with load values very close to each other, blade 1 unexpectedly, has much lower loads in the LE sensor; even more unexpected are the loads in the TE sensor that have slightly increasing trend but with opposite sign compared to the other 2 blades TE signals. Despite these very marked differences, when blade 1 signals are combined (using equation A.6) to calculate the edgewise signal, they provide a very consistent and matching signal with blade 2 and 3 seen in Figure 5.6. This different behavior of blade 1 sensors might be caused by a pitch offset on the sensors installation or by a non correct installation of the strain gauges; it is likely that this set up error is compensated by the combination of the two corresponding sensors that eliminated this bias.

5.2.3 Wind Turbine SMV5 vs. Wind Turbine SMV6

In Figure 5.8 the SU and CP sensors of the 3 blades of both SMV5 and SMV6 are plotted against wind speed .

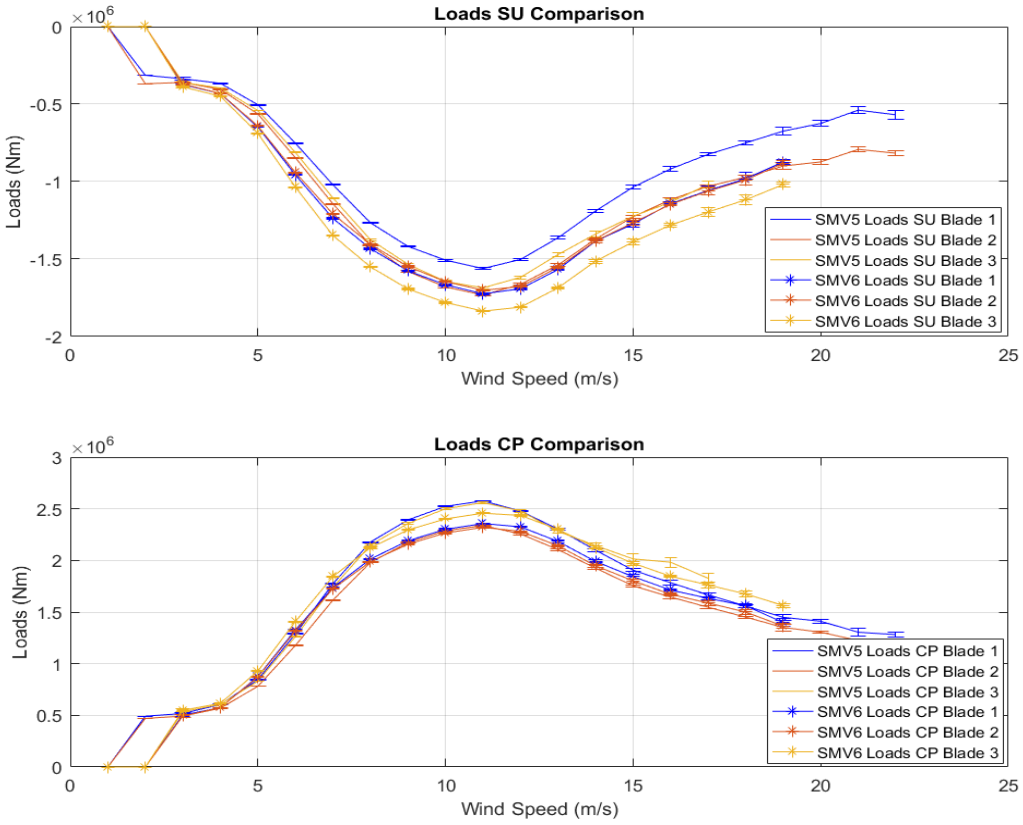

Figure 5.8: Comparison of the 3 blades SU and CP sensors in SMV5 and SMV6. The error bars represent the 95% confidence interval.

For both the SU and CP sensors a very consistent pattern is seen for all the 3 blades of each wind turbine; the small difference is most likely due to the envelope of uncertainty derived by the not perfect installation of the strain gauges sensors in a really difficult environment like the inside of a wind turbine blade. As a conclusion all the flapwise loads signals of the 3 blades of both SMV5 and SMV6 can be used for a reliable normal operation and active wake farm control strategies loads and fatigue analysis.

In Figure 5.9 the LE and TE sensors of the 3 blades of both SMV5 and SMV6 are plotted against each other.

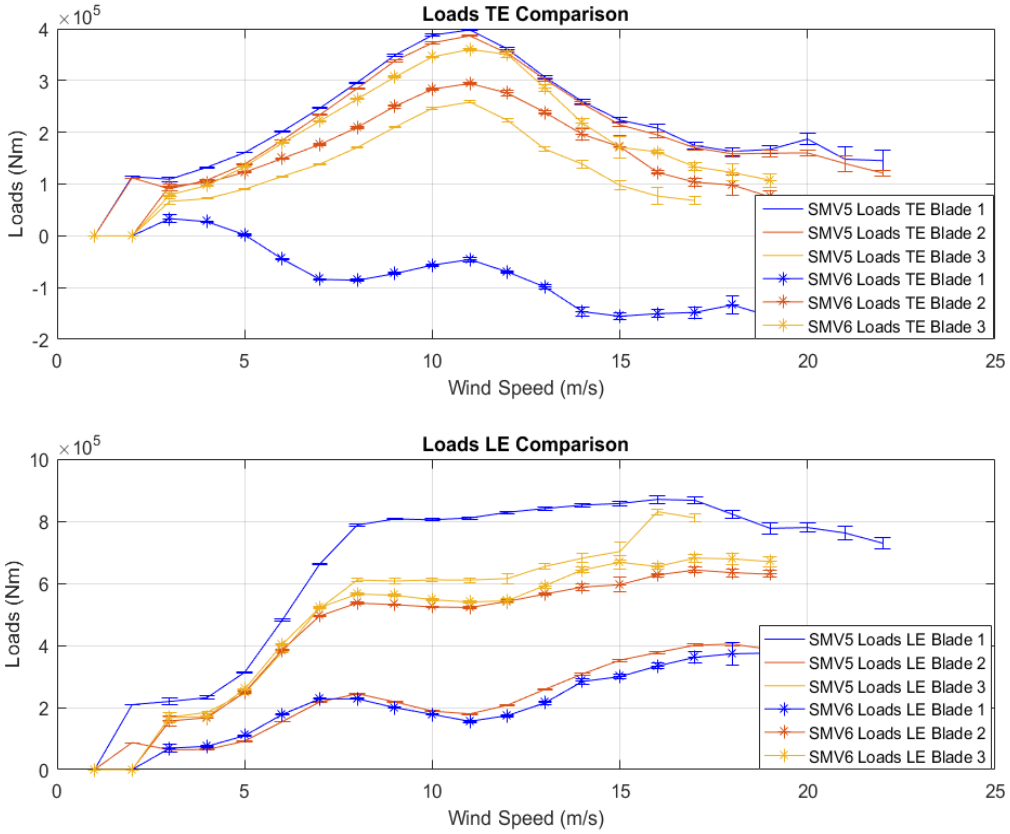

Figure 5.9: Comparison of the 3 blades TE and LE sensors in SMV5 and SMV6. The error bars represent the 95% confidence interval.

It can be observed that the LE and TE sensor loads signals have less consistency and much more variability; this is most likely due to the higher degree of difficulty in installing the sensors in the edgewise direction since the surface of the supporting structural beam inside the blade is very rough making it difficult to install the sensor in the right position. Said so it can still be seen both LE and TE graphs contains some signals that are very different and that cannot be explained by the envelope of uncertainty because the loads difference is very noticeable. These signals are (as seen previously): SMV5 LE blade 2 signal, SMV6 LE blade 1 signal and SMV6 TE blade 1 signal. This difference could be explained by a pitch offset on the sensors installation, by a non correct installation of the strain gauges or by a non correct gluing of the sensors on the blade internal surface. After extensive analysis of the data no definite reason for this behaviour is found.

5.3 Summary

In the load validation the distributions of the flapwise and edgewise loads for both the turbines (and for all the 3 blades) have been analyzed with very similar trends and values seen in both turbines. The flapwise loads distributions are mainly dominated by thrust, as a consequence loads rise up to the time when the turbine starts pitching and then they decrease. The edgewise loads distributions are predominately affected by the gravity forces acting on the blades and they are rarely disturbed by wind speed (thrust). These loads are much smaller compared to the flapwise ones due to the loads from the two sides of the cycle compensating each other when the mean is calculated.

Then to understand the reason why some blades behaved differently, the single sensors that have been used to recreate the flapwise and edgewise signals have been also analyzed and compared to each

other.

It can be concluded that the SMV5 edgewise loads signal of blade 2 is not reliable (so it is not used) due to the unexpected behaviour in both the edgewise boxplot analysis and in the single TE and LE signal analysis. The SMV6 edgewise loads signal of blade 1 is considered still reliable due to the consistency of the combined LE and TE signals shown in the edgewise boxplot analysis that most likely eliminated this bias present in these 2 sensors; as a consequence this anomaly is considered not relevant in the normal operation and active wake farm control strategies loads and fatigue analysis.

6 Fatigue Loads Calculation and Validation

The edgewise and flapwise loads have been calculated and validated in the previous chapters for both wind turbines. Loads are not really indicative for the analysis of possible changes in the lifetime durability of wind turbine rotor components. In order to assess the changes in material properties due to the application of loads over a period of time, fatigue loads need to be calculated and analyzed. Fatigue in wind turbines is mainly caused by the presence of recurring cyclic loads that are able to provoke cumulative high-cycle fatigue (more than 10000 cycles are needed for structural failure [30]) damage on rotor components of a wind turbine [30]. The validation of fatigue loads has to make sure that the detected field measurement behave in the expected way and are representative of the actual fatigue loads encountered by the turbine blades.

6.1 Fatigue Loads Calculation

The major part of the wind turbine rotor fatigue loads are occurring during power production operation and as a consequence, only this operating mode is analyzed in this project.

The fatigue loads have been calculated following the International Standards: Measurement of mechanical loads (IEC 61400-13:2016) [30]. Usually fatigue is represented and analyzed using a fatigue load cycle spectra that utilizes the rainflow algorithm giving the possibility to use the Palmgren-Miner linear damage rule and the Whöler curve for the calculation of fatigue [30].

The Palmgren-Miner linear damage rule assumes that every different cycle provoke some damage d_i and that all the damages are then combined in the total sum of damage D_{total} (Equation 6.1); when the total damage D_{total}, defined by the summation of the used cycles d_i (n_i/N_i), reaches the value of 1, failure occur [30].

$$D_{total} = \sum \frac{n_i}{N_i} < 1 \tag{6.1}$$

The Whöler curve assumes that in a log-log S-N curve (Strain over Number of cycles), the number of cycles that lead to failure (N) at a given load (S) is given by the linear relationship shown in Equation 6.2) [28]):

$$N = C * S^{-m} \tag{6.2}$$

where C and m are properties of the material.

Since the total damage D_{total} relies on the load at the intersection between the S-N curve and the y-axis (S_0), as seen in the following equation 6.3.

$$D_{total} = \frac{1}{S_0^m} \sum n_i * S_i^m \tag{6.3}$$

The preferred way of calculating fatigue loads is 1Hz damage equivalent load (DEL). This in order to facilitate the comparison between fatigue contributions from the different wind speeds. The damage equivalent load is the cyclic load that when occurs n_{eq} times (in the case of wind turbines 1Hz for 10 minutes = 600) induces the same fatigue damage as the observed turbulent flow at a specific wind speed [32].

$$D_{total} = \frac{n_{eq} * S_{eq}^m}{S_0^m} = \frac{1}{S_0^m} \sum_i n_i * S_i^m \tag{6.4}$$

$$\implies S_{eq} = \left(\frac{\sum n_i * S_i^m}{n_{eq}} \right)^{\frac{1}{m}} \tag{6.5}$$

In this thesis the damage equivalent loads (DEL) cycle counts have been calculated using the rainflow counting algorithm on each 10-min load time series. This algorithm, implemented as a function by Matlab, will be briefly explained below and it is divided into 2 main parts [30]:

1. In the first part the load time series are simplified into signal made of peaks and dips; the extremes are filtered to a minimum chosen size and then identified.
2. In the second part, the cycle counting procedure takes place; the main idea is to turn the load signal by 90° and to consider each peak as a point where the water starts to flow and count the half cycles that happen every time the flow gets interrupted. The flow is interrupted:
   - every time the flow arrives to the end of the time series;
   - every time the opposite peak is bigger in magnitude;
   - every time the flow merges with another flow.

   This counting procedure is repeated for each dip and then all the half-cycles of the same magnitude are combined to calculate the DEL [33].

In the next section the calculated fatigue loads will be analyzed and validated.

6.2 10-min DEL Fatigue Loads Validation Under Normal Operating Conditions

Before the analysis of the DEL (Damage Equivalent Loads) time-series statistics, some basic filters have been applied to the DEL data set in order to filter out the erroneous data that were more than one order of magnitude higher than the majority of the data; the same filters that have been applied to the operating conditions of the wind turbine in the load validation (Section 5.2), in order to select only the time-series where the wind turbine is operating, have been applied. Other filters have been applied in order to select only the wind directions where both turbines are outside the wake created by neighbouring wind turbines (between 230° and 320°) so that DEL are not influenced by the increased turbulence intensity and decreased wind speed occurring inside the wake. In this validation only the specific period where the turbine was operating normally has been selected (meaning that no wind farm active wake control strategies have been applied).

After these filters have been applied, the mean DEL values (for both flapwise and edgewise directions) of the 3 blades in both wind turbines have been analyzed using box plot graphs. Box plot representation is very convenient when dealing with 3 groups of data sets (blade 1, blade 2 and blade 3) with big amounts of data because they are able to display data distribution through their quartiles within small space.

It needs to be remembered that fatigue equivalent loads (DEL) of a wind turbine, come from the variation of the loads in time and they do not heavily depend on the mean level of the loads.

In this analysis, the wind flow characteristics have been taken from the data of WindCube V2.

6.2.1 Wind Turbine SMV5

In Figure 6.1 SMV5 boxplot of the mean of the DEL of each filtered 10-min time series is shown for both the flapwise and the edgewise directions for all 3 blades.

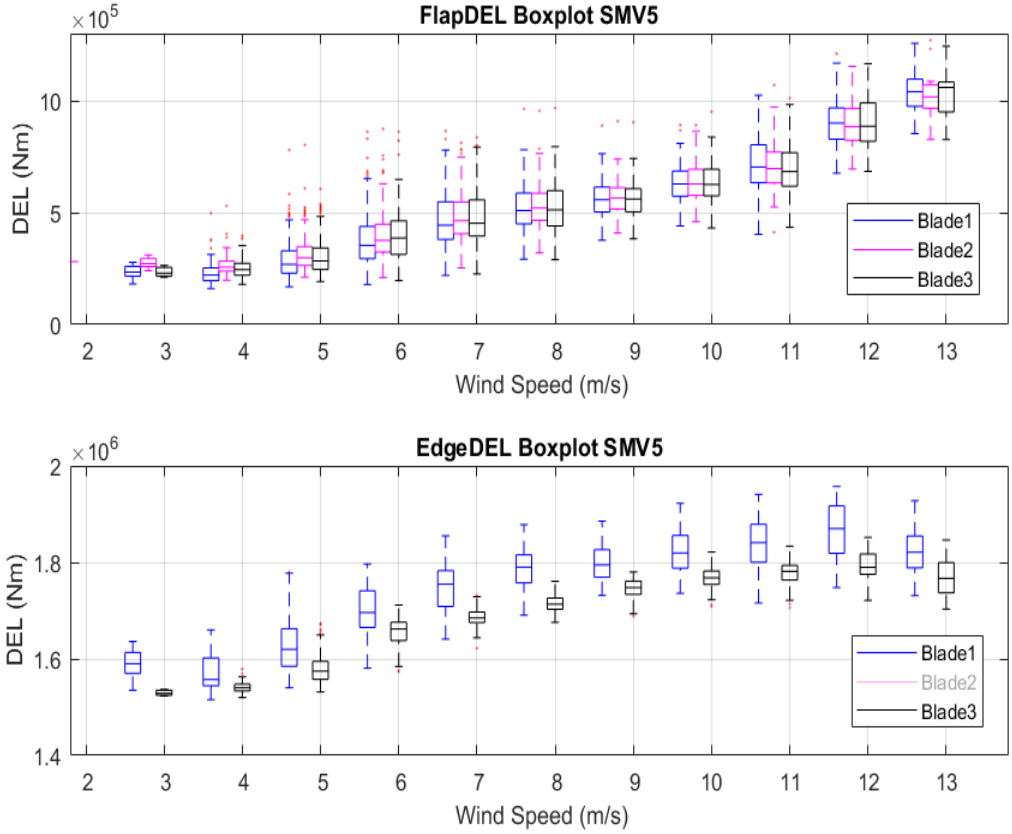

Figure 6.1: Boxplot of the flapwise and edgewise DEL signals for SMV5

The first box plot, seen in Figure 6.1, shows the distribution of the the flapwise DEL of the three blades as a function of wind speed; it presents a strongly increasing trend with a constant slope up to 11 m/s (when the turbine starts pitching); than the slope increases slightly up to 13 m/s (limited due to data availability). This trend is expected since the flapwise motion is strongly affected by turbulence; as wind speed increases, also the wind speed standard deviation increases rising the variation of the loads impressed on the blade flapwise direction [32]. This increased variation that shapes flapwise DEL loads increases even more when the turbine starts pitching; this could be due to the pitch control induced vibrations. The same trend is seen in both Albert Meseguer et al. paper [25] and in Jennifer Rinker report [32]. Comparing the flapwise DEL boxplots of the 3 different blades it can be seen a very consistent trend for all the 3 blades with very similar median and interquartile range (IQR) showing consistency and reliability in SMV5 flapwise DEL data.

The second boxplot, seen in Figure 6.1, shows the distribution of the the edgewise DEL of the three blades as a function of wind speed; it presents a slightly increasing trend up to 11-12 m/s where the maximum is reached, then the edgewise DEL start decreasing. This increasing trend might look surprising initially since it has been previously stated that edgewise motion is dominated by gravitational effects (expected not to change much with increasing wind speed) [32]. However, the variation of the edgewise DEL is much smaller than the one of flapwise DEL with respect to the mean value. This is expected since the edgewise motion is not totally unaffected by turbulence; as a consequence a much smaller relative increase in edgewise DEL loads is expected [32]. The same trend is also seen in both Albert Meseguer et al. paper [29] and in Jennifer Rinker report [32]. Comparing the edgewise DEL boxplots of the 2 different blades it can be seen a consistent trend with blade 3 having slightly lower values; this small difference is most likely due to the envelope of uncertainty of both loads and DEL calculations.

As expected, the edgewise DEL are around one order of magnitude higher than the the flapwise DEL due to to the periodicity and magnitude of occurrence of the gravitational loads on this specific direction.

6.2.2 Wind Turbine SMV6

In Figure 5.4 SMV6 boxplot of the mean of the DEL of each filetered 10-min time series is shown for both the flapwise and the edgewise directions for all 3 blades. Due to the consistency and similarity of these DEL boxplots to the ones of wind turbine SMV5, the DEL analysis previously done for wind turbine SMV5 (in Section 6.2.1) is equally valid for wind turbine SMV6.

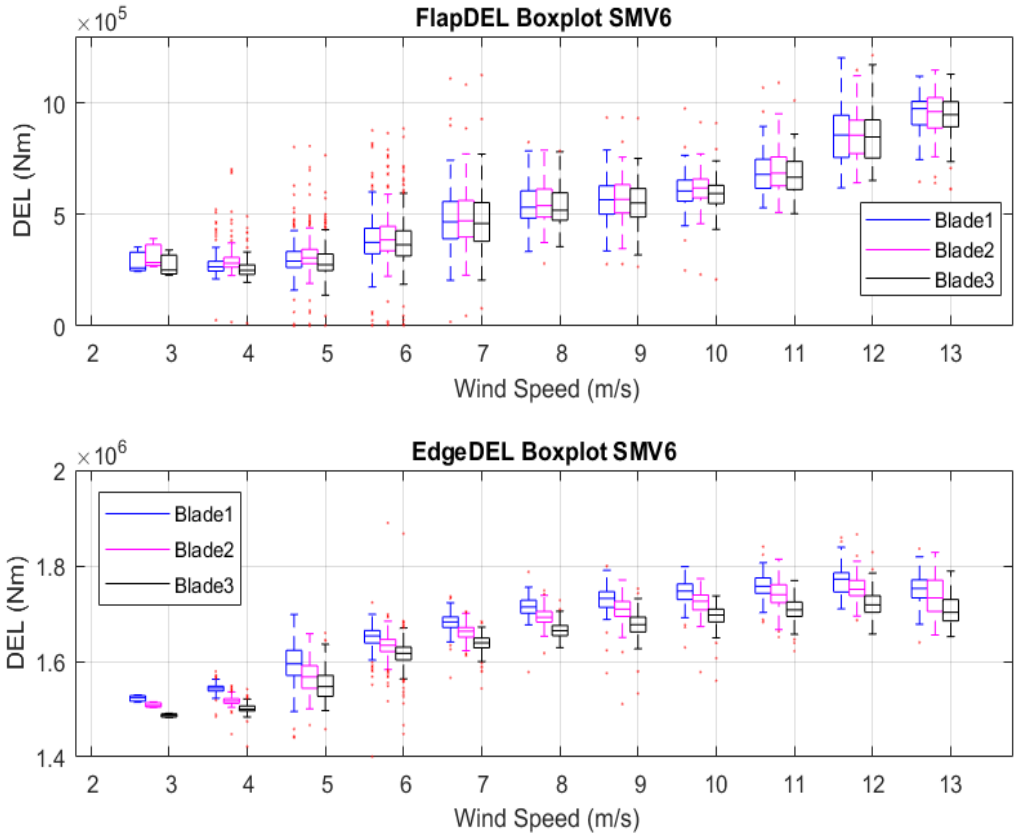

Figure 6.2: Boxplot of the flapwise and edgewise DEL signals for SMV6

7 Loads and Fatigue Analysis Under Normal Operation

After a quick analysis of the data availability in the second field campaign, an evaluation of the wind turbine loads and fatigue under normal operation is done in order to being able to compare and assess the loads and fatigue variations when active wake control strategies are applied. In the analysis of normal operation, the dependency of fatigue loads is evaluated with respect of the atmospheric conditions (wind direction, wind shear and turbulence intensity).

7.1 Data Availability

The data availability of all the sensors during the second field measurement campaign (June 2017-March 2018) is shown in Figure 7.1. The second measurement campaign include 24266 10-min time series for SMV5 and 23732 10-min time series for SMV6.

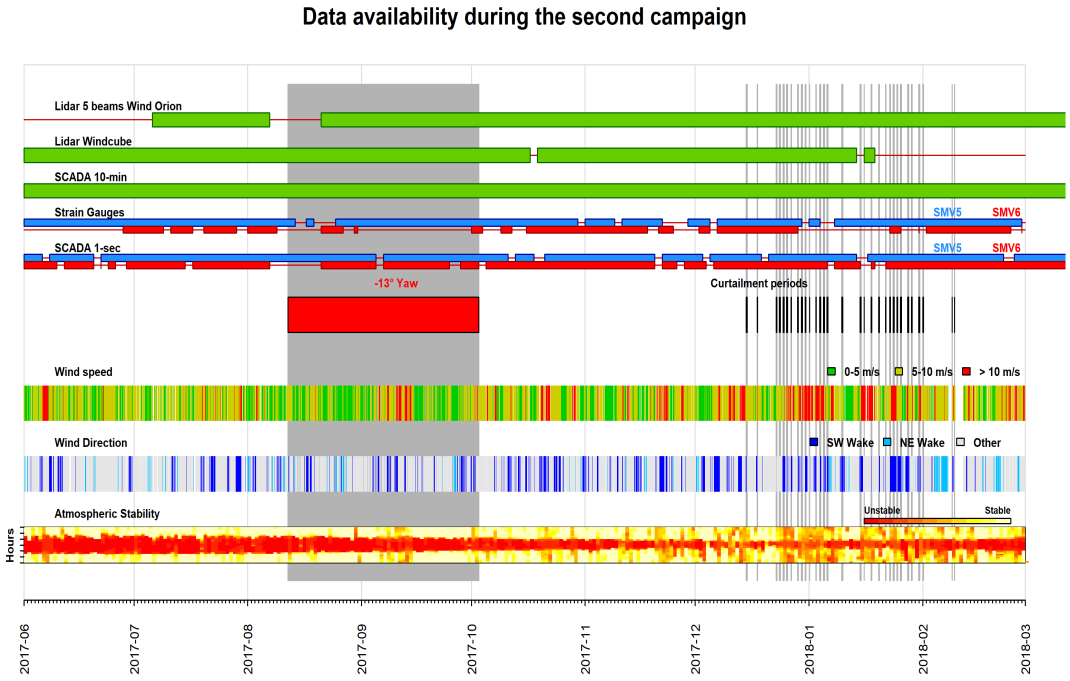

Figure 7.1: Data availability and atmospheric conditions during the second field campaign. Figure created by ENGIE Green.

Normal operation periods are considered the periods when the wind farm is operating without the implementation of active wind farm wake control strategies; Figure 7.1 shows clearly that there are two main periods where no control strategies have been applied:

1. between 1st June 2017 and 13th August 2017;
2. between 4th October 2017 and 14th December 2017.

Unfortunately the first period hasn't been used due to the maintenance operations taking place during those months; during maintenance operations the parameters and characteristics of the wind turbines are modified and as a consequence the data from this period would not match the normal operation data. The period used for the loads and fatigue analysis under normal operation is the second. Data availability of all the measuring devices is generally good with only few short periods of missing data for the strain gauges and SCADA data for both turbines. Due to these missing data and to the noisy characteristics of SCADA signals (since they are located downstream to the rotor), it has been decided

to rely on the lidar Windcube V2 data for the find flow characteristics (wind speed, wind direction, wind shear and turbulence intensity).

7.2 Normal Operation Loads Analysis

Normal operation means that the turbines are producing power without the activation of any wind farm control strategy, in the same manner that they would in a traditional wind farm. This means that the same basic filters explained and applied in section 5.2 and 6.2 have been applied. In addition the data have been restricted to the normal operation period between 4th October 2017 and 14th December 2017 seen in section 7.1.

In this analysis, normal operation has been divided into two main categories depending on the main ambient wind direction: the first category is operation subjected to wake conditions and the second category is operation subjected to no-wake conditions (see Figure 7.2). Wind turbine SMV5 is subjected to SMV6 wake conditions when the ambient wind direction is between ∼180° and ∼230° (alignment at 207°); wind turbine SMV6 is subjected to SMV7 wake conditions when the ambient wind direction is between ∼150° and ∼200° (alignment at 173.5°). Generally both wind turbines should experience no-wake conditions throughout the remaining wind directions if no other turbines are present. However in this specific case, no-wake conditions have been chosen when the ambient wind direction is between ∼230° and ∼320°; this because of the presence of other further away wind turbines in the wind farm positioned to the North/North-East of SMV5, SMV6 and of the WindCube V2 and because of consistency in the turbulence intensity and shear factor distribution (mostly due to the specific roughness of each wind direction) .

The wind flow characteristics have been taken from the data of WindCube V2. The flapwise loads of each blade have been normalized with the flapwise mean load values at 11 m/s of that blade during no-wake conditions; this because at 11 m/s maximum flapwise loads are reached when the turbine is subjected to no-wake. This normalization choice is used also in the edgewise direction to keep consistency so all the edgewise loads values of each blade have been normalized with the edgewise mean loads at 11 m/s (wind speed corresponding to the maximum flapwise loads). This choice is made in order to simplify the analysis of each blade relative changes during the different wake/no-wake conditions. The focus of this thesis is not on the absolute loads values but on the relative changes. Due to more restrictive filtering, data are available only for wind speeds up to 13 m/s.

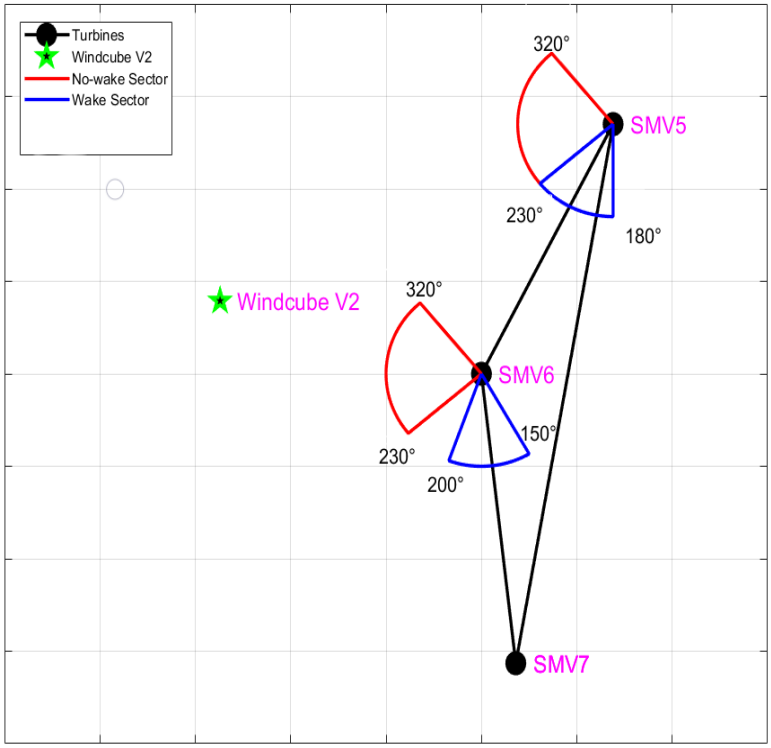

Figure 7.2: Wake and no-wake sector analyzed in this thesis.

7.2.1 Flapwise Mean Loads Under Normal Operation

In Figure 7.3 SMV5 and SMV6 flapwise mean loads are shown as a function of ambient wind speed for both the wake and no-wake conditions.

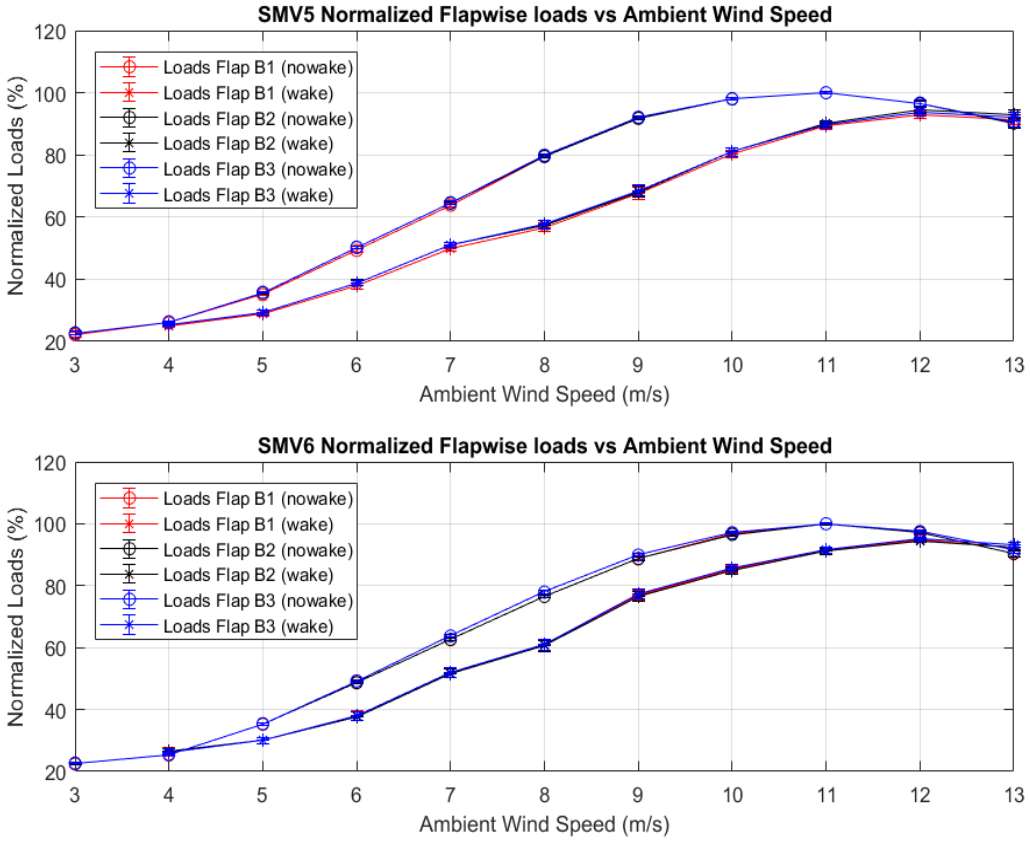

Figure 7.3: SMV5 and SMV6 normalized flapwise loads as a function of ambient wind speed for wake and no-wake conditions. The error bars represent the 95% confidence interval.

The first graph seen in Figure 7.3 shows how the flapwise loads of SMV5 varies with ambient wind speed for both wake and no-wake conditions. The graph shows high consistency in the behavior of all the 3 different blades that matches almost perfectly. The trend seen for the no-wake condition flapwise loads has been already seen in section 5.2.1 and it is caused by the dominance of thrust force in this direction (similarly to Figure 5.4 but upside down due to the normalization). The trend seen for the wake condition flapwise loads is the same but it is shifted to the right; this means that for the same ambient wind speed loads under wake conditions are significantly lower with a maximum difference of 32% at both ambient wind speeds of 8 m/s and 9 m/s. This happens because during wake conditions, the wind speed perceived by the turbine is lower compared to the ambient wind speed, meaning that lower loads at each wind speed are observed. This also explains why during wake conditions, flapwise loads still rise after 11 m/s (point where, under no-wake conditions, the blade are fully pitched to keep constant power); inside the wake the downwind turbine "feels" the wind speed of 11m/s when the ambient wind speed is higher than 12 m/s.

The same trends seen in the flapwise loads of SMV5 both wake and no-wake conditions are also seen in the flapwise loads of SMV6 (second graph seen in Figure 7.3). It needs to be pointed out that a significantly smaller difference in flapwise loads is observed in SMV6 with a maximum difference of 26% at the ambient wind speeds of 6 m/s. A reason for this smaller difference could be a more invasive influence on the wind flow characteristics of a small forest present to the South of the wind farm that is mostly present in SMV6 wake range while only partially in SMV5 wake range. The presence of this forest increases the surface roughness and could eventually increase the turbulence intensity facilitating air mixing and so decreasing wind speed deficit inside the wake of SMV7 on SMV6. Another reason could be that when the ambient wind direction is below 170°, SMV6 wake enters the Windcube V2

range (lowering the perceived ambient wind speed by the Windcube V2 compared to the real ambient wind speed seen by SMV6). This means that the correct flapwise loads curve could be more shifted to the right, leading to an increase of the loads difference between wake and no-wake conditions to values similar to the ones observed in SMV5. Less plausible is the idea that such a slightly larger distance beween SMV7 and SMV6 (0.1D more) could impact loads so significantly.

7.2.2 Edgewise Mean Loads Under Normal Operation

In Figure 7.4 SMV5 and SMV6 edgewise mean loads are shown as a function of ambient wind speed for both the wake and no-wake conditions.

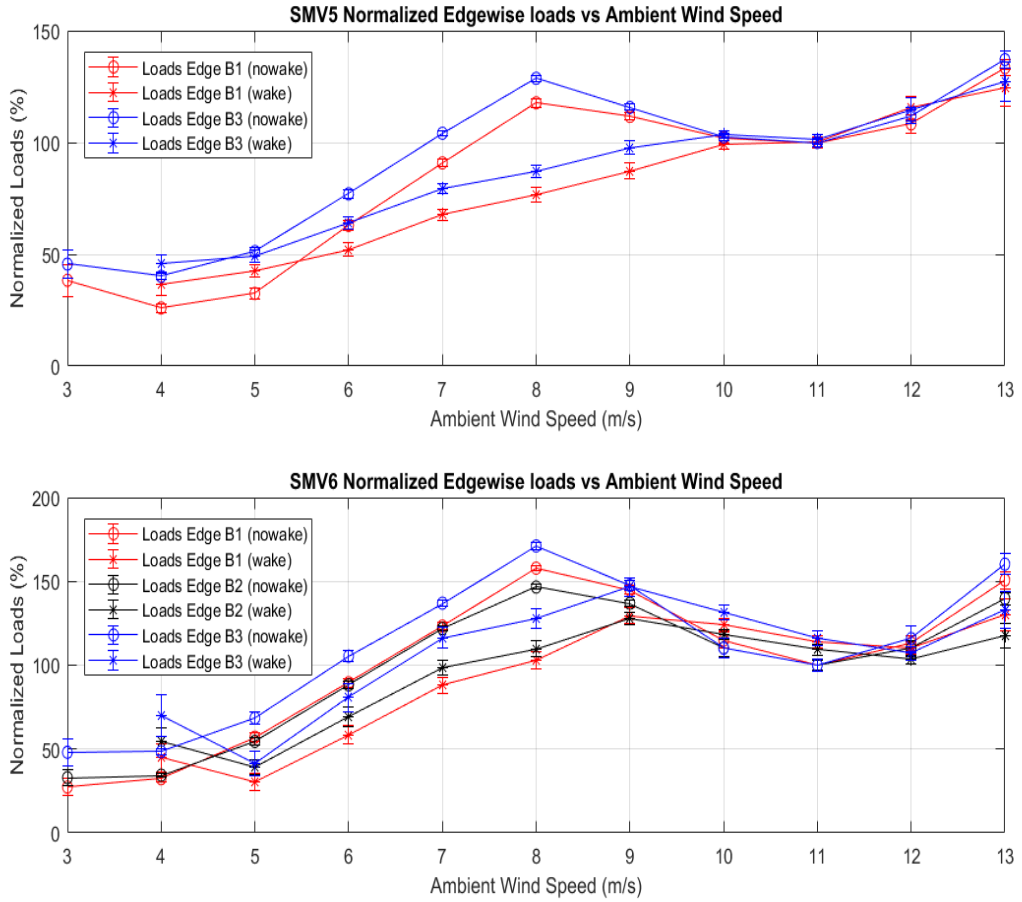

Figure 7.4: SMV5 and SMV6 normalized edgewise loads as a function of ambient wind speed for wake and no-wake conditions.. The error bars represent the 95% confidence interval.

The first graph seen in Figure 7.4 shows how the edgewise loads of SMV5 varies with ambient wind speed for both wake and no-wake conditions. The graph shows less consistency in the behavior of blades 1 and 3 compared to the flapwise loads; this difference is most likely due to the same reasons explained in section 5.2.3, mainly envelope of uncertainty and increased difficulty in the installation of the strain gauge sensors in the edgewise direction. The trend is mainly affected by gravity forces. Even in the edgewise direction lower loads are observed for the wake conditions especially at ambient wind speeds between 7 m/s and 9 m/s. The maximum difference of 42% is at the ambient wind speeds of 8 m/s (for B1 of both turbines). However, for unknown reasons, SMV5 does not show a very clear shifted trend for the edgewise loads in wake conditions. This shift is slightly more visible in the edgewise loads of SMV6 up to 10 m/s. It can be concluded that edgewise loads show a similar trend (with lower loads) during wake

conditions, but the clear shift of loads (due to lower encountered wind speed during wake conditions) is less noticeable and clear. This is due to the very marginal influence of thrust in the edgewise direction.

7.3 Normal Operation Fatigue Loads (DEL) Analysis

The normal operation fatigue loads analysis also uses the same filters applied in the normal operation loads analysis seen in the section 7.2. The same normal operation period between the 4th October 2017 and the 14th December 2017 has been used. Fatigue loads dependence on wind speed has been examined in section 6.2 where fatigue loads under normal operation have been validated. The fatigue loads dependence on varying wind direction, wind shear and turbulence intensity will be analyzed in the following sections in order to increase the understanding of effects that these parameters have on fatigue. Fatigue loads are strongly affected by the amount of thrust force applied. Since the thrust force is dependent on wind speed, in order to have a reliable analysis, the DEL values have been normalized with the average no-wake DEL value at their specific wind speed. This specific DEL normalization for each wind speed is meant to decrease as much as possible the effect of wind speed (thrust) on the blades DEL to clearly observe the effects that wind direction, wind shear (for the calculation of the wind shear parameter see Appendix B) and turbulence intensity have. No-wake conditions have been used in order to eliminate the alternated results caused by the wake.

DEL however are not only heavily affected by the wind speed but they are also affected by wind shear and more importantly by turbulence intensity; for this reason the average DEL values at each specific wind speed used for the normalization, have been calculated only for specific wind shear and turbulence intensity ranges where DEL has limited variability. With these filters it is easier to analyze how DEL change with increasing wind shear and turbulence intensity.

Figure 7.5 shows the flapwise DEL of both turbines (SMV5 and SMV6) as a function of turbulence intensity and wind shear. The data have been filtered for no-wake conditions and the wind speed range selected is between 6.5m/s and 8.5m/s (wind speeds where more data are available) to decrease the effect of wind speed on DEL.

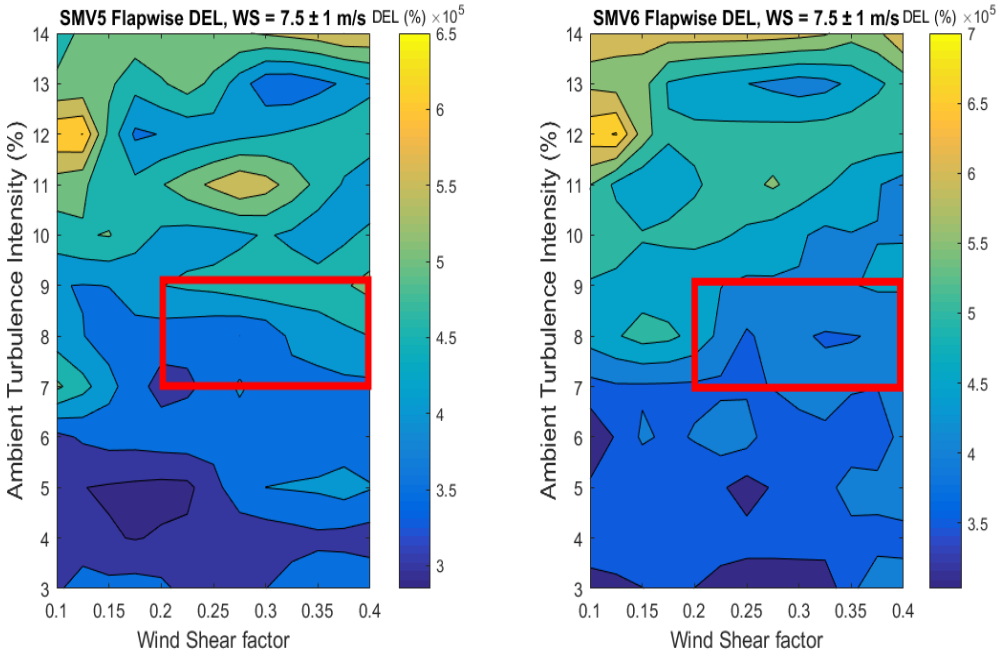

Figure 7.5: SMV5 and SMV6 flapwise DEL contour plots, wind speed = 7.5 ± 1 m/s

In Figure 7.5, it can be observed that the sensitivity of the flapwise DEL to wind shear is higher for higher turbulence intensities, whereas the flapwise DEL sensitivity to turbulence intensity is higher

for lower wind shear. As a consequence taking into consideration confidence in the data and assuming that flapwise DEL behaves similarly at all the wind speeds, the normalization ranges (where DEL are more constant) chosen have been: turbulence intensity between 7% and 9% and wind shear parameter between 0.2 and 0.4.

A recap on the normalization used in the normal operation DEL analysis is shown below:

- Wind Speed: all DEL values have been normalized with the average no-wake DEL value at their specific wind speed;
- Wind Direction: No-wake wind direction has been chosen for both SMV5 and SMV6 (between 230° and 320°);
- Wind Shear: wind shear parameter has been restricted between 0.2 and 0.4;
- Turbulence Intensity: turbulence intensity has been restricted between 7% and 9%.

7.3.1 Flapwise DEL vs Wind Direction

The first atmospheric characteristic analyzed is wind direction. In the wind direction analysis no restrictions on the data have been applied because: turbulence intensity and wind shear restrictions would have limited the range of wind directions while in this analysis the whole range of wind directions is needed in order to see the wake effects on DEL and also they would have decreased the amount of data significantly.

Figure 7.6 shows the flapwise DEL of both turbines (SMV5 and SMV6) as a function of wind direction.

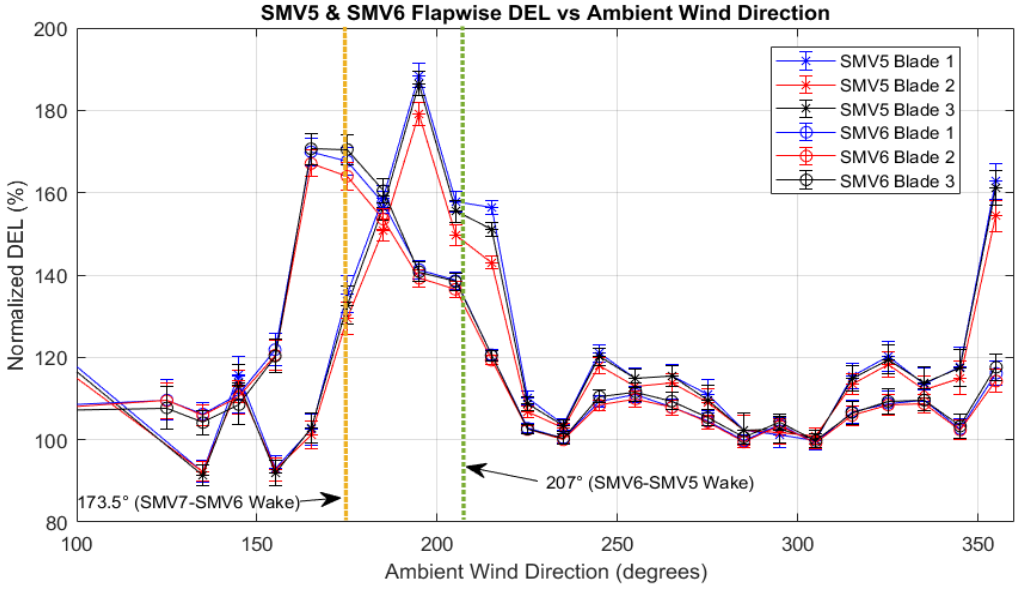

Figure 7.6: SMV5 and SMV6 normalized flapwise loads as a function of ambient wind direction. The error bars represent the 95% confidence interval.

In Figure 7.6 the wake effects on the flapwise DEL are very evident in both the wind turbines; also the consistency of all the 3 blades of each turbine is very high. SMV5 and SMV6 flapwise DEL have almost identical flat trend in the region between 230° and 340° where no-wake conditions are encountered; here DEL are slightly above 100% most likely due to higher turbulence intensities compared to the range used in normalization (average TI at the site is between 10% and 11%). SMV5 DEL have a very sharp increase up to the normalized DEL value of 189% (blade 1) starting at ∼155° and ending at ∼230° corresponding to the expected wake wind directions. The same thing is observed for SMV6 with an increase up to the normalized DEL value of value 171% (blade 3) starting at ∼145° and ending at ∼230°. In the region between ∼30° and ∼100° also a flat trend close to the normalized value of 100%

is expected; however, due to the low amount of data, this region is not shown. SMV5 also see another peak after ∼340° with a DEL increase up to the normalized DEL value of value of 161%; this increase in DEL is also due to the wake effect created by the presence of the other wind turbines of the wind farm aligned in a row almost perfectly going from North to South (∼5°). In SMV6 this increase is less pronounced because the wake of the other wind turbines happens at wind directions higher than 5° (up to ∼30°). As expected fatigue loads increase very significantly in wake conditions with values that for both turbines almost double the fatigue loads under no-wake conditions. The reason for this increase in fatigue is most likely the increase in turbulence intensity caused by the wake; the increase in turbulence intensity combined with the imbalance of the rotor loads in the presence of half-wake rises the variation of the loads in time (main cause of increased fatigue).

Figure 7.7 shows in particular the wake sectors of SMV5 and SMV6 for a more in depth analysis of these wind direction ranges.

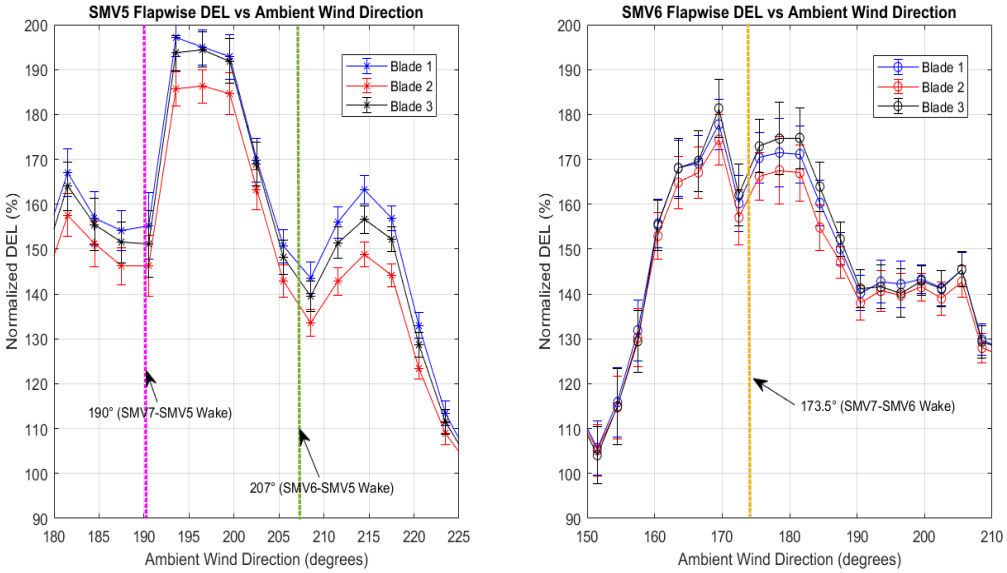

Figure 7.7: SMV5 and SMV6 normalized flapwise loads as a function of wake wind directions. The error bars represent the 95% confidence interval.

The fist noticeable thing, in SMV5 wake sector, is that the flapwise DEL peak is not symmetrical to the aligned wake direction of 207° and the peak happens at ∼195°. Two other smaller peaks are observed at ∼182° and ∼215°. The second noticeable thing is that the dips between the 3 peaks correspond to the aligned wakes direction of both the turbines SMV5 and SMV7 on the turbine SMv5. The presence of these peaks is most likely caused by the presence of the half-wakes present to the right and to the left of the aligned wakes direction (190° and 207°). When the wind direction is between ∼190° and ∼207°, SMV5 is subjected to the combined half wake of both SMV6 and SMV7 driving up the flapwise fatigue loads to its maximum. Surprisingly the magnitude of the peak caused by the half wake of SMV7 (167% at 182° (blade1)) is higher compared to the magnitude of the peak caused by the half wake of SMV6 (163% at 215° (blade3)). Due to SMV7 larger distance of 7.2D compared to SMV6 3.7D it was expected that the influence of the wake caused by SMV7 would have been smaller compared to the one caused by the closer SMV6. This is probably due to the effect of the forest located South of the wind farm that increase ambient turbulence intensity for these particular wind direction consequently increasing fatigue.

SMV6 flapwise DEL peak is quite symmetrical to aligned wake direction of 173.5°; two minor peaks are present to the left and to the right of the wind direction 173.5°. They are most likely caused by the presence of half-wake that is characterized by the highest fatigue loads inside the wake sector, however due to the uncertainty present, conclusions on the causes of the peaks need to be taken cautiously. Also in SMV6 wake sector there is an asymmetrical steady region between ∼190° and ∼210° where DEL stays

almost constant to the value of around 140%. The reason for this region is the presence of the same forest to the South of the wind turbine that appears to be the thickest and most affecting between ∼190° and ∼210° as seen in Figure 7.8

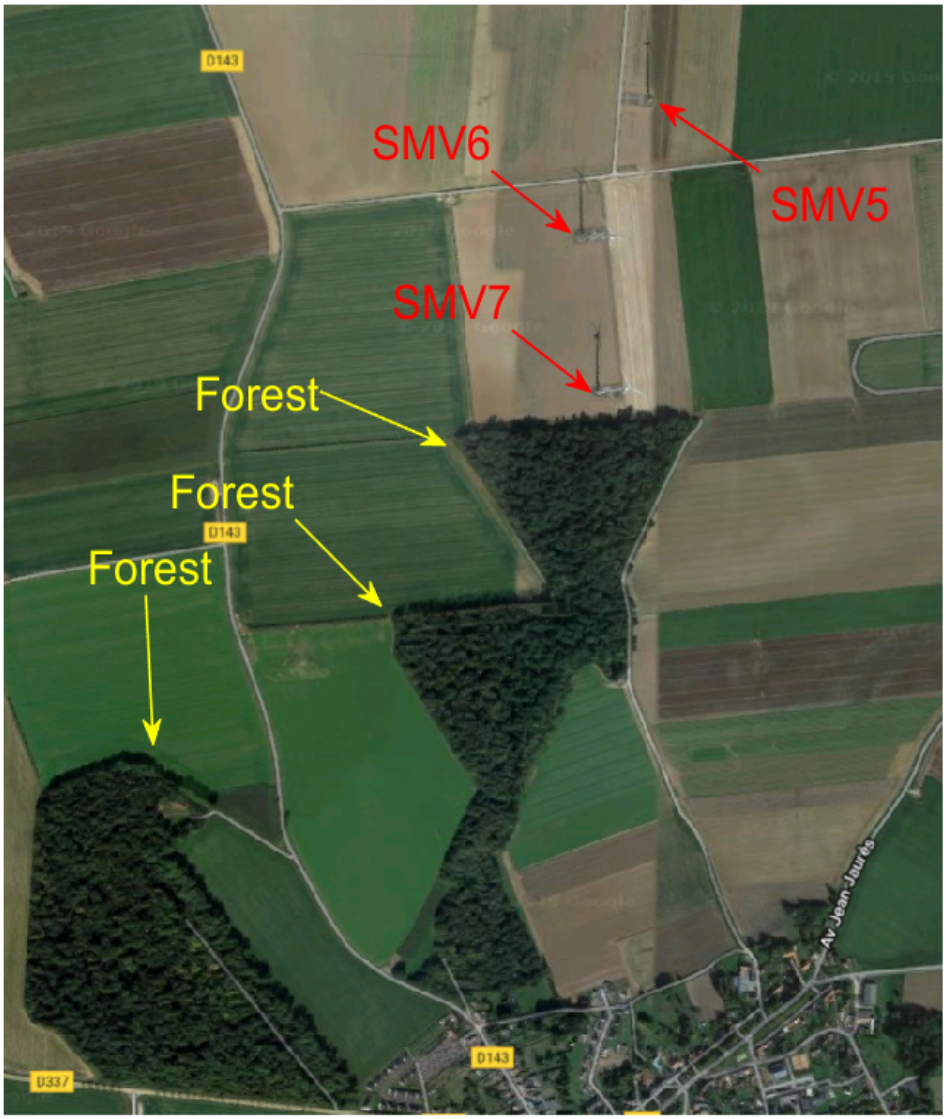

Figure 7.8: Aerial footage of the forests present to the South of the wind farm. Image retrieved from Google Maps.

In order to see what are the wind speeds more influenced by this increase in fatigue, the flapwise DEL for each separated wind speed of turbine SMV5 (blade 1) have been plotted as a function of wind direction in Figure 7.9.

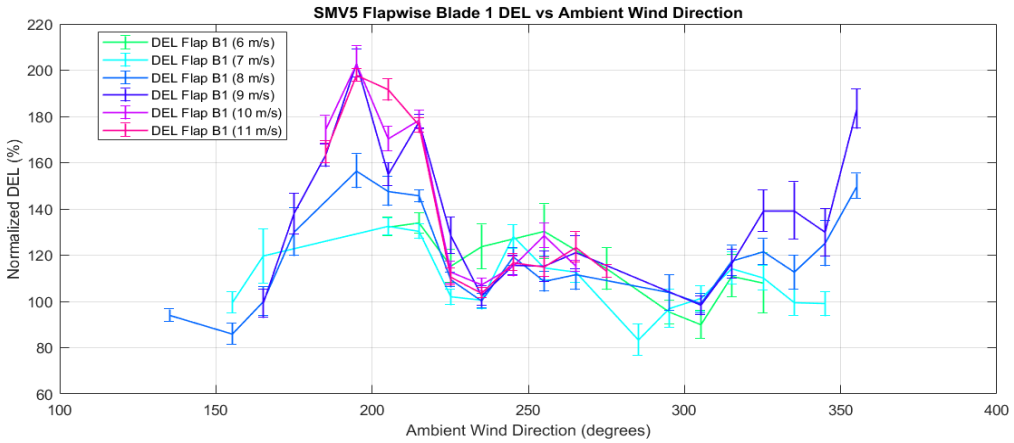

Figure 7.9: Normalized SMV5 blade 1 flapwise DEL of each wind speed as a function of wind direction.

Figure 7.9 displays a clear trend that sees higher wind speeds having a more pronounced relative increase compared to lower wind speeds. The difference is quite impressive; the increase is above the normalized DEL value of 195% at 11 m/s and it decreases quite regularly down to 8 m/s. Then for wind speeds below 8 m/s, the increase is below the normalized DEL value of 160% but for these wind speeds there is scarcity of data at around 200° (where the peak should be) decreasing the reliability of the values. This trend was expected due to the dependence of flapwise loads on thrust and also the dependence of the wake strength on the thrust of SMV6. Since the highest loads (and thrust) in SMV6 are seen between 10 m/s and 11 m/s, the strongest wake is expected to be seen at these wind speeds. As a consequence also the increase in flapwise fatigue is expected to be the highest between 10 m/s and 11 m/s.

7.3.2 Edgewise DEL vs Wind Direction

For the same reason explained in the flapwise DEL wind direction analysis no restrictions on the data have been applied. The flapwise trends and features explained in section 7.3.1 are also seen in the edgewise direction (see Figures 7.10, 7.11 and 7.12). Due to the similarity of these edgewise DEL trends to the flapwise ones, the DEL analysis (in section 7.3.1) previously done for the flapwise DEL is equally valid for the edgewise DEL. The only major difference is that the magnitude of the increased fatigue due to the wake effect is much less, with ranges between 103% and 106%. This is explained by the limited effect that variations in turbulence intensity have on this direction that is mostly dominated by gravitational effects (explained in section 6.2.1).

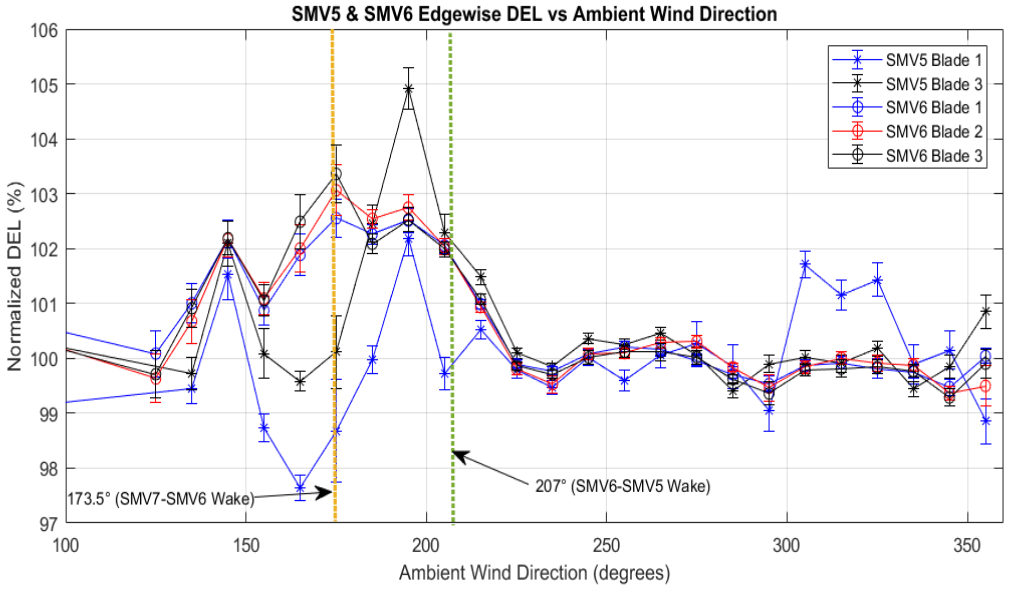

Figure 7.10: SMV5 and SMV6 normalized edgewise loads as a function of ambient wind direction. The error bars represent the 95% confidence interval. The error bars represent the 95% confidence interval.

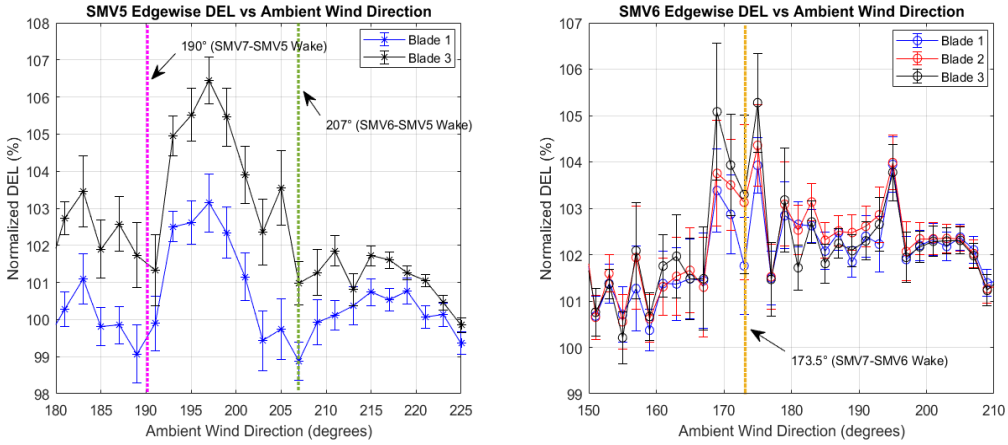

Figure 7.11: SMV5 and SMV6 normalized edgewise loads as a function of wake wind directions. The error bars represent the 95% confidence interval.

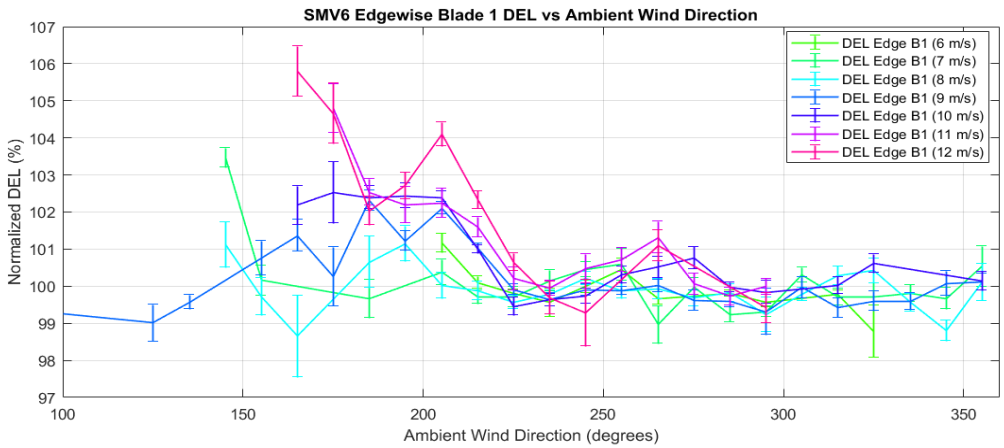

Figure 7.12: Normalized SMV5 blade 1 edgewise DEL of each wind speed as a function of wind direction. The error bars represent the 95% confidence interval.

7.3.3 Flapwise DEL vs Wind Shear

The second atmospheric characteristic analyzed is wind shear. In the wind shear analysis turbulence intensity has been restricted in the range between 7% and 9%; this range, as seen in Figure 7.5, is characterized by low flapwise DEL sensitivity for turbulence intensity. This means that in this specific range it is possible to analyze how fatigue loads vary with respect to wind shear without major influence from turbulence intensity. Wind direction has been restricted to no-wake conditions (between 225° and 320°) to avoid any influence by the wake.

Figure 7.13 shows the flapwise DEL of both turbines (SMV5 SMV6) as a function of wind shear (for the calculation of the wind shear parameter see Appendix B).

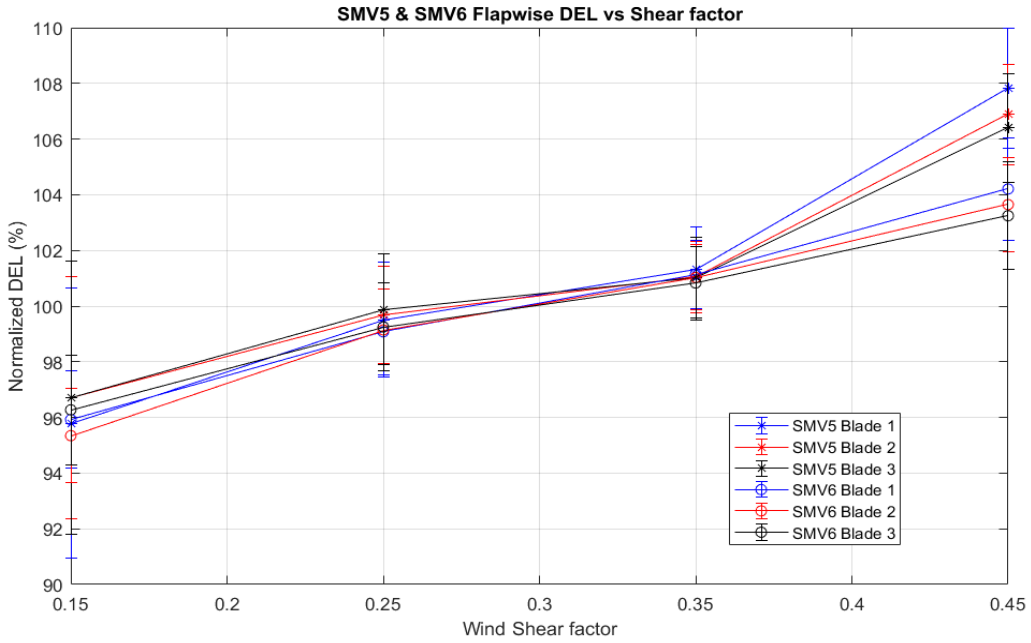

Figure 7.13: SMV5 and SMV6 normalized flapwise DEL as a function of shear factor. The error bars represent the 95% confidence interval.

Both wind turbines share a similar trend that does not show a marked increase in flapwise DEL

as wind shear increases but rather a more slowly growing trend that leads to a slight increase overall in loads; this increase of more than 10% in flapwise DEL is generally consistent for SMV6 while is a slightly lower in SMV5. This trend is expected especially in modern large scale wind turbines where the difference between the mean wind speed between the top and the bottom part of the rotor can be important particularly when atmospheric stability is high (when atmospheric stability is high, stratification of the boundary layer leads to the creation of high wind shear [9]). Variation in loads increases because blades are subjected to higher loads when they are located in the part of the rotor further away from the ground creating cyclical higher loads (once per revolution) that lead to increase fatigue loads as observed in Figure 7.13.

Normalized flapwise DEL loads of the wind turbine SMV6 are observed to be up to ∼4% lower compared to the ones of turbine SMV5 at the wind shear factor of 0.45. This difference is most likely due to the small difference in the DEL sensitivity used in the normalization as seen in Figure 7.5 (SMV5 and SMV6 have been normalized independently).

It can be concluded that the wind shear affects slightly flapwise DEL with a maximum increase of a little more than 10% through the wind shear range available from the data. The edgewise DEL of both turbines (SMV5 and SMV6) as a function of wind shear are not analyzed due to the extremely small sensitivity to changes in wind shear, most likely due to the dominance of gravitational based effect on this direction (for the graphs see Appendix C).

7.3.4 Flapwise DEL vs Turbulence Intensity

The third atmospheric characteristic analyzed is turbulence intensity. In this analysis wind shear has been restricted in the range between 0.25 and 0.45; this range, as seen in Figure 7.5, is characterized by low flapwise DEL sensitivity to wind shear. This means that in this specific range it is possible to analyze how fatigue loads vary with respect to turbulence intensity without the influence (rather small) from wind shear. Wind direction has been restricted to no-wake conditions (between 225° and 320°) to avoid any influence by the wake.

Figure 7.14 shows the flapwise DEL of both turbines (SMV5 and SMV6) as a function of turbulence intensity (estimated at hub height by the Windcube V2 as the 10 min standard deviation of the wind speed divided by the mean wind speed; it needs to be also noted that generally lidar measurement of turbulence intensity is not the most reliable).

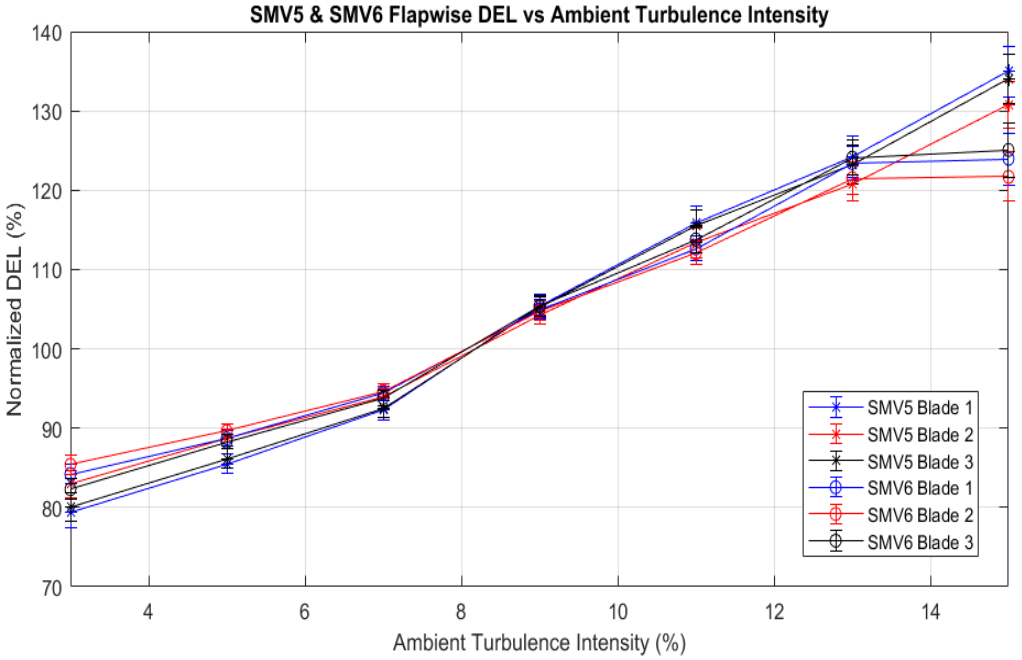

Figure 7.14: SMV5 and SMV6 normalized flapwise DEL as a function of turbulence intensity. The error bars represent the 95% confidence interval.

A marked increase in flapwise DEL as turbulence intensity increases is seen consistently in all the 6 blades of the two wind turbines. This increase is maximum in the case of SMV5 blade 1 with an increase from 79% to 135% (of normalized DEL) from 3% to 13% turbulence intensity. This trend is expected because, as explained in section 2.2.5, turbulence is referred to random fluctuations of the air flow (called gusts) that significantly increase or decrease the mean wind speed for periods up to 20 seconds; since loads (especially in the flapwise direction) are strongly dependent on wind speed (thrust), the fluctuations in wind speed correspond also in loads fluctuations leading to increased fatigue loads [9].

As in the analysis of wind shear, normalized flapwise DEL loads of the wind turbine SMV5 are observed to be up to 10% lower at 15% turbulence intensity compare to the ones of turbine SMV6. This difference is most likely due to the small difference in the DEL sensitivity used in the normalization as seen in Figure 7.5 (SMV5 and SMV6 have been normalized independently).

It can be concluded the turbulence intensity affects strongly flapwise DEL with a maximum increase of slightly more than 56% through the turbulence range available from the data. The edgewise DEL of both turbines (SMV5 and SMV6) as a function of turbulence intensity is not analyzed due to the extremely small sensitivity to changes in turbulence intensity, most likely due to the dominance of gravitational based effect on this direction (for the graphs see Appendix C).

7.4 Summary

The loads analysis under normal operation mainly confirmed that, for the same ambient wind speed, loads are significantly lower inside the wake due to the presence of the wind speed deficit in this region. This trend is seen in both the flapwise and the edgewise loads directions.

The dependency of fatigue with respect of the atmospheric conditions showed significant increases in the fatigue loads inside the wake sector up to 60-70% more for single wake and ∼90% for double wake compared to the sector with no-wake. This is due to the increased turbulence intensity present in the wake region. This analysis also showed a significant sensitivity of fatigue loads with respect to turbulence intensity. On the other end much smaller sensitivity with respect to wind shear has been observed. These trends are seen in both the flapwise and the edgewise loads directions; the only the difference is that the

magnitude of the increased fatigue due to the wake effect is much less in the edgewise direction. This is explained by the limited effect that variations in turbulence intensity have on this direction that is mostly dominated by gravitational effects.

8 Loads and Fatigue Analysis Under Curtailment Strategy

This chapter analyzes in dept the effects of a curtailment strategy on the loads and fatigue of both the upstream (SMV6) and the downstream (SMV5) turbines. The availability of the data used (collected during the second measurement campaign) is assessed and then the curtailment strategy applied is discussed in details. The results obtained from the curtailment strategy, on both turbines, are compared to the ones with similar inflow conditions during normal operation in order to have a trustfully comparison.

8.1 Curtailment Strategy Applied in the Second Field Test

During the second field campaign, the curtailment strategy has been applied on the upstream turbine (SMV6). Unlike the usual approach where nominal power is derated by a certain percentage, in this field test a predefined curtailed power curve has been used; this curtailment curve is generally used for limiting the turbine noise and is called the Senvion MM82 SMII type B power curve. This power curve is shown in Figure 8.1 along with the normal operation Senvion MM82 power curve and the curtailed power curve applied.

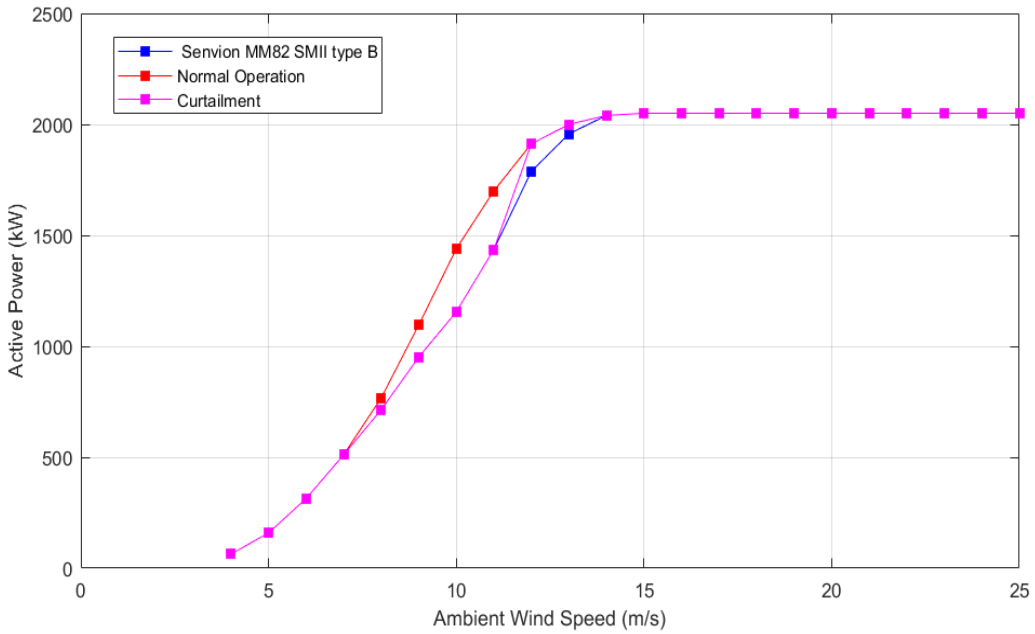

Figure 8.1: Normal operation, Senvion MM82 power curve and curtailment strategy power curves implemented in the second campaign.

Wind Speed [m/s]	Difference between Normal Operation Power and the Senvion MM82 SMII type B power [%]	Difference between Normal Operation Power and Curtailment Power [%]
8	-7.2%	-7.2%
9	-14.2%	-14.2%
10	-21.9%	-21.9%
11	-16.8%	-16.8%
12	-6.7%	-0%
13	-2.2%	-0%

Table 8.1: Difference between normal operation and curtailment strategy active power curves. Power values not shown for confidentiality reasons.

In the Senvion MM82 SMII type B power curve curtailment starts at 7 m/s and ends at 14 m/s with a maximum planned power reduction of more than 20% seen at 10 m/s (Table 8.1). However in the second field test curtailment was applied up to 11 m/s. For wind speeds higher than 11 m/s, normal operation power curve was used. This curtailment is considered not significant because the power is curtailed by a maximum of 22% before rated power while usually rated power is included in the decrease. As a consequence the observations of the impact on both the upstream and downstream turbines are expected to be quite difficult due to the small curtailment implemented.

In order to make the curtailment as automated as possible, the curtailed power curve have been implemented in the wind turbine control system so that it could be activated automatically through the wind turbine sensors. During the curtailment period, the derating has been activated and deactivated every hour between 10pm and 5am as seen in Figure 8.2.

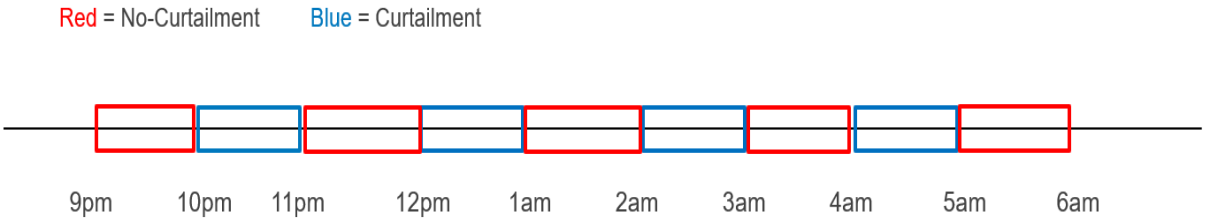

Figure 8.2: Representation of the curtailment strategy night activation

This was done to compare the effect of the control strategy with the same atmospheric conditions as for the normal operation case, and thus be able to quantify the changes with an improved accuracy. The choice of winter period during the night time was to limit changes in stability and thus in atmospheric conditions. This approach has been used also in [34]. However, even inside the hours where curtailment was activated, it was effectively implemented only when the ambient wind direction was between 180° and 230° (wake sector SMV5 caused by SM6) and when the wind speed was between 5 m/s and 11 m/s (wind speed range where curtailment strategy was expected to be effective [35]).

8.2 Data Availability

The data availability of all the sensors during the application of the second field measurement campaign curtailment strategy (14 December 2017 - 9 February 2018) is shown in Figure 8.3.

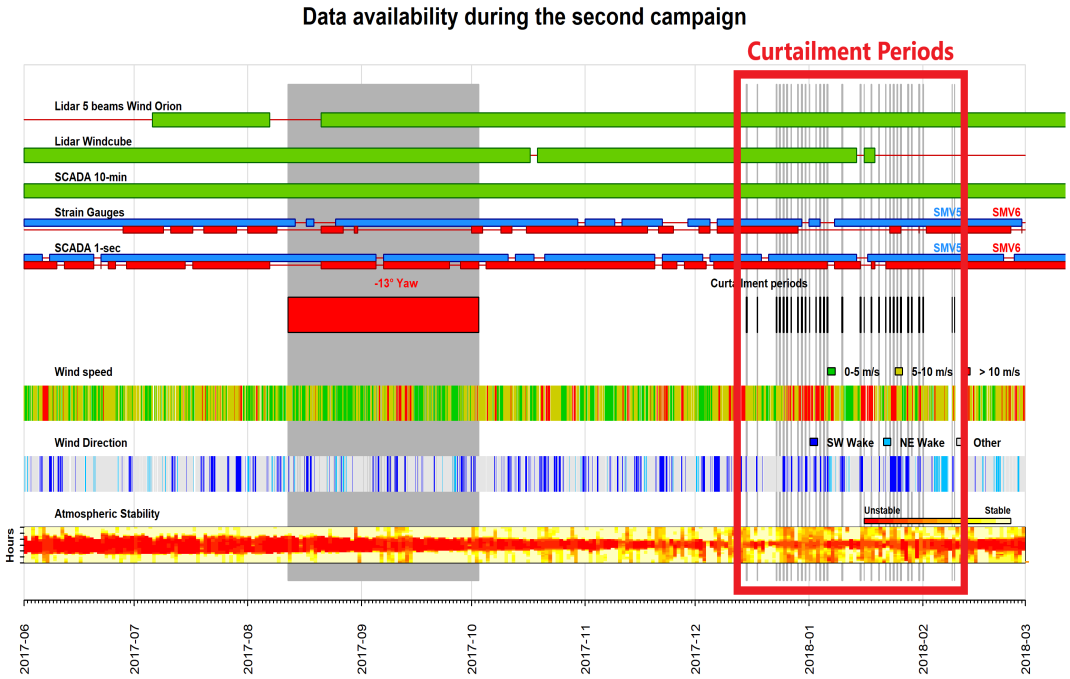

Figure 8.3: Data availability and atmospheric conditions during the second field campaign. Figure created by ENGIE Green.

Curtailment periods correspond to the grey vertical lines inside the red box. Figure 8.3 shows the availability of the main sensors used to asses atmospheric conditions, loads and fatigue; Windcube V2 stopped working in the last period, unfortunately lowering the amount of data available; it can also be noticed that the strain gauges of SMV6 stopped working for a prolonged period of time throughout January. These two major losses of valuable data, combined with the activation of the curtailment strategy only with specific atmospheric conditions (discussed later), restricted the activated curtailment data of 63h to only 9h used in the upstream turbine (SMV5) analysis and to only 9.5h used in the downstream turbine (SMV6) analysis. Due to the different sensor availability in the two turbines, only 4h of curtailment measurement period is available when the sensors of both turbines are working simultaneously as it can be seen in Figure 8.4.

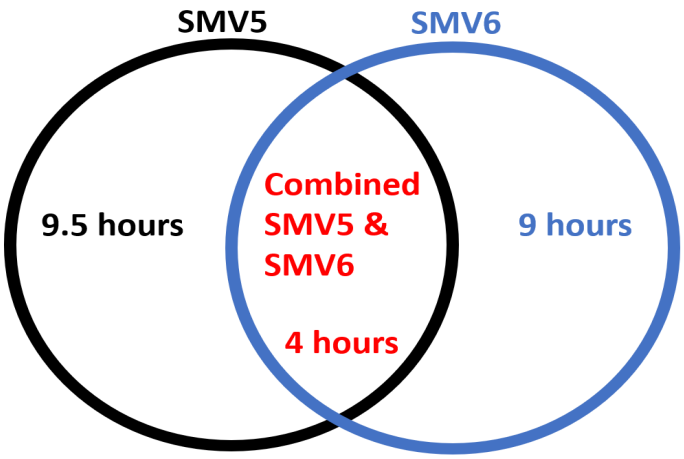

Figure 8.4: SMV5 and SMV6 data availability after filtering

8.3 Normal Operation Period Selection

In order to truly assess the impact of this curtailment strategy on loads and fatigue compared to normal operation, the inflow conditions of the normal operation periods used as comparison need to be as close as possible to the inflow conditions of the curtailment strategy periods. This is due to the sensitivity of loads and fatigue with respect to atmospheric conditions like wind speed, turbulence intensity and wind shear shown in section 7.3. For the curtailment strategy two different methods of selecting normal operation periods have been used:

- the first method (called normal operation method 1) applied also in [34] to ensure the consistency in inflow conditions, uses the no-curtailment periods (corresponding to the red squares in Figure 8.2) between curtailment periods (corresponding to the blue squares in Figure 8.2) making the very reasonable assumption that the atmospheric conditions on average would not change much in the range of an hour during night time (measured period between December 2017 and February 2018). This assumption is reasonable with a large amount of data, however after taking only the no-curtailment periods previous and subsequent the valid curtailment periods, only 14.6h of normal operation (no-curtailment) have been available.
- the second method (called normal operation method 2) was developed for this thesis and aimed to find for each curtailment period available (a total of 57 10-min averages for SMV5 and 54 10-min averages for SMV6), periods inside the full normal operation span (October 2017-December 2017) that have similar atmospheric conditions. The filters applied to select the periods with similar inflow conditions are the following:

  1. Average wind speed: $\pm$ standard deviation (wind speed) divided by 2;
  2. Average wind direction: $\pm 10°$;
  3. Average turbulence intensity: $\pm 1\%$;
  4. Average wind shear parameter: ± 0.1;

  Beside turbulence intensity, that was the most influential filter, these filters have been selected considering data availability; a compromise had to be found between having a good data availability and the selectivity of the inflow conditions. This method increases the data availability of normal operation to 58.2h for SMV5 and to 51.5h for SMV6.

The two methods will be analyzed and the results will be compared. In theory both methods should provide normal operation periods with very similar inflow conditions to the curtailment periods; however the second method normal operation periods are from fall season while the first method normal operation periods are from winter season, so moderate differences in the distributions are expected due to changes in stability, air pressure and temperature (air density). Very similar inflow conditions would have been expected between the downstream turbine SMV5 and the upstream turbine SMV6, though Figure 8.4 shows that only 4h of curtailment measurements are available with all the sensor working for both turbines. This rises the possibility of differences in the atmospheric conditions between the curtailment periods of the two turbines and due to the low data availability, it has been chosen to use all the curtailment periods available in each turbine. This should not affect the trends since the comparison and the analysis of loads and fatigue is made for each single turbine independently. In this chapter loads have not been normalized due to simplicity and also because the loads are plotted as a function of wind speed eliminating the effect of different wind speeds (affecting thrust) plotted together.

8.4 Upstream Wind Turbine SMV6

In this section loads and fatigue are analyzed for the upstream turbine SMV6; data from the curtailed period will be compared with the ones selected using both the normal operation method 1 and method 2 explained in the section 8.3. As previously stated, in order to have comparable data, the inflow conditions of the data compared need to be similar; as a consequence the analysis starts with an assessment of the inflow conditions followed by loads fatigue analysis. Due to the consistency in the results of all the 3 blades of each turbine, only blade 1 of both turbines is shown.

Figure 8.5 and Figure 8.6 represent respectively the ambient turbulence intensity and the wind shear parameter as a function of ambient wind speed (taken from Windcube V2) for SMV6 selected periods.

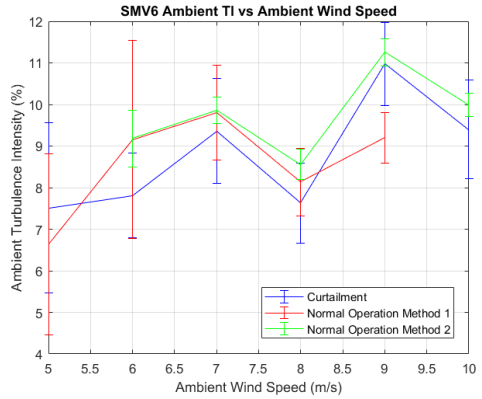

Figure 8.5: Ambient turbulence intensity as a function of ambient wind speed. The error bars represent the 95% confidence interval.

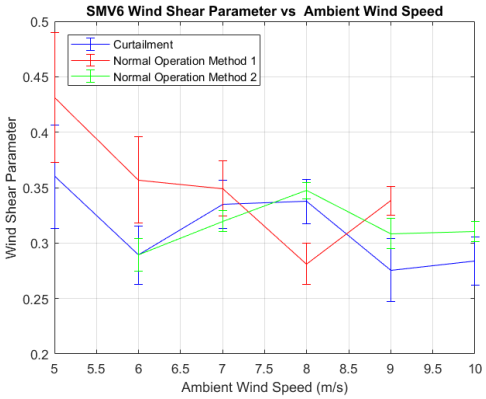

Figure 8.6: Wind shear parameter as a function of ambient wind speed. The error bars represent the 95% confidence interval.

The values between the 3 data sets do not present any major differences that could have majorly affected loads and fatigue loads analysis beside a slightly lower turbulence intensity at 9 m/s in the normal operation method 1 period. The curtailment period has generally lower values however, the sizes of the error bars show a large dispersion and underlie the low amount of data available. A bigger difference in wind shear is seen between the normal operation method 1 period and the other 2 periods; this difference is not very significant especially because of the lower sensitivity of fatigue to this parameter. Generally, consistent inflow conditions for a reliable analysis are observed in the curtailment period in the normal operation method 1 period and in the normal operation method 2 period.

After the inflow conditions have been analyzed, edgewise and flapwise loads are plotted and studied. Figure 8.7 and Figure 8.8 represent respectively the flapwise blade loads and the edgewise blade loads as a function of ambient wind speed (taken from Windcube V2) for SMV6 selected periods.

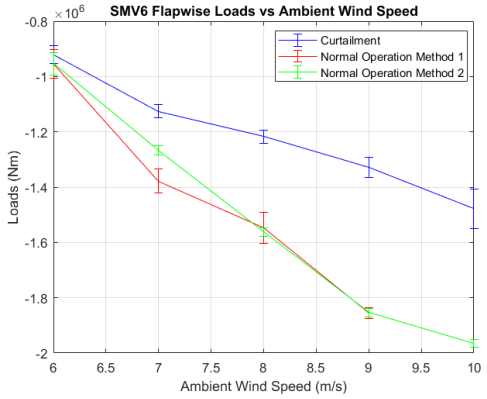

Figure 8.7: Flapwise loads as a function of ambient wind speed. The error bars represent the 95% confidence interval.

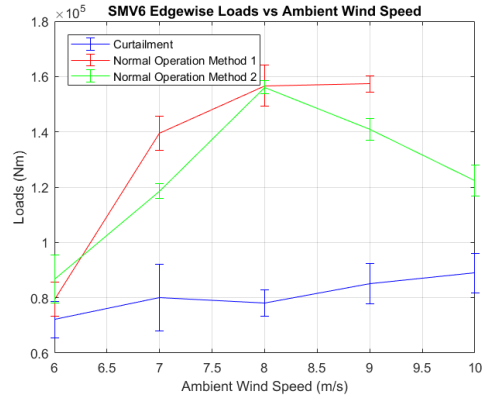

Figure 8.8: Edgewise loads as a function of ambient wind speed. The error bars represent the 95% confidence interval.

Both the flapwise and edgewise loads show that loads of the curtailment period are significantly lower compared to the ones of the normal operation periods. Normal operation method 1 and 2 periods have almost matching levels of loads. The decrease in loads is expected because curtailing the power of wind turbine SMV6, implies a decrease in the thrust coefficient and so in the thrust force acting on the rotor

(see Figure 8.9). Reductions in thrust are also generally related to reductions in wind turbine blade loads and tower moments [29].

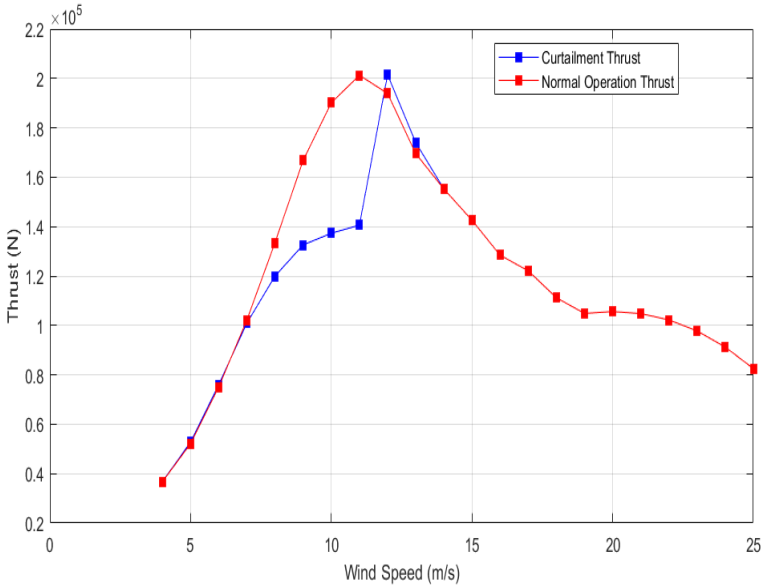

Figure 8.9: Normal operation and curtailment strategy thrust curves implemented in the second campaign. The C_t used has been given by the manufacturer.

Wind Speed [m/s]	Expected Difference in Thrust [%]	Difference in Flapwise Blade Loads (method 1) [%]	Difference in Flapwise Blade Loads (method 2) [%]	Difference in Edgewise Blade Loads (method 1) [%]	Difference in Edgewise Blade Loads (method 2) [%]
6	-1%	-4%	-4%	-10%	-19%
7	-1%	-20%	-12%	-54%	-39%
8	-11%	-24%	-25%	-67%	-67%
9	-23%	-33%	-33%	-59%	-49%
10	-32%	–	-28%	–	-31%

Table 8.2: Difference between normal operation periods and curtailment strategy period thrust and loads (the C_t used has been given by the manufacturer).

Table 8.2 represents the changes in the expected thrust, flapwise and edgewise loads when curtailment strategy is applied. Since thrust is the main force acting on the flapwise direction of the blades, the changes in loads (especially in the flapwise direction) are generally expected to follow the changes in thrust. This general trend is observed, however it seems that there is a shift down in the percentages difference between the expected thrust and the flapwise loads of both methods. This shift might be caused by an earlier effective implementation of the curtailment strategy in the field data due to the presence of turbulence or due to the presence of some hysteresis effects; this idea is confirmed by the differences in rotor speeds and in pitch angles that start to be significant at 7 m/s as seen in Figure 8.10 and 8.11. Also the smaller decrease in loads at 10 m/s is explained by the differences in rotor speed and in pitch angle; at this speed, normal operation periods reached rated rotor speed while the rotor speed in the curtailment period is still increasing (due to the early pitching): this decreases the difference with respect to 9 m/s. Another reason could be that SMV6 is partially in the wake of SMV7 when the curtailment sector starts (at 180°) so the perceived wind from this sector could be lower.

Decrease in thrust was not expected to have major influences on the edgewise loads however this direction saw the largest decreases in loads. This is most likely due to the large decrease in the rotor speed.

It can be concluded that loads on the curtailed turbine show a significant decrease in both the flapwise direction, with a maximum decrease of 33% (at 9 m/s) compared to both normal operation methods, and in the edgewise direction, with a decrease of 67% (at 8 m/s) compared to both normal operation methods. It can also be said that theoretical thrust differences between curtailment and normal operation periods are quite an accurate indication of loads variation but they do not take into account the possibility of early activation of the curtailment strategy due to turbulence.

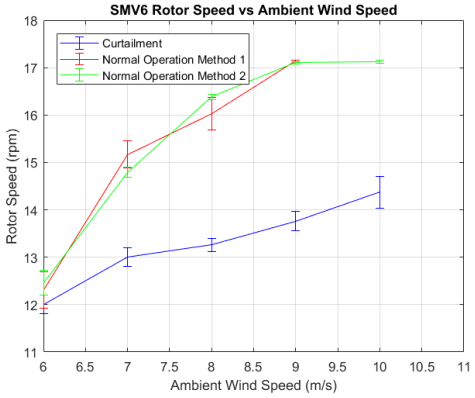

Figure 8.10: Rotor speed as a function of wind speed. The error bars represent the 95% confidence interval.

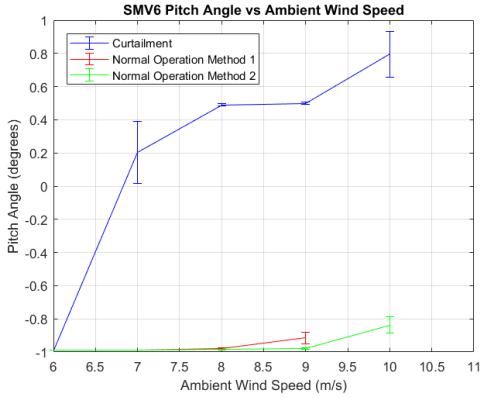

Figure 8.11: Pitch angle as a function of wind speed. The error bars represent the 95% confidence interval.

Figure 8.12 and Figure 8.13 represent respectively the flapwise blade fatigue loads and the edgewise blade fatigue loads as a function of ambient wind speed (taken from Windcube V2) for SMV6 selected periods.

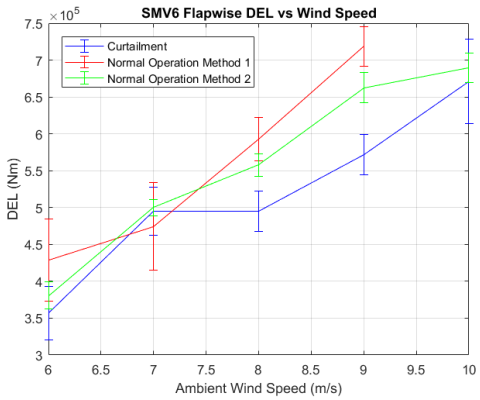

Figure 8.12: Flapwise fatigue loads as a function of ambient wind speed. The error bars represent the 95% confidence interval.

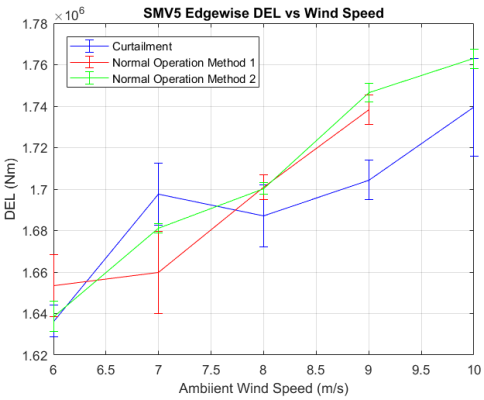

Figure 8.13: Edgewise loads as a function of ambient wind speed. The error bars represent the 95% confidence interval.

Wind Speed [m/s]	Difference in Flapwise Blade DEL (method 1) [%]	Difference in Flapwise Blade DEL (method 2) [%]	Difference in Edgewise Blade DEL (method 1) [%]	Difference in Edgewise Blade DEL (method 2) [%]
6	-18%	-6%	-1%	-0%
7	+4%	-1%	+2%	+1%
8	-18%	-12%	-1%	-1%
9	-22%	-14%	-2%	-2%
10	–	-3%	–	-1%

Table 8.3: Difference between normal operation periods and curtailment strategy period fatigue loads.

Fatigue equivalent loads (DEL) of a wind turbine come from the variation of the loads in time so, due to similar inflow conditions, lower loads are expected to lead to lower fatigue. Flapwise DEL under the curtailment period have similar values compared to the normal operation method 1 and 2 periods up to 7 m/s; after this wind speed, DEL under curtailment operations decrease significantly compared to the other 2 periods. A similar trend is observed in the edgewise direction but with decreases much less significant. At 7 m/s curtailment period DEL show a sudden jump that increases the DEL up to normal operation periods level if not higher in the edgewise direction. This increase in fatigue loads can be explained by looking at Figure 8.11; here it can be seen that this wind speed corresponds to the highest increase in pitch angle during the curtailment period. This large change in pitch angle might induce significant vibration to the blade increasing fatigue loads significantly. After this wind speeds, significant lower flapwise fatigue loads are observed during the curtailment period with a maximum decrease of 22% (9 m/s) compared to normal operation method 1 period and of 14% (9 m/s) compared to normal operation method 2 period. Fatigue loads on the edgewise direction decrease much less during the curtailment period; this is probably caused by similar loads variations due to gravitational effects between normal operation periods and curtailment period even though loads are lower in the curtailment period.

It can be concluded that fatigue loads on the curtailed turbine show a significant decrease in the flapwise direction, with a maximum decrease between 14% and 22% (9 m/s) depending on which normal operation period is used for comparison. In the edgewise direction a much smaller maximum decrease of 2% (9 m/s) is observed on the curtailment period compared to both normal operation method periods.

8.5 Downstream Wind Turbine SMV5

In this section loads and fatigue are analyzed for the downstream turbine SMV5; data from the curtailed period will be compared with the ones selected using both the normal operation method 1 and method 2 explained in the previous section. As previously stated, in order to have comparable data, the inflow conditions of the data compared need to be similar; as a consequence the analysis starts with an assessment of the inflow conditions followed by loads fatigue analysis. Due to the consistency in the results of all the 3 blades of each turbine, only blade 1 of both turbines is shown.

Figure 8.14 and Figure 8.15 represent respectively the ambient turbulence intensity and the wind shear parameter as a function of ambient wind speed (taken from Windcube V2) for SMV5 selected periods.

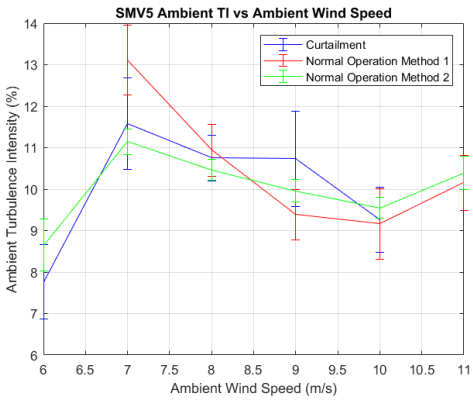

Figure 8.14: Ambient turbulence intensity as a function of ambient wind speed. The error bars represent the 95% confidence interval.

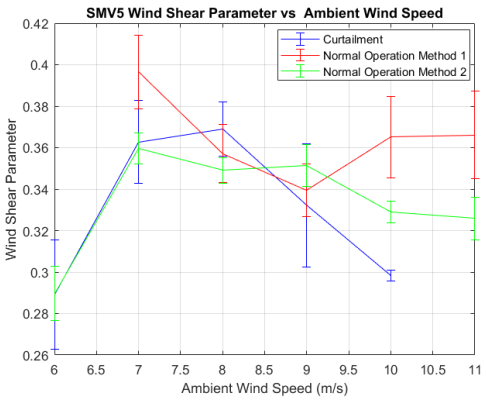

Figure 8.15: Wind shear parameter as a function of ambient wind speed. The error bars represent the 95% confidence interval.

The ambient turbulence intensity in all the 3 data set shows a similar trend where lower wind speeds are more likely to have higher turbulence whereas higher wind speeds tend to have lower turbulence. This trend is due mainly to the definition of turbulence intensity (as the wind speed at the denominator becomes bigger, turbulence intensity decreases). The values of turbulence are very similar between the 3 data sets with error bars (95% confidence interval) overlapping everywhere beside at 7 m/s; here the turbulence intensity of the normal operation method 1 period is higher compared to the normal operation method 2 period. Wind shear also behaves very similarly to turbulence intensity with very similar trends and values. A bigger difference in wind shear is found at 10 m/s where none of the error bars are overlapping.

Generally, consistent inflow conditions for a reliable analysis are observed in the curtailment period, normal operation method 1 period and normal operation method 2 period. The presence of higher wind shear at 10 m/s for the normal operation method 1 period will not be taken into consideration since the differences in the wind shear are not considered too relevant due to the lower sensitivity of fatigue to this parameter. These graphs also show that the assumption done for the method 1 (atmospheric conditions on average would not change much in the range of an hour during night time) is not reliable with low amount of data for these two parameters.

Figure 8.16 shows the local turbulence intensity as a function of the ambient wind speed (taken from the SCADA system of SMV5) for SMV5 selected periods.

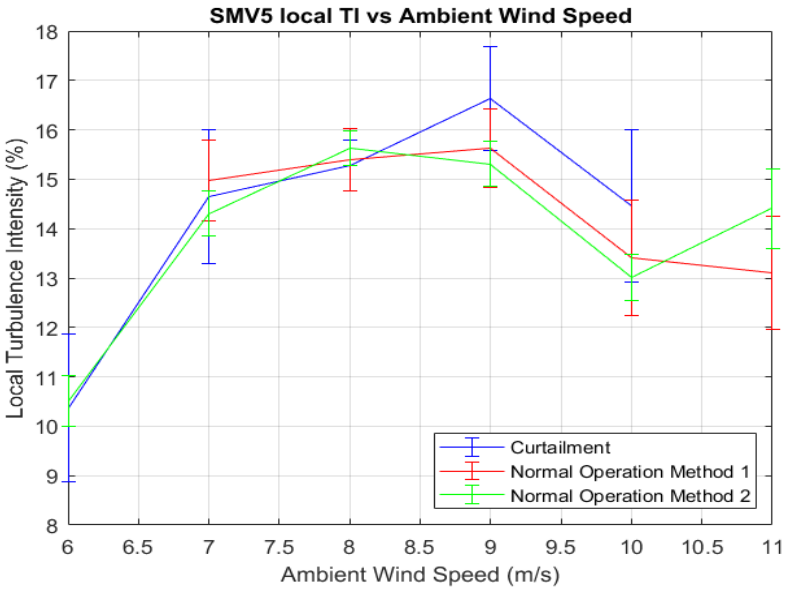

Figure 8.16: Turbulence intensity as a function of wind speed. The error bars represent the 95% confidence interval.

The perceived turbulence intensity is expected to be generally higher, compared to the ambient turbulence intensity, due to the position of the SCADA system right inside the wake of SMV6. Turbulence intensity in the curtailment period was expected to be lower compared to normal operation methods due to the reduced thrust impressed by the curtailed SMV6 turbine on the flow of air reducing the strength of turbulence intensity; however no major decrease is seen in the curtailment period having values close to the other 2 periods; at 9 m/s and 10 m/s turbulence intensity from the curtailment period is slightly higher than the normal operation methods but still with overlapping error bars showing the significant spread of the data.

After the inflow conditions have been analyzed, edgewise and flapwise loads are plotted and studied. Figure 8.17 and Figure 8.18 represent respectively the flapwise blade loads and the edgewise blade loads as a function of ambient wind speed (taken from Windcube V2) for SMV5 selected periods.

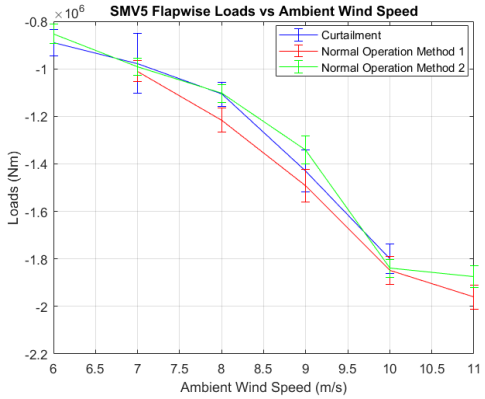

Figure 8.17: Flapwise loads as a function of ambient wind speed. The error bars represent the 95% confidence interval.

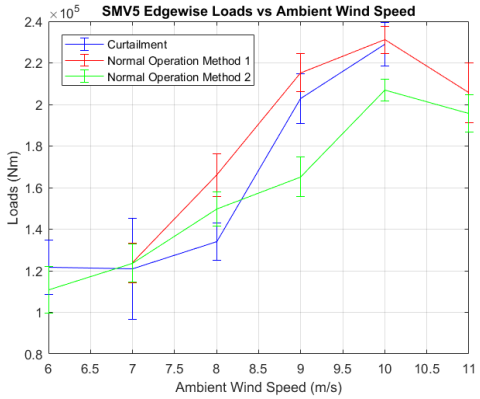

Figure 8.18: Edgewise loads as a function of ambient wind speed. The error bars represent the 95% confidence interval.

Flapwise loads are expected to be generally higher for the curtailment period compared to the normal operation methods due to the theoretical wind deficit reduction [17]; Figure 8.17 shows matching flapwise loads levels between the curtailment period and the normal operation method 2 period, while

normal operation method 1 period has slightly higher flapwise loads. Slightly higher edgewise loads are also observed for the normal operation method 1 period. In theory the loads of the 2 normal operation methods should be very similar; this difference is most likely due to the different seasons of the data that influence other factors (rather than turbulence intensity and wind shear) like stability, air density and temperature. It is needed to keep also in mind that the lower availability of data in both the curtailment and normal operation method 1 period increases their level of uncertainty.

It can be concluded that no major reductions have been observed between loads (flapwise and edgewise) of the curtailment period and the normal operation method 2; reductions up to 9% (8 m/s) in the flapwise direction have been observed between the curtailment period and the normal operation method 2 period. This could be due to a too small change in the wind speed deficit caused by the weak curtailment. However the limited amount of data available and the inconsistency in the 2 normal operation periods results show that uncertainty is high; the difference between the 2 normal operation period results can be considered as the uncertainty of the normal operation periods.

Figure 8.19 and Figure 8.20 represent respectively the flapwise blade fatigue loads and the edgewise blade fatigue loads as a function of ambient wind speed (taken from Windcube V2) for SMV5 selected periods.

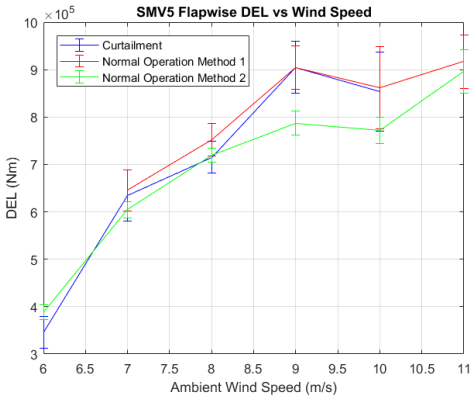

Figure 8.19: Flapwise fatigue loads as a function of ambient wind speed. The error bars represent the 95% confidence interval.

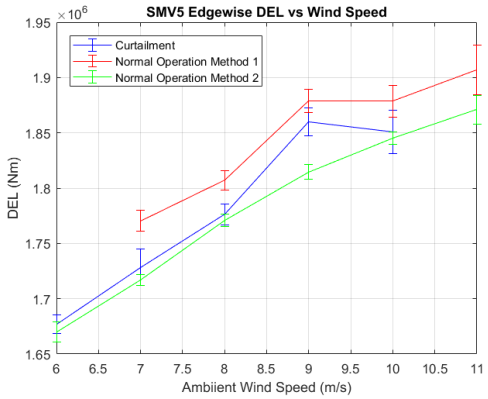

Figure 8.20: Edgewise fatigue loads as a function of ambient wind speed. The error bars represent the 95% confidence interval.

Figure 8.19 shows that flapwise DEL have very similar values between the curtailment period and the normal operation method 1 period while the normal operation method 2 period flapwise DEL have similar values up to 8 m/s; after this point normal operation method 2 period flapwise DEL are consistently lower (up to 14% at 9 m/s) than those of the other 2 periods. Figure 8.20 shows that edgewise DEL have very similar values between all 3 the periods; normal operation method 1 period has marginally higher edgewise DEL in the range of 1%. Interestingly both graphs underline a general higher similarity between the trends of the curtailment period and the normal operation method 1 period (where data have been collected on close temporal proximity). This result could mean that normal operation method 1 is able to match all the inflow conditions (not only wind shear and TI) more precisely compared to method 2; indeed filters used in method 2 did not take into account atmospheric stability and other parameters that change seasonally and that most likely affects these results. However due to the uncertainty no conclusions on the performance of these two methods can be drawn.

It can be concluded that no major reductions have been observed between fatigue loads of the curtailment period and the normal operation periods, most likely due to a too small change in the wind speed deficit and turbulence intensity caused by the weak curtailment. Like in the load analysis, also the fatigue loads inconsistency in the 2 normal operation period results shows that uncertainty is high; the difference between the 2 normal operation periods results can be considered as the uncertainty of the normal operation periods.

8.6 Summary and Discussion

The performance of the curtailment strategy on the reduction of loads and fatigue loads between an upstream wind turbine (SMV6) and a downstream wind turbine has been examined in this chapter. The data used in this analysis have been taken from the second campaign of field tests in the SMARTEOLE project.

The analysis made on the downstream turbine SMV5 showed no significant reductions in either loads or fatigue loads. This can be explained by the possible mixing of two distinctive phenomena that are taking place in the wake of the upwind turbine SMV6 and that have effect on fatigue loads. The implementation of the curtailment strategy decreases the velocity deficit in the wake with consequent increase in loads and fatigue but, at the same time, reduces turbulence intensity (decreases loads and fatigue). It is not known which of these effects is predominant but, for small inter-spacing distances, the decreased wind deficit has the highest relevance [17]; indeed no major decrease in wake-added turbulence intensity could be measured. This explains why loads and fatigue do not vary significantly in both edgewise and flapwise direction. Also the quite large loads and fatigue difference between the normal operation method 1 and 2 periods underlines the uncertainty in the measurements for SMV5 since in theory they should be matching.

On the other end, the analysis made on the upstream turbine SMV6 showed a significant decrease in the flapwise direction loads (maximum decrease of 33% at 9m/s) and fatigue (maximum decrease of 22% at 9m/s); the edgewise direction also saw a decrease in loads (maximum decrease of 67% at 8m/s) and in fatigue (maximum decrease of 2% at 9m/s). The reductions are due to the implementation of the curtailment strategy that, by increasing pitch angle and decreasing the rotor speed and the thrust force acting on the rotor, reduces loads and fatigue.

The two methods of selecting normal operation periods with similar inflow conditions to the curtailment period, gave similar results in both loads and fatigue of the upstream turbine SMV6. On the other end, loads and fatigue results in the downstream turbine SMV5 were less consistent and with a high degree of uncertainty. This is likely due to the more variable inflow conditions (due to the presence of the wake) and also to the different seasons in which the measurements were taken that could have changed the way the wake behaves. Logically a longer period of measurements would be ideal and could have canceled out these differences in seasons but, if not possible, a shorter temporal average of the data (lower than 10-min averages) could be helpful to increase the data availability and to more precisely characterize the inflow conditions.

The curtailment strategy has shown a good potential in the reduction of loads and fatigue in both the flapwise and edgewise direction of the upstream turbine. However no major benefits on the downstream turbine in terms of loads and fatigue reduction have been observed with enough certainty. It has been shown in [35] that, with the implementation of a power production optimization process made on the curtailment strategy, the combined power can be expected to increase up to 2%. The sum of increased combined power and decreased blade loads on the upstream turbine make this strategy still promising.

For this strategy only blade loads and fatigue have been analyzed because they are the major source of loads that are then distributed throughout the whole turbine. However, the changes in the drive-train and tower loads and fatigue may still be quite different and could change the potential benefits of this strategy.

After the analysis of the whole wake sector (from 180° to 230°), a more selective analysis regarding the full wake sector (from 195° to 215°) was attempted in order to see clearer trends caused by the curtailment strategy in the sector where the wake effects are the highest. Unfortunately due to the low amount of data especially in the curtailment strategy period, it was impossible to obtain reliable trends.

9 Loads and Fatigue Analysis Under Yaw-Control Strategy

This chapter analyzes in dept the effects of a yaw-control strategy on the loads and fatigue of both the upstream (SMV6) and the downstream (SMV5) turbines. The availability of the data used (collected during the second measurement campaign) is assessed and then the curtailment strategy applied is discussed in details. The results obtained from the yaw-control strategy, on both turbines, are compared to the ones observed with similar inflow conditions during normal operation in order to have a trustfully comparison.

9.1 Yaw-control Strategy Applied in the Second Field Test

During the second field campaign, the yaw-control strategy has been applied on the upstream turbine (SMV6). The wind turbine has been unintentionally misaligned, this because the support on which is fixed the wind vane has been involuntarily moved during a maintenance operation creating a yaw-error for the wind turbine. The value of the yaw-angle applied on the upstream turbine SMV6 has been estimated approximately by comparing the SCADA sensor yaw-position data with the Windcube V2 wind direction at hub height. During the second measurement campaign a mean yaw-offset of -13° is observed. The convention used in this chapter is opposite to the one used in [20] and showed in Figure 2.7: a positive value for the yaw-angle means that the wind turbine is leading the wind (the value of the nacelle position is higher than the value of the wind direction) while a negative value for the yaw-angle means that the wind turbine is lagging the wind (the value of the nacelle position is lower than the value of the wind direction).

9.2 Data Availability

The data availability of all the sensors during the application of the second field measurement campaign yaw-control strategy (13 August 2017 - 3 October 2017) is shown in Figure 9.1.

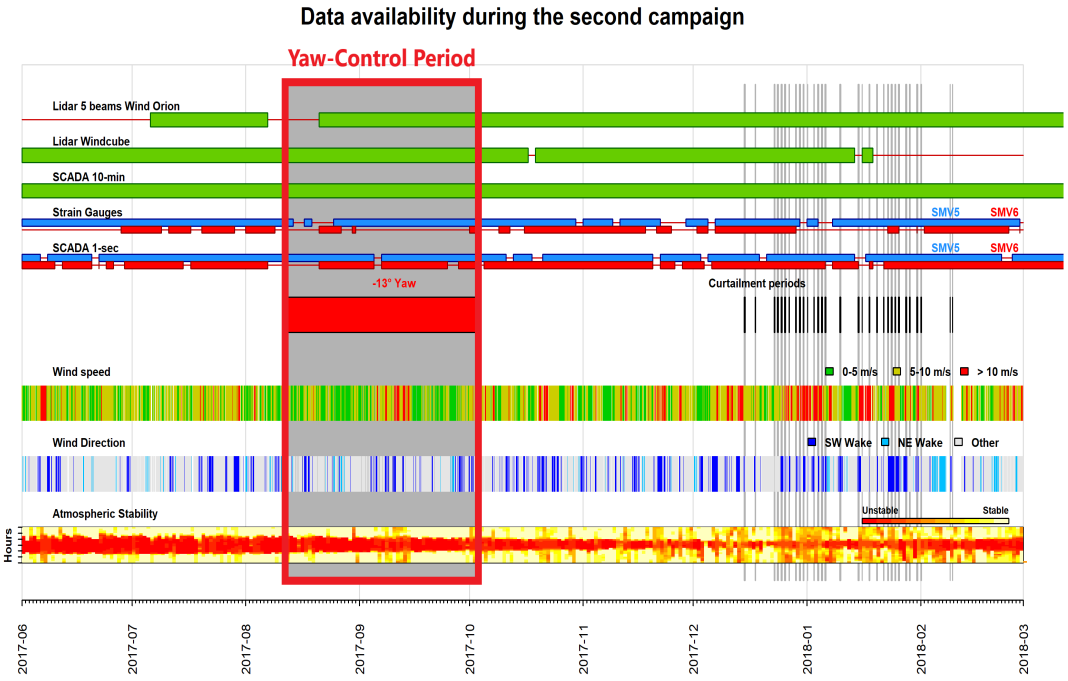

Figure 9.1: Data availability and atmospheric conditions during the second field campaign. Figure created by ENGIE Green.

The yaw-control period corresponds to the grey section inside the red box. Figure 9.1 shows the

availability of the main sensors used to asses atmospheric conditions, loads and fatigue. It can be noticed the lack of data available in the SMV6 strain gauges due to malfunctioning causing major losses of valuable data. All the other sensors have good data availability inside the yaw-control period. Since the yaw-error persisted at all wind atmospheric conditions, the upstream turbine had 34.5h of data available (out of 51.3h) while the downstream turbine had only 19.7h of data available (out of 58.8h), because only the wind directions subjected to the upstream turbine wake are of interest (between 180° and 230°). In Figure 9.2 the yaw-offset angle is shown as a function of wind speed for the 34.5h SMV6 available data. The yaw-offset angle has an average of -12.4° and it is observed to be consistent after 5 m/s so wind speeds below this mark will not be considered. This brings the average offset angle to -13°.

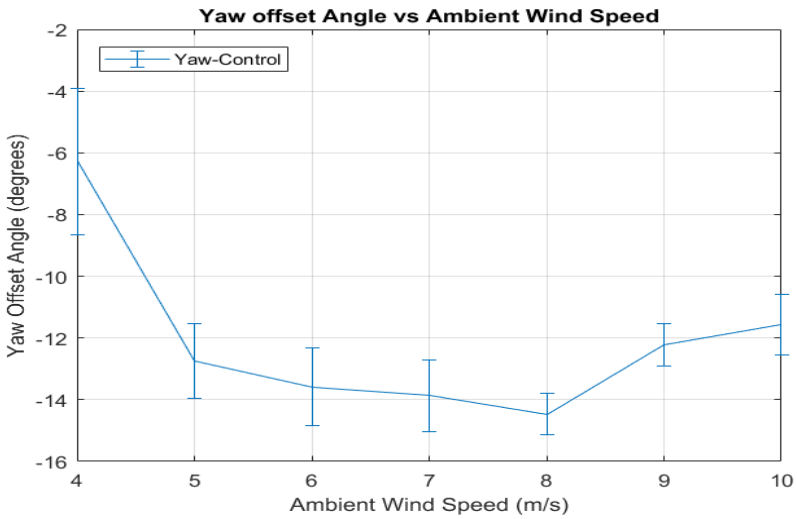

Figure 9.2: SMV6 yaw-offset angle as a function of ambient wind speed. The error bars represent the 95% confidence interval.

9.3 Normal Operation Period Selection

In order to truly asses the impact of this yaw-control strategy on loads and fatigue compared to normal operation, the inflow conditions of the normal operation period, as in the curtailment strategy, need to be as close as possible to the inflow conditions of the curtailment strategy period. This is due to the sensitivity of loads and fatigue with respect to atmospheric conditions like wind speed, turbulence intensity and wind shear shown in section 7.3. In the yaw-control strategy, the method of selecting normal operation period is similar to method 2 used in the curtailment strategy: this method (called normal operation) aims to find for each yaw-control period available (a total of 118 10-min averages for SMV5 and 207 10-min averages for SMV6), periods inside the full normal operation span (June 2017-March 2018) that have similar atmospheric conditions. The filters applied to select the periods with similar inflow conditions are the following:

1. Average wind speed: ± standard deviation (wind speed) divided by 2;
2. Average wind direction: ±10°;
3. Average turbulence intensity: ±1%;
4. Average wind shear parameter: ±0.1;

As for the curtailment strategy, beside turbulence intensity that was the most influential filter, these filters have been selected considering data availability; a compromise had to be found between having a good data availability and the selectivity of the inflow conditions. This method create a data availability for normal operation of 59.9h for SMV5 and of 158.7h for SMV6. This big difference is due to the different wind direction filters: as previously said for SMV5 wind direction was limited between 180° and 230° to see the effect of SMV6 wake on it; while SMV6 was limited to the no-wake wind direction

between 200° and 360° since the yaw-error persisted at all wind atmospheric conditions.

9.4 Upstream Wind Turbine SMV6

In this section loads and fatigue are analyzed for the upstream turbine SMV6; data from the yaw-controlled period will be compared with the ones filtered using the normal operation selection method explained in section 9.3. As previously stated, in order to have comparable data, the inflow conditions of the data compared need to be similar; as a consequence the analysis starts with an assessment of the inflow conditions followed by loads fatigue analysis. Due to the consistency in the results of all the 3 blades of each turbine, only blade 1 of both turbine is shown.

Figure 9.3 and Figure 9.4 represent respectively the ambient turbulence intensity and the wind shear parameter as a function of ambient wind speed (taken from Windcube V2) for SMV6 selected periods.

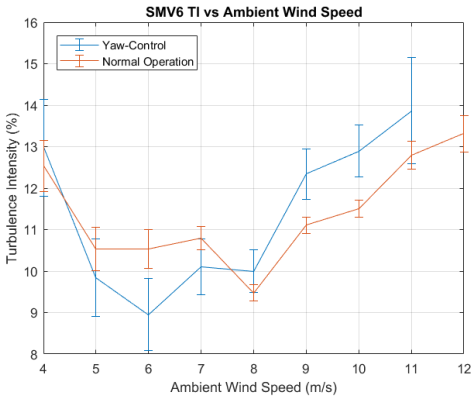

Figure 9.3: Ambient turbulence intensity as a function of ambient wind speed. The error bars represent the 95% confidence interval.

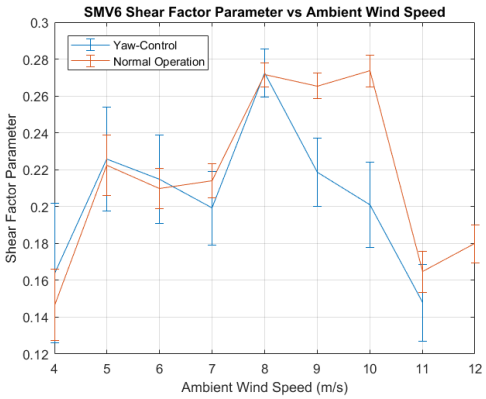

Figure 9.4: Wind shear parameter as a function of ambient wind speed. The error bars represent the 95% confidence interval.

The ambient turbulence intensity trend is very similar between the yaw-control period and the normal operation period. Also the wind shear trends are similar. Generally lower wind shear and higher turbulence intensity are observed after 8 m/s in the yaw-controlled period. In these particular periods an interesting trend is seen: the wind speeds with higher wind shear also have lower turbulence intensity. This effect is generally dependent on atmospheric stability as this parameter dictates the vertical motion of the air. Generally consistent inflow conditions for a reliable analysis are observed in the yaw-controlled period and in the normal operation period.

After the inflow conditions have been analyzed, edgewise and flapwise loads are plotted and studied. Figure 9.5 and Figure 9.6 represent respectively the flapwise blade loads and the edgewise blade loads as a function of ambient wind speed (taken from Windcube V2) for SMV6 selected periods.

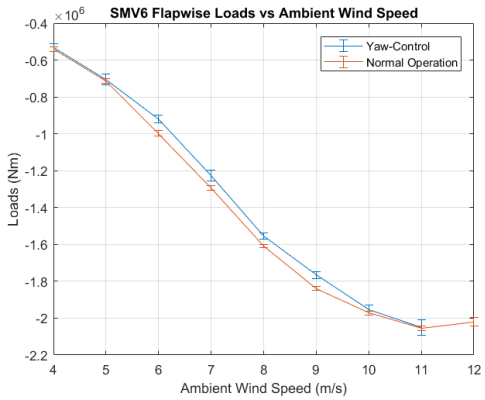

Figure 9.5: Flapwise loads as a function of ambient wind speed. The error bars represent the 95% confidence interval.

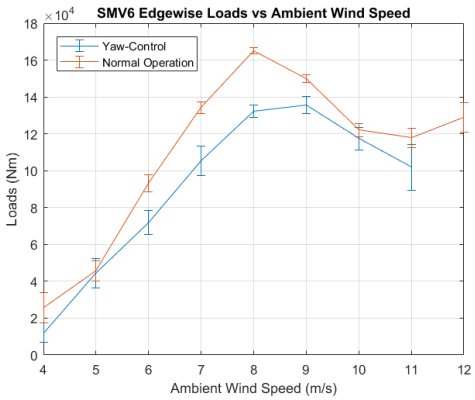

Figure 9.6: Edgewise loads as a function of ambient wind speed. The error bars represent the 95% confidence interval.

Wind Speed [m/s]	Difference in Flapwise Blade Loads [%]	Difference in Edgewise Blade Loads [%]
4	-1%	-72%
5	-1%	-3%
6	-8%	-26%
7	-5%	-24%
8	-3%	-22%
9	-4%	-10%
10	-1%	-4%
11	-0%	-14%

Table 9.1: Difference between normal operation period and yaw-control strategy period loads.

The upstream turbine SMV6 is subjected to a significant decrease in loads in both the flapwise and edgewise directions. Table 9.4 shows a maximum loads decrease between the normal operation period and the yaw-controlled period of 8% (6 m/s) in the flapwise direction and 72% (4 m/s) in the edgewise direction. The main reason for this decrease in flapwise loads is similar to what has been seen in the curtailed upstream turbine SMV6 and it is most likely linked to a decrease of the "effective" thrust force acting on the rotor. When a turbine has a yaw-misalignment only the perpendicular component of the velocity crosses the rotor area, therefore the thrust force is divided in 2 components, one parallel and one perpendicular to the rotor [36]. The perpendicular force acting on the rotor is the "effective" thrust force and its formula is shown below:

$$Thrust_{\perp} = \frac{1}{2} * C_T \rho A (U_0 \cos\gamma)^2 \tag{9.1}$$

where A is the area, C_T is the thrust coefficient, ρ is the air density, U_0 is the wind velocity at the disk and γ is the yaw-angle. It can be noted that $\cos(13°)^2$ is approximately 5%, therefore the decrease in flapwise loads is consistent with the expected decrease in thrust.

As a consequence the parallel component of the force will be exerted on the flow creating a distortion in the wake and a consequent decrease in wake intensity [36]. This is confirmed by the lower rotor speed experienced by the rotor during the yaw-controlled period not caused by any increase in pitch angle but caused by the decreased perceived wind (and as a consequence thrust) as seen in Figure 9.7 and 9.8. Interestingly Table 9.4 shows that, even if the turbine SMV6 is yawed, at 11 m/s the difference in flapwise loads (thrust) decreases to 0%. This can be explained by looking at Figure 9.8 where it can

be seen that under yaw-control the turbine pitch less at 11 m/s, this compensate the effect of the yaw resulting in the same thrust and loads.

Decrease in thrust was not expected to have major influences on the edgewise loads, however this direction saw the largest decreases in loads. This could be caused by a combination of the lower rotor speed experienced by the yawed rotor (even though the difference is quite small) and the decrease in thrust.

It can be concluded that loads on the yawed turbine show a significant decrease in both the flapwise direction, with a maximum decrease of 8% compared to normal operation, and in the edgewise direction, with a maximum decrease of 72% compared to normal operation.

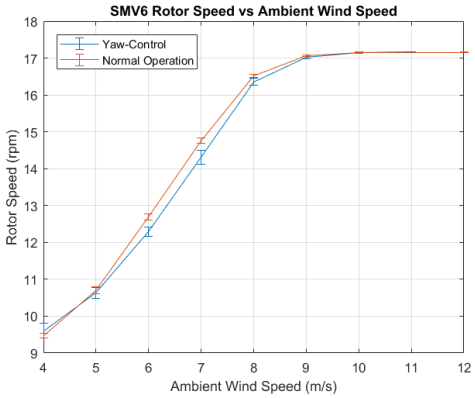

Figure 9.7: Rotor speed as a function of wind speed. The error bars represent the 95% confidence interval.

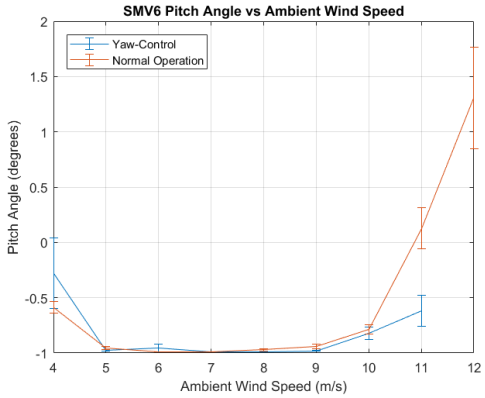

Figure 9.8: Pitch angle as a function of wind speed. The error bars represent the 95% confidence interval.

Figure 9.9 and Figure 9.10 represent respectively the flapwise blade fatigue loads and the edgewise blade fatigue loads as a function of ambient wind speed (taken from Windcube V2) for SMV6 selected periods.

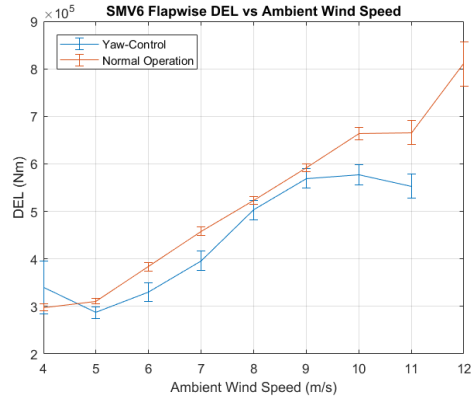

Figure 9.9: Flapwise fatigue loads as a function of ambient wind speed. The error bars represent the 95% confidence interval.

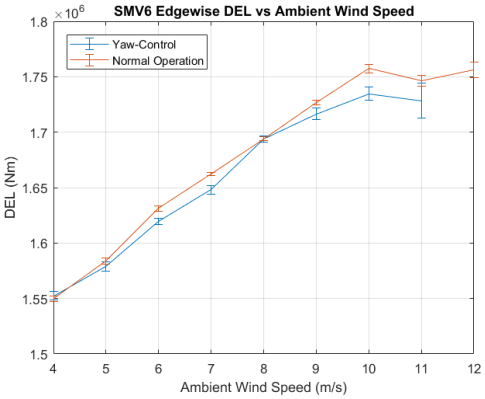

Figure 9.10: Edgewise fatigue loads as a function of ambient wind speed. The error bars represent the 95% confidence interval.

Wind Speed [m/s]	Difference in Flapwise Blade DEL [%]	Difference in Edgewise Blade DEL [%]
4	+13%	+0%
5	-8%	-0%
6	-15%	-1%
7	-15%	-1%
8	-4%	-0%
9	-4%	-1%
10	-14%	-1%
11	-19%	-1%

Table 9.2: Difference between normal operation period and yaw-control strategy period fatigue loads.

Fatigue equivalent loads (DEL) of a wind turbine come from the variation of the loads in time and they do not heavily depend on the mean level of the loads so generally the decreases observed in SMV6 loads do not necessarily mean a decrease in DEL; however here, since the inflow conditions (especially turbulence intensity) are very similar, also a decrease in the loads should correspond to a decrease in fatigue. Flapwise DEL in the yaw-control period are constantly lower compared to the normal operation with a maximum decrease of 19% at 11 m/s. Edgewise DEL in the yaw-control period are also constantly lower compared to the normal operation with a maximum decrease of 1.3% at 10 m/s. This trend of lower fatigue loads for wind speeds below rated is also shown in [21]. In this research article simulations of the NREL 5 MW reference turbine performed with the aeroelastic simulation tool HAWC2 show that the blade fatigue reduction depends on the turbulence level with reductions up to 20% at low turbulence intensities. This value is very close to the one obtained in this thesis. This reduction in fatigue loads of the yawed turbine has been investigated in [37]. Here is concluded that given a normal shear layer, and given the direction of rotation of most turbines, by yawing the turbine counterclockwise (as it is done in the SMARTEOLE field test), there is effective reduction of the angle of attack variation in 1P; this is because at the bottom of the rotation, the blades are advancing into the flow, while they are retreating from faster flow at the top, thus reducing the apparent speed variation across the rotor.

Nevertheless flapwise fatigue loads are generally expected to increase when the wind turbine is yawed, this because misaligned inflow conditions change the blade aerodynamics (angle of attack, lift and drag) with the azimuthal position creating additional cyclic loads variation increasing fatigue [38]. This trend is shown in [20] and where flapwise fatigue loads are shown to increase with nonzero yaw-angle. The same paper showed that edgewise fatigue loads decrease with decreasing yaw-angle (using this thesis convention explained in section 9.1).

It can be concluded that fatigue loads on the yawed turbine show a significant fatigue decrease in the flapwise direction, with a maximum decrease of 19% (11 m/s) compared to the normal operation period used for comparison. In the the edgewise direction a much smaller general decrease of 1% is observed on the yaw-controlled period compared to normal operation period.

9.5 Downstream Wind Turbine SMV5

In this section loads and fatigue are analyzed for the downstream turbine SMV5; data from the yaw-controlled period will be compared with the ones selected using the normal operation selection method explained in the section 9.3. As previously stated, in order to have comparable data, the inflow conditions of the data compared need to be similar; as a consequence the analysis starts with an assessment of the inflow conditions followed by loads fatigue analysis. Due to the consistency in the results of all the 3 blades of each turbine, only blade 1 of both turbine is shown.

Figure 9.11 and Figure 9.12 represent respectively the ambient turbulence intensity and the wind shear parameter as a function of ambient wind speed (taken from Windcube V2) for SMV5 selected

periods.

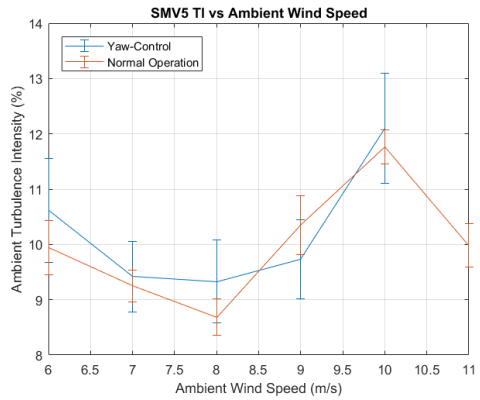

Figure 9.11: Ambient turbulence intensity as a function of ambient wind speed. The error bars represent the 95% confidence interval.

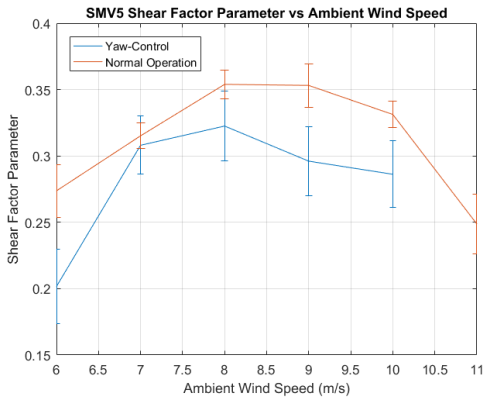

Figure 9.12: Wind shear parameter as a function of ambient wind speed. The error bars represent the 95% confidence interval.

It can be observed that the turbulence intensity trend is very similar between the yaw-control period and the normal operation period. For this specific periods the expected trend, where lower wind speeds are more likely to have higher turbulence, whereas higher wind speeds tend to have lower turbulence, is not observed. Also the wind shear trends are similar, with a generally lower wind shear observed in the yaw-controlled period. This lower value can be explained by the different seasons when the measurement were taken: yaw-controlled period took place in the late summer months with generally less stable atmospheric conditions compared to winter and as a consequence increased turbulence (slightly higher values in the yaw-controlled period) and decreased wind shear. Generally, consistent inflow conditions for a reliable analysis are observed in the yaw-controlled period and in the normal operation period.

After the inflow conditions have been analyzed, edgewise and flapwise loads are plotted and studied. Figure 9.13 and Figure 9.14 represent respectively the flapwise blade loads and the edgewise blade loads as a function of ambient wind speed (taken from Windcube V2) for SMV5 selected periods.

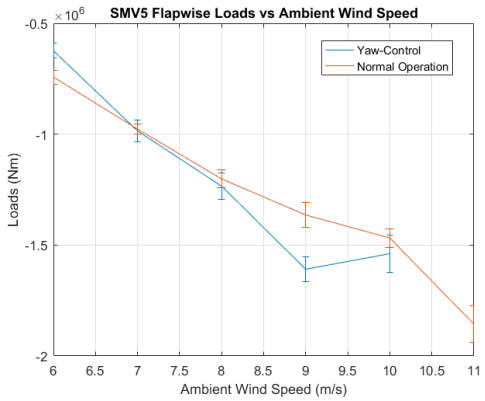

Figure 9.13: Flapwise loads as a function of ambient wind speed. The error bars represent the 95% confidence interval.

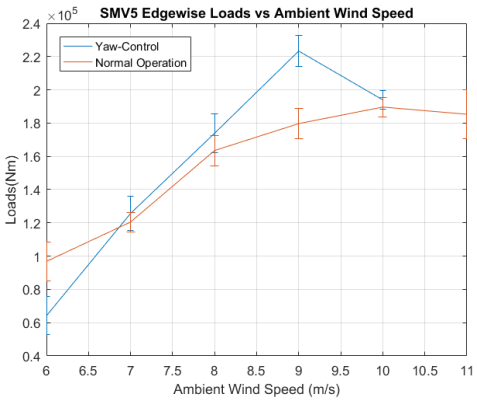

Figure 9.14: Edgewise loads as a function of ambient wind speed. The error bars represent the 95% confidence interval.

Both flapwise and edgewise loads have similar loads up to 8 m/s for both the yaw-controlled and the normal operation periods. After the ambient wind speed of 8 m/s loads experience a jump with the peak at 9 m/s. This peak is also visible in the rotor speed as a function of ambient wind speed (graph shown in Figure 9.16) but no pitch angle increase is seen at 9 m/s (Figure 9.17). In order to investigate this

unexpected behavior the average wind direction has been plotted as a function of ambient wind speed to see if major differences are present at 9 m/s (see Figure 9.15).

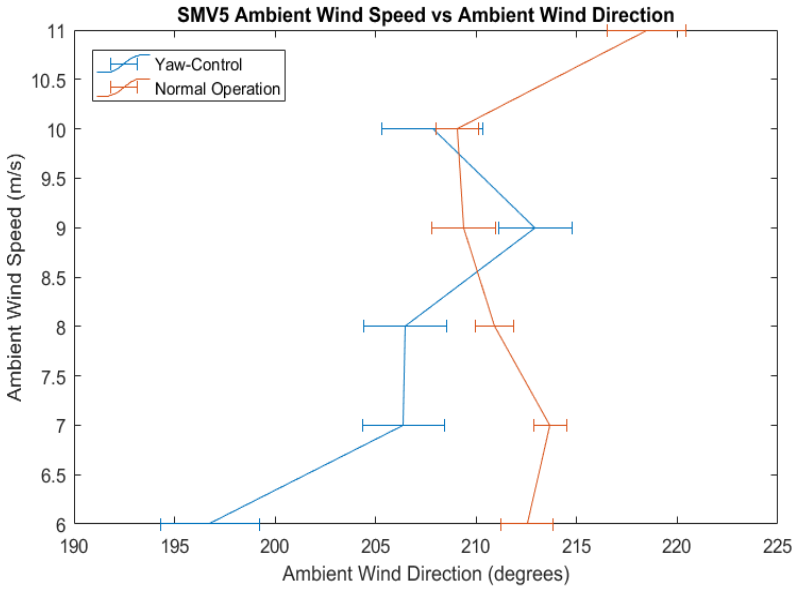

Figure 9.15: Turbulence intensity as a function of wind speed. The error bars represent the 95% confidence interval.

It can be seen that at 9 m/s a major shift in the observed trend is seen; the yaw-controlled period has always wind speeds closer to the wake center (∼205°) except at 9 m/s where the opposite trend occurs. This can explain the peak present at 9 m/s that is most likely due to the presence of more points in the yaw-controlled period close to half-wake conditions. This increases the loads and rotor speed significantly. Also it can be noted that also at 7 m/s and 8 m/s the loads of the normal operation period could be higher due to the same effect. This underlines the uncertainty observed in the SMV5 loads trends.

Beside the values at 9 m/s in the yaw-controlled period, no major changes have been observed between loads (flapwise and edgewise) of the yaw-controlled period and the normal operation period suggesting that the differences in average wind direction previously explained could have distorted the visible trends.

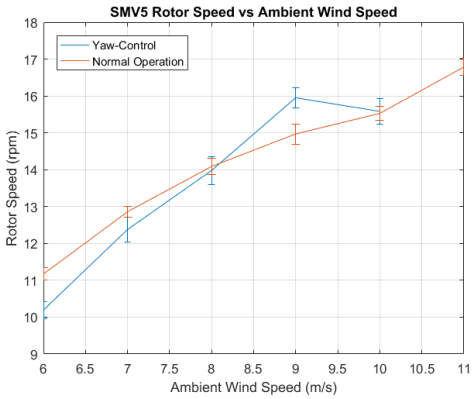

Figure 9.16: Rotor speed as a function of wind speed. The error bars represent the 95% confidence interval.

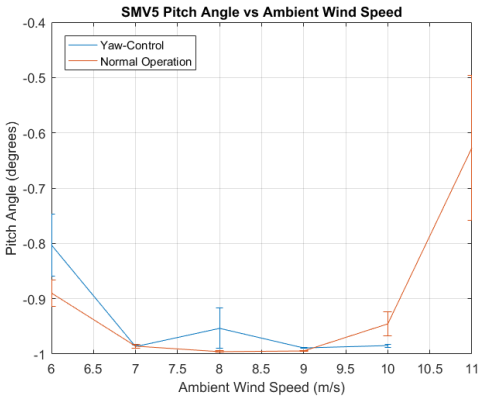

Figure 9.17: Pitch angle as a function of wind speed. The error bars represent the 95% confidence interval.

Figure 9.18 shows the local turbulence intensity as a function of the ambient wind speed (taken from

the SCADA system of SMV5) for SMV5 selected periods.

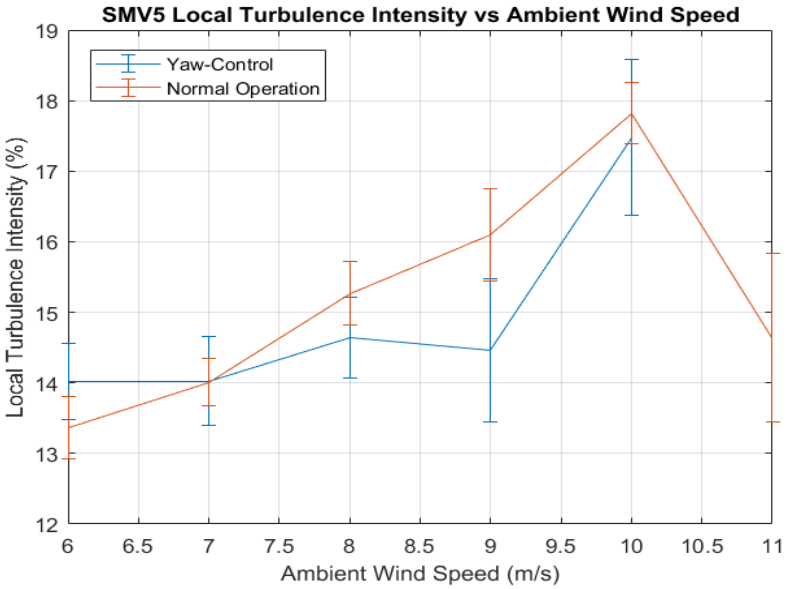

Figure 9.18: Turbulence intensity as a function of wind speed. The error bars represent the 95% confidence interval.

As it is observed, the local turbulence intensity is expected to be generally higher compared to the ambient turbulence intensity due to the position of the SCADA system right inside the wake of SMV6. Also no major changes are seen in the perceived turbulence intensity trends compared to the ambient turbulence intensity trends.

Changes in the downstream turbine loads strongly depend on the changes in the deviation angle θ (as seen in Figure 2.6) since the distance is fixed. Therefore, depending on the distance, the downstream turbine could be exposed to no-wake conditions or partial wake conditions. Using the wake deflection model developed in [36] the deviation angle θ can be estimated using the following Equation 9.2 [36]:

$$\theta = \frac{\frac{C_t}{2}\cos^2(\gamma)\sin(\gamma)}{1+\beta\frac{x}{D}} \tag{9.2}$$

where γ is the yaw-angle (-13°), C_t is the thrust coefficient ($\sim$0.8 for the wind speeds available), β is the wake expansion coefficient (0.1 suggested value in [36]) and x is the distance in diameters (3.7D). This method gives a deviation angle θ of 3.6°. Even though this method is more reliable for the far wake, where turbulence intensity is the dominant force, it gives an idea of the magnitude of this angle and consequently of the wake shift.

In order to confirm this shift in the wake, the SMV5 flapwise DEL and the active power produced have been plotted as a function of wind direction for both the normal operation period and the yaw-controlled period with the hope to see a counterclockwise shift in the wake effects. Unfortunately no clear shift has been observed in either the flapwise DEL plot or the power produced plot. For the graphs see Appendix D.

Figure 9.19 and Figure 9.20 represent respectively the flapwise blade fatigue loads and the edgewise blade fatigue loads as a function of ambient wind speed (taken from Windcube V2) for SMV5 selected periods.

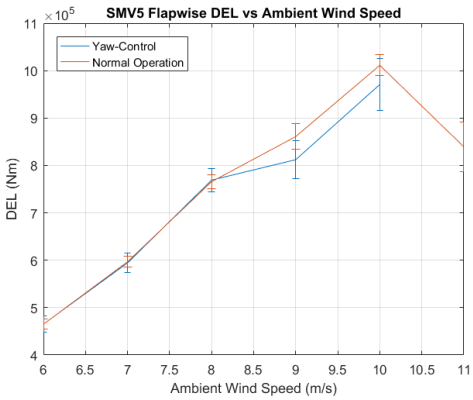

Figure 9.19: Flapwise fatigue loads as a function of ambient wind speed. The error bars represent the 95% confidence interval.

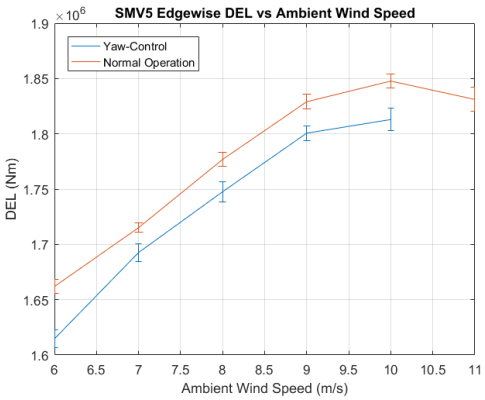

Figure 9.20: Edgewise fatigue loads as a function of ambient wind speed. The error bars represent the 95% confidence interval.

Wind Speed [m/s]	Difference in Edgewise Blade DEL
6	-3%
7	-1%
8	-2%
9	-2%
10	-2%

Table 9.3: Difference between normal operation period and yaw-control strategy period edgewise loads.

Flapwise fatigue loads of the yaw-control and normal operation periods have similar values up to 8 m/s, then the yaw-control period has slightly lower values. However the yaw-control period error bars are quite large and they overlap with the normal operation period showing less reliability (also due to the lower amount of data). This decrease is most likely connected to the increase in loads seen previously at the same ambient wind speed and, for the same reasons explained in the loads section (because of the difference in average wind direction), no conclusions can be drawn from it even though higher fatigue loads were expected due to rotor imbalance at 9 m/s. On the other end a slight decrease in the edgewise fatigue loads is observed with consistency throughout the different wind speeds even where rotor speed and loads increase. The reason for this decrease, only seen on the edgewise direction, is unknown since the effects of the yaw-control on the wake flow characteristics were expected to be more predominant on the flapwise direction.

It can be concluded that no major reductions have been observed between fatigue loads of the yaw-controlled period and those of the normal operation period in the flapwise direction. In the edgewise direction a minor decrease in loads in the range of 1% to 3% is observed. However no satisfying reasons have been found in the analysis to explain this decrease.

One of the main reasons why no major changes are observed, beside all the analysis made, is that here the analysis is made for the whole wake sector. This means that since the wake resembles a Gaussian distribution, a shift of few degrees in the wake distribution will be weakly felt because only the tail of the wake distribution (where the loads and fatigue are less affected) is not seen by the downwind turbine (see Figure 9.21). To solve this problem, a more selective analysis regarding the full wake sector (from 195° to 215° rather than from 180° to 230°) is done in order to see clearer trends caused by the curtailment strategy in the sector where the wake effects are the highest.

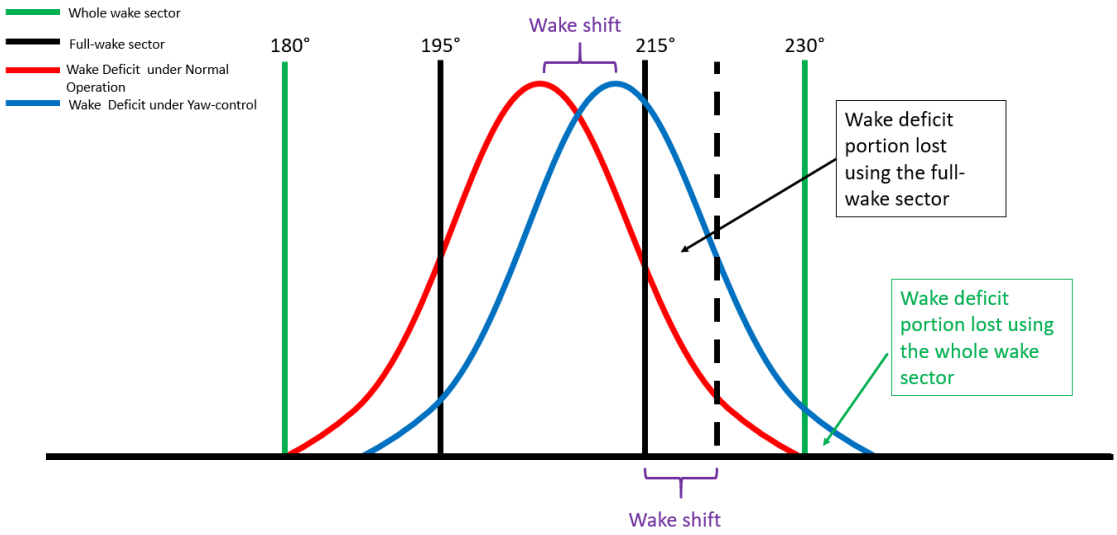

Figure 9.21: Wake deficit shift.

Inflow conditions are not shown due to the similarity with the ones of the whole wake sector. Figures 9.22, 9.23, 9.24 represent respectively the flapwise blade loads, the edgewise blade loads and the power produced as a function of ambient wind speed (taken from Windcube V2) for SMV5 selected periods (full-wake sector).

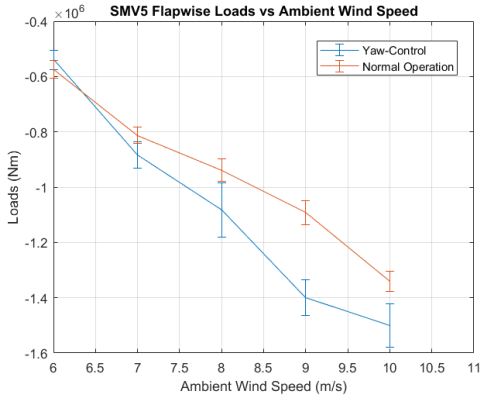

Figure 9.22: Flapwise loads as a function of ambient wind speed (full-wake sector)). The error bars represent the 95% confidence interval.

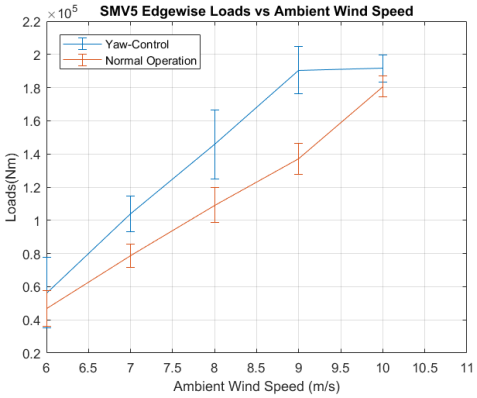

Figure 9.23: Edgewise loads as a function of ambient wind speed (full-wake sector). The error bars represent the 95% confidence interval.

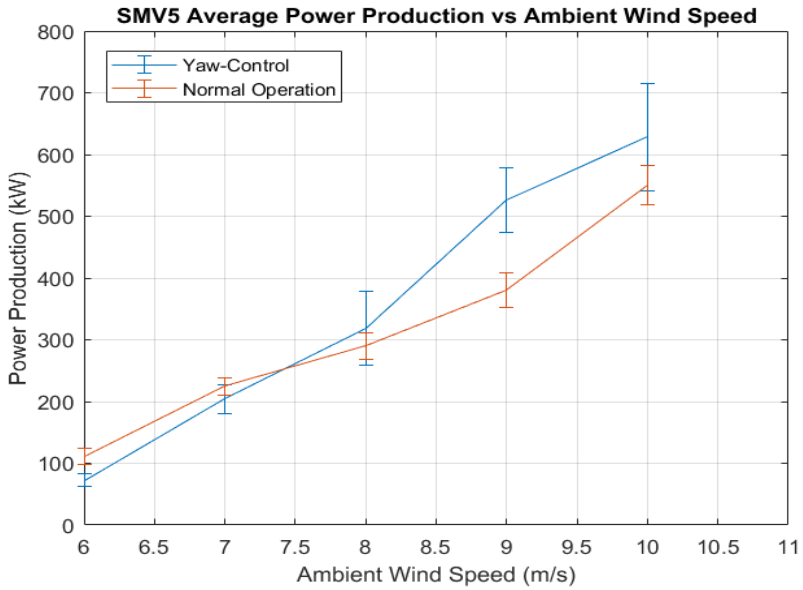

Figure 9.24: Power produced as a function of wind speed (full-wake sector). The error bars represent the 95% confidence interval.

Wind Speed [m/s]	Difference in Flapwise Blade Loads [%]	Difference in Edgewise Blade Loads [%]	Difference in Active Power Production [%]
6	-6%	+19%	-42%
7	+8%	+27%	-10%
8	+14%	+29%	+9%
9	+25%	+33%	+32%
10	+11%	+6%	+13%

Table 9.4: Difference between normal operation period and yaw-control strategy period loads.

It can be noted that for the full-wake region, loads in the yaw-controlled period are higher than the normal operation period up to the value of 25% (9 m/s) in the flapwise direction and up to the value of 33% (9 m/s) in the edgewise direction. This trend is expected because by steering the wake of turbine SMV6, the wake wind deficit is reduced resulting in an increase in power (Figure 9.24) up to 32% (9 m/s) and as a consequence in loads. This trend is much more visible in the full wake most likely due to a bigger percentage of the wake sector analyzed being shifted out of the full-wake sector (195° to 215°) compared to the whole sector analyzed previously (180° to 230°)(see Figure 9.21).

Figure 9.25 and Figure 9.26 represent respectively the flapwise blade fatigue loads and the edgewise blade fatigue loads as a function of ambient wind speed (taken from Windcube V2) for SMV5 selected periods (full-wake sector).

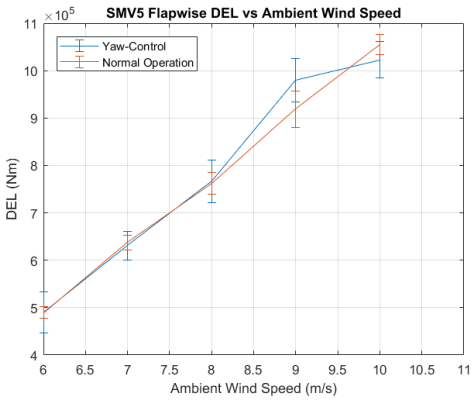

Figure 9.25: Flapwise fatigue loads as a function of ambient wind speed (full-wake sector)). The error bars represent the 95% confidence interval.

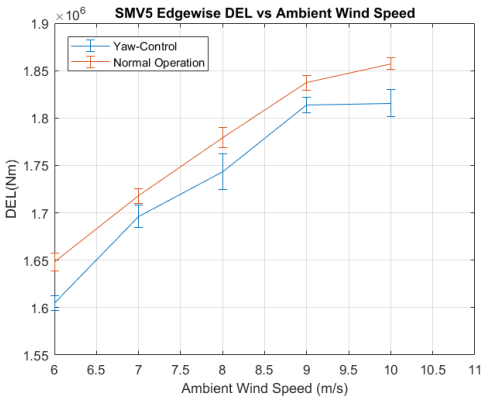

Figure 9.26: Edgewise fatigue loads as a function of ambient wind speed (full-wake sector). The error bars represent the 95% confidence interval.

An increase in fatigue loads was expected due to the increase observed in the loads and due to the increased possibility of half-wake situations caused by the wake deflection. However fatigue loads do not show major increases in the flapwise direction. In the edgewise direction an unexpected slight decrease similar to the one seen in the whole wake analysis is observed. A similar trend showing no increase in fatigue loads is seen in [21], where simulations, carried out with HAWC2 for the aero-servo-elastic model and DWM for the wake modelling conducted on a 2.3 MW machine, showed load and fatigue alleviation towards negative yaw angles with higher reductions at lower turbulence intensities.

It can be concluded that the analysis of the full-wake sector is able to highlight more precisely the loads and fatigue trends because of the less variation of wake influence inside the selected range. The analysis of the full-wake sector showed the potential of the yaw-controlled strategy; the downwind turbine SMV5 showed an increase in power production due to the weaker wake wind speed reduction without showing a major increase in fatigue loads. Therefore is recommended to use the full-wake sector for the analysis of the downwind turbine loads and fatigue during a yaw-control strategy especially when limited amount of data is available.

9.6 Summary and Discussion

The performance of the yaw-control strategy on the reduction of loads and fatigue loads between an upstream wind turbine (SMV6) and a downstream wind turbine has been examined in this chapter. The data used in this analysis have been taken from the second campaign of field tests in the SMARTEOLE project.

The analysis made on the downstream turbine SMV5 showed no significant reductions in the flapwise loads. This can be explained by the quite large wake sector taken for the analysis (between 180° and 230°); this was done in order to keep the amount of data available to a level where trends were recognizable and reliable. However, by taking such a large sector, not only the full-wake is captured but also the tails of the wake. Since the deviation angle generated is quite small, it is likely that only one tail of the wake distribution was yawed away not changing loads significantly. This could explain why loads do not vary significantly in both edgewise and flapwise directions. Also no significant decrease was found in the flapwise fatigue loads since the trend observed was not consistent and reliable most likely due to the possible faulty measurement present at 9 m/s. The edgewise fatigue loads saw a slight decrease up to 3%; no plausible explanation has been found for this trend beside some light differences in the inflow conditions. Due to the possible effect previously mentioned, the smaller full-wake sector (195° to 215°) was also analyzed with the hope that clearer trends would have been seen despite the lower amount of data. Trends showed an important increase in flapwise loads (up to 25% at 9 m/s), in the edgewise loads (up to the value of 33% at 9 m/s) and in power produced (up to 32% at 9 m/s). No major changes have been detected in the fatigue loads.

On the other end, the analysis made on the upstream turbine SMV6 showed a significant decrease in the flapwise direction loads (maximum decrease of 8% at 6m/s) and fatigue (maximum decrease of 19% at 11m/s); the edgewise direction also saw a decrease in loads (maximum decrease of 72% at 4m/s) and in fatigue (maximum decrease of 1.3% at 10m/s). The decreases are due to the implementation of the yaw-control strategy; this creates a misalignment with the incoming flow changing the blade aerodynamics like thrust, lift and drag, lowering loads and fatigue. The effects on loads and fatigue generated on the yawed turbines are very conflicted in literature; many studies also found increases in fatigue loads mainly due to the creation of additional cyclic loads variation.

The yaw-control strategy has shown a good potential in the reduction of loads and fatigue in both the flapwise and edgewise directions of the upstream turbine. Despite initially no major effects have been seen on the downstream turbine in terms of loads and fatigue reduction due to the large wake sector analyzed, a significant increase in loads and power without any significant increase in fatigue loads have been observed in the narrower full-wake sector showing a promising trend. Due to the close proximity between the two turbines it can be argued that possibly a higher yaw-offset could highlight more clearly major loads variation trends without narrowing the wake sector analyzed; however it has been shown that inside the full-wake sector clearer trends are seen due to a bigger percentage of the wake sector analyzed being shifted out of the analyzed wake sector. Also a more consistent and verified yaw-control strategy could increase the potential for load reduction quite significantly. A potentially good strategy is to apply this strategy only in some partial wake conditions where it is possible to deflect the wake completely out of the downstream turbine; this is especially suitable for small inter-spacing distances like in this case.

Due to the limited amount of data no trends were analyzed for wind speeds above rated where more significant loads and fatigue increases are possible [37].

Also for this strategy only blade loads and fatigue have been analyzed because they are the major source of loads that are then distributed throughout the whole turbine. However, the changes in the drive-train and tower loads and fatigue may still be quite different and could change the potential benefits of this strategy. In [20] field data, increases in the blade fatigue loads for the yawed turbine are associated with increases in the tower top bending moment for both misalignment directions while the tower base bending moment increases only with positive yaw angles (convention used in this thesis). Before drawing conclusions more analysis on these types of loads need to be done especially considering the variability of the results.

10 Conclusions

Wind energy is a rapidly expanding and evolving sector that is in the need of constant innovation to be competitive with other power generation technologies. Research and development are key factors for the decrease in the price of energy generated by wind turbines, and this is the reason why the development and the implementation of active wind farm wake control strategies have become increasingly important over the last couple of years. The main idea behind these strategies is to control the wind turbines inside the wind farm collectively with the goal of mitigating the wake effect interactions, increasing the wind farm total power production and decreasing the turbines loads and fatigue.

The impact on power production of these wind farm control strategies has been the main focus recently; indeed many simulations and experiments collectively showed that increase in power production is possible with the value of the gains varying a lot depending on the inflow conditions and on the wind farm characteristics. Less focus has been given to loads analysis where the few experiments and simulations performed in literature give contrasting and very inconsistent results that change quite dramatically with varying inflow conditions.

The French National Research Agency SMARTEOLE project implemented two wind farm control strategies in an operating wind farm called La Sole du Moulin Vieux and owned by Engie Green in order to assess the performance of these strategies on a commercial wind farm with very dynamic inflow conditions. The two wind farm control strategies applied are the curtailment strategy and the yaw-control strategy.

This master thesis is based on the data collected during the second field campaign of the SMARTEOLE project (June 2017- March 2018) where the curtailment strategy was implemented applying the turbine noise reduction Senvion MM82 SMII type B power curve and the yaw-control strategy was caused by an error in maintenance that created an average yaw error of -13°. The examination and investigation of the second field campaign showed and confirmed the difficulty in the detection of reliable trends due to the large variability of inflow conditions during different periods throughout the 10 month long measuring campaign and due also to the limited amount of data available caused by faults in sensors and by the limited temporal application of the control strategies.

The calibration procedure of the strain gauges data turned out to be quite challenging due to the huge amount of data initially available and due to the many steps involved in the calculation of the temperature correction. However no major losses of data have occurred during this process; beside a minor quantity of data that was out of scale, almost all sensors data behaved as it was expected (only one sensor behaved unexpectedly).

The loads calculated after the calibration procedure have been filtered for clear outliers that were not in a realistic loads range; the loads data validation showed the possibility of a non correct installation of the strain gauges (non correct gluing of the sensors on the blade internal surface) that led to the conclusion that the edgewise signal of blade 2 was unusable and that, thanks to the installation of two sensors in the same load direction, the edgewise signal of blade 1 was considered still reliable due to the consistency of the combined LE and TE signals shown in the edgewise boxplot analysis. This shows that the installation of strain gauges sensors in the edgewise loads direction is quite challenging due to the rough surface inside the blade in this direction. However the application of 2 sensors in the same loads direction has multiples advantages:

- the behavior of the 2 sensors can be compared to make sure they behave similarly and if it does so, it can be combined to have a more reliable signal;
- if one sensor does not work or it gives faulty results but the other one is fine, data from this direction can still be used.
- if the offset is consistent in both the sensors, the bias created by this offset can be compensated by the other sensor and so the error can be eliminated when the signals are combined.

Fatigue loads were calculated after the loads validation procedure following the International Standards Measurement of mechanical loads (IEC 61400-13:2016) and they have also been filtered for clear outliers that were not in a realistic fatigue range but due to the previous filtering done on the loads, very few outliers have been found.

Normal operation analysis showed, as expected, that fatigue is very sensible to inflow conditions; fatigue showed an overall increase of around 10% in the range of wind shear parameters available (from 0.15 to 0.45) and an overall increase of around 56% in the range of turbulence intensities available (from 3% to 15%). Fatigue loads are more sensible to turbulence intensity compared to wind shear as a consequence in order to have a reliable fatigue comparison, the turbulence intensity of the inflow needs to be very similar. Unfortunately, no other inflow condition parameters like stability, air density, air pressure and temperature have been analyzed as they could have noticeable effects on the loads [39]. As expected, loads in the wake decreased by a maximum of 32% (8 and 9 m/s) in SMV5 and by a maximum of 26% (6 m/s) in SMV6 due to the wind speed deficit present in the wake. Fatigue loads inside the wake sector went up by 60-70% for single wake and 90% for double wake compared to the sector with no-wake; this is due to the increase in turbulence intensity in the wake.

Then the impact of the 2 wake control strategies has been quantified and compared to the normal operation period. For the curtailment strategy two different methods of selecting the normal operation period with similar inflow conditions have been tried due to the lack of data in the curtailment period. In the first method data have been selected from the same nights where curtailment strategy was applied for one hour every two. This method assumed that, on average, inflow conditions did not change much in one hour. In the second method data matching the curtailment period inflow conditions have been selected from the normal operation period (October 2017-December 2017). The inflow conditions of the data selected by both methods have been very similar to each other and to the curtailment period. However loads and fatigue were matching only in the upstream turbine SMV6 where loads decreased up to 33% (at 9 m/s) in the flapwise direction and up to 67% (at 8 m/s) in the edgewise direction. Fatigue loads on the curtailed turbine show a significant decrease in the flapwise direction, with a maximum decrease between 14% and 22% (9 m/s) depending on which normal operation period is used for comparison. In the edgewise direction a much smaller maximum decrease of 2% (9 m/s) is observed on the curtailment period compared to both normal operation methods periods. In the downstream turbine no clear trend has been detected due to the inconsistency in the loads and fatigue of the normal operation data selected with the two methods; this shows high uncertainty in the results (should have been very similar). The change in the season where the data of the two different methods have been taken (late summer against winter) could have played a role but this difference is not seen in SMV6. Most likely low amount of data and increased turbulence (caused by the wake) lead to inconsistency in the trends.

In the yaw-control strategy, data matching the yaw-control period inflow conditions have also been selected from the normal operation period (October 2017-December 2017). Also here inflow conditions matched well and the upstream turbine SMV6 showed a decrease up to 8% (at 9 m/s) in the flapwise direction loads and up to 72% (at 9 m/s) in the edgewise direction loads. Fatigue also decreased up to 19% (at 11 m/s) in the flapwise direction loads and up to 1.3% (at 10 m/s) in the edgewise direction for the upstream turbine. Literature shows very conflicting fatigue trends in the yawed turbine; similar results are shown in [21] where the blade fatigue reduction depends on the turbulence level with reductions up to 20% at low turbulence intensities. One explanation for this reduction is that by yawing the turbine counterclockwise, there is effective reduction of the angle of attack variation in 1P (discussed in [37]). Opposite results are shown in [20] with both simulations and the field-derived results confirming this trend of increased fatigue loads with both positive and negative yaw-misalignment. Such different results are most likely due to the very high sensitivity to inflow conditions like turbulence intensity and by the different types of wind turbines analyzed. The downstream turbine SMV5 showed no significant reductions in the flapwise loads and fatigue when the whole wake was analyzed but, when only the full-wake was analyzed, a significant increase in loads and power produced, without any significant increase in fatigue loads have been observed. This underlines the potential of the yaw-controlled strategy to increase power production without significantly increasing fatigue.

It needs to be highlighted that, due to the low amount of data and due to the very high sensibility

of loads and especially fatigue trends while applying active wake control strategies, the results of the strategies observed in this thesis have significant uncertainty and that more research needs to be done in order to draw final conclusions on the effectiveness of these wind farm control strategies,

Recommendations

The most obvious recommendation is to try to collect as much data as possible for both the normal operation period and for the active wake control strategy period. Due to the high sensitivity of loads and fatigue to inflow conditions it is recommended that the data are collected during the same season for both the normal operation period and the wake control strategy period.

Sensors with the same sampling frequency are also recommended to be synchronized in order to facilitate and accelerate the data analysis process.

If a short period of data measurement is available, it is suggested to use data averages of 1 or 2 minutes to increase the number of data available to detect trends. Also a better characterization of the inflow conditions is possible due to the less variability of inflow conditions.

The presence of two sensors for each loads direction is also recommended in order to have a more reliable analysis of the data with the possibility of using only one sensor if malfunctioning happens.

Analysis of tower and nacelle loads would be also beneficial for a more comprehensive understanding of the loads reduction potential of these wake control strategies.

Bibliography

1. I. Kumusanac, D. Fraile, G. Brindley. “Wind Energy in Europe in 2018: Trends and statistics”. In: Wind Europe (2019),
2. F.D. McAuliffe, J. Murphy, K. Lynch, C. Desmond, J.A. Norbeck, L.M. Nonas, Y. Attari, P. Doherty, J.D. Sorensen, J. Giebhardt, C. Lopez, S. Hildebrandt, S. Potestio and V. Godavarthi. “Driving Cost Reductions in Offshore Wind: the leanwind project final publication”. In: Leanwind (2017),
3. European Technology and Innovation Platform on Wind Energy. “Strategic Research and Innovqtion Agenda 2018 ”. In: ETIP Wind (2018)
4. A. Crespo, J. Hernandez, and S. Frandsen. “Survey of modelling methods for wind turbine wakes and wind farms”. In: Wind energy 2.1 (1999), pp. 1–19.
5. B. Sanderse. “Aerodynamics of wind turbine wakes - Literature review”. Tech. rep. Energy research Center of the Netherlands, 2009
6. J. Højstrup. “Spectral coherence in wind turbine wakes”. Journal of Wind Engineering and Industrial Aerodynamics, 80:137–146, 1999.
7. R.J. Barthelmie, S.T. Frandsen, K. Hansen, J.G. Schepers, K. Rados, W. Schlez, A. Neubert, L.E. Jensen, and S. Neckelmann. “Modelling the impact of wakes on power output at Nysted and Horns Rev”. In European Wind Energy Conference, 2009.
8. Erich Hau. “Wind Turbines: Foundamentals, Technologies, Application, Economics”. In: Loads and Structural Stresses Chapter 6 (1999), pp.161-180
9. H. A. Madsen, K. Thomsen. “Analysis of Wind Turbine Loads”. (2011), pp. 133-157
10. M. O. L. Hansen. “Aerodynamics of Wind Turbines”. (2008), pp.139-146
11. L.J. Vermeer, J.N. Sorensen, A. Crespo. “Wind Turbine Wake Aerodynamics”. (2003), pp. 493-502
12. P. Volund. “Loads on a horizontal axis wind turbine operating in a wake”. In: Van Hulle FJL, Smulders PT, Dragt JB, editors. EWEC’91 (1991). p. 605–9
13. H. Stiesdal. “Wake loads on the Bonus 450 kW II turbine”. 14th BWEA Wind Energy Conference (1992), p. 183–9
14. J.A. Dahlberg, M. Poppen, S.E. Thor. “Load/fatigue effects on a wind turbine generator in a wind farm”. EWEC’91 (1991). p. 251–5.
15. S. Frandsen, K. Thomsen. “Change in fatigue and extreme loading when moving wind farms offshore”. Wind Eng (1997)
16. M. Mirzaei, T. Göçmen, G. Giebel, P.E. Sørensen, N.K. Poulsen. “Turbine Control Strategies for Wind Farm Power Optimization”. 2015 American Control Conference.
17. S.K. Kanev, F.J. Savenije, W.P. Engles. “Active wake: An approach to optimize the lifetime operation of wind farms”. Wind Energy Research Centre of the Netherlands (ECN). Wiley (2018).
18. C. Galinos, T.J. Larsen, M. Mirzaei. “Impact on wind turbine loads from different down regulation control strategies ”. Journal of Physics: Conference Series 1104 (2018).
19. K. Boorsma. “Active Wake Control by Pitch Adjustment: Analysis of field measurements”. Wind Energy Research Centre of the Netherlands (ECN)(2015).
20. R. Damiani, S. Dana, J. Annoni, Paul Fleming, J. Roadman, J. van Dam and K. Dykes. “Assessment of wind turbine component loads under yaw-offset conditions”. European Academy of Wind Energy (2018).
21. K.A. Krag and M.H. Hansen. “Load alleviation of wind turbines by yaw misalignment”. Department of Wind Energy, Technical University of Denmark. Wiley (2013).
22. A.M. Urbán, T.J. Larsen, G.C. Larsen, D.P. Held, E. Dellwik, D. Verelst. “Optimal yaw strategy for optimized power and load in various wake situations”. Journal of Physics: Conference Series 1102 (2018).
23. J.W. Wagenaar, L.A.H. Machielse, J.G. Schepers. “Controlling Wind in ECN’s Scaled Wind Farm”. Wind Energy Research Centre of the Netherlands (ECN)(2012).
24. S. Macri, O. Coupiac, A. Leroy, N. Girard . “Experimental analysis of the wake dynamics of a modelled wind turbine during yaw manoeuvres”. Journal of Physics: Conference Series 1037 (2018).
25. Agence Nationale pour la Recherche, the SMARTEOLE national project. Available at: http://www.agencenationale-recherche.fr/?Project=ANR-14-CE05-0034. [Accessed: 2019-04-10]

26. S. Aubrun, D. Averbuch, S. Baleriola, C. Braud, M. Boquet, P. Devinant, T. Duc, N. Girard, F. Guillemin, E. Guilmineau, A. Leroy, D. Nelson-Gruel, D. Peaucelle. "SMARTEOLE: Improve the Wind Energy Efficiency Through the Use of Smart Rotors". Final report - ANR Project n° 14-CE05-0034. March 22, 2019.
27. HBM. 2019. Optical strain sensor fundamentals.
Available at: https://www.hbm.com/en/7256/optical-strain-sensor-fundamentals/. [Accessed 2019-04-16]
28. HBM. 2019. What is a fiber bragg grating?
Available at: https://www.hbm.com/en/4596/what-is-a-fiber-bragg-grating/. [Accessed 2019-04-16]
29. A. Meseguer, T. J. Larsen, J. Rinker, H. Villanueva. "V52 Model Validation: Simulation and Measurements Comparison". DTU Wind Energy Report (2017).
30. P.H.Madsen. "Recommended practices for wind turbine testing and evaluation: Fatigue Loads". International Energy Agency Programme (1990).
31. IEC 61400-13:2016, "Wind turbines - Part 13: Measurement of mechanical loads". International Standard (2016).
32. J.Rinker. "Variation of mean value and short-term DELs vs. wind speed for select loads in DTU 10 MW RWT". DTU Vindenergi Report 2018 (2018).
33. M. O. L. Hansen. "Aerodynamics of Wind Turbines". (2008), pp.157-161
34. P. Fleming, J. King, K. Dykes, E. Simley, J. Roadman, A. Scholbrock, P. Murphy, J.K. Lunquist, P. Moriarty, K. Fleming, J. van Dam, C. Bay, M. Mudafort, H. Lopez, J. Skopek, M. Scott, B. Ryan, G. Guersnay and D. Brake. "Initial results from a field campaign of wake steering applied at a commercial wind farm". European Academy of Wind Energy (2019).
35. T. Duc, G. Giebel, T. Gocmen, M. Korpas, O. Coupiac. "Optimization of wind farm power production using innovative control strategies". DTU Wind Energy. DTU Wind Energy Master Thesis M, Vol.. 0161 (2017).
36. A. Jimenez, A. Crespo and E. Migoya. "Application of a LES technique to characterize the wake deflection of a wind turbine in yaw". Wind Energy 13.6 (2010).
37. J.R. White, B.L. Ennis and T.G. Herges. "Estimation of Rotor Loads Due to Wake Steering". Sandia National Laboratories (2018).
38. D.S. Zalkind and L.Y. Pao. "The Fatigue Loading Effects of Yaw Control for Wind Plants". 2016 American Control Conference (2016).
39. M. Salih, M.Q.Taha, M.K. Alawsaj. "Performance analysis of wind turbine systems under different parameters effect".International Journal of Energy and Environment (2012).

Appendix

A Example of Loads Calculation from the Strain Gauges Wavelength Signal

After the fitting parameters a, b, c, d, e have been calculated in the temperature law as shown in section 4.4, from the instantaneous temperature measurement λ_T^t, and using the temperature law derived above, the values λ_{TD}^t and λ_{TS}^t are calculated using the following formulas:

$$\lambda_{TD}^t = a(\lambda_T^t)^2 + b\lambda_T^t + c \tag{A.1}$$

$$\lambda_{TS}^t = d(\lambda_T^t) + e \tag{A.2}$$

Assuming for example that:

- λ_T^t = 1527 nm;
- a = 0.1241;
- b = -378.51;
- c = $2.901e^{+05}$;
- d = -0.0425;
- e = 65.4489.

$$\lambda_{TD}^t = 0.1241 * (1527)^2 - 378.51 * (1527) + 2.901e^{+05} = 1483nm \tag{A.3}$$

$$\lambda_{TS}^t = -0.0425 * (1527) + 65.4489 = 0.55nm \tag{A.4}$$

After the temperature correction has been made through the use of the temperature law, ΔM_0 is the peak to peak variation of the gravity loads and it is calculated using the following formula:

$$\Delta M_0 = M_g * \sqrt{(2)} * cos(tilt) \tag{A.5}$$

Assuming for example that:

- Mass = 6350 Kg;
- l = 12 m;
- g = 9.80665 m/s^2;
- tilt = 5°;
- Mg = Mass*g*l = $7.47e^{+05}$ Nm .

$$\Delta M_0 = 7.47e5 * \sqrt{(2)} * cos(5) = 10.52e^{+05}Nm \tag{A.6}$$

Then, by comparing the instantaneous strain measurement of the sensor λ_S^t with these calculated values, the resulting instantaneous strain M^t from the loads can be computed with the equation 4.2 that can be rewritten as:

$$M^t = (\lambda_S^t - \lambda_{TD}^t)\frac{\Delta M_0}{\lambda_{TS}^t} \tag{A.7}$$

Assuming for example that:

- λ_S^t = 1482 nm.

$$M^t = (1482 - 1483) * \frac{10.52e^{+05}}{0.55} = -1.91e^{+06}Nm \tag{A.8}$$

It needs to be noted that the values utilized are just an example and do not represent real values used for the calibration in this thesis.

B Wind Shear Parameter Calculation

The wind shear parameter has been calculated using the wind speed data at 11 different height (40m, 50m, 60m, 70m, 80m, 90m, 100m, 120m, 140m, 160m, 200m) taken from the Windcube V2. The wind shear parameter (also called shear exponent) has been determined using the power-law wind profile of the following Equation B.1:

$$U(z) = U_{ref}\Big(\frac{z}{z_{ref}}\Big)^{\alpha} \tag{B.1}$$

where U_{ref} is the wind speed at 80m, z_{ref} is 80m and α has been found as the value that best fits each 10-min Windcube V2 data at the 12 different height (the Matlab Nonlinear least-squares solver has been used).

C Normal Operation Loads Edgewise Fatigue (DEL) Analysis

C.0.1 Flapwise DEL vs Wind Shear

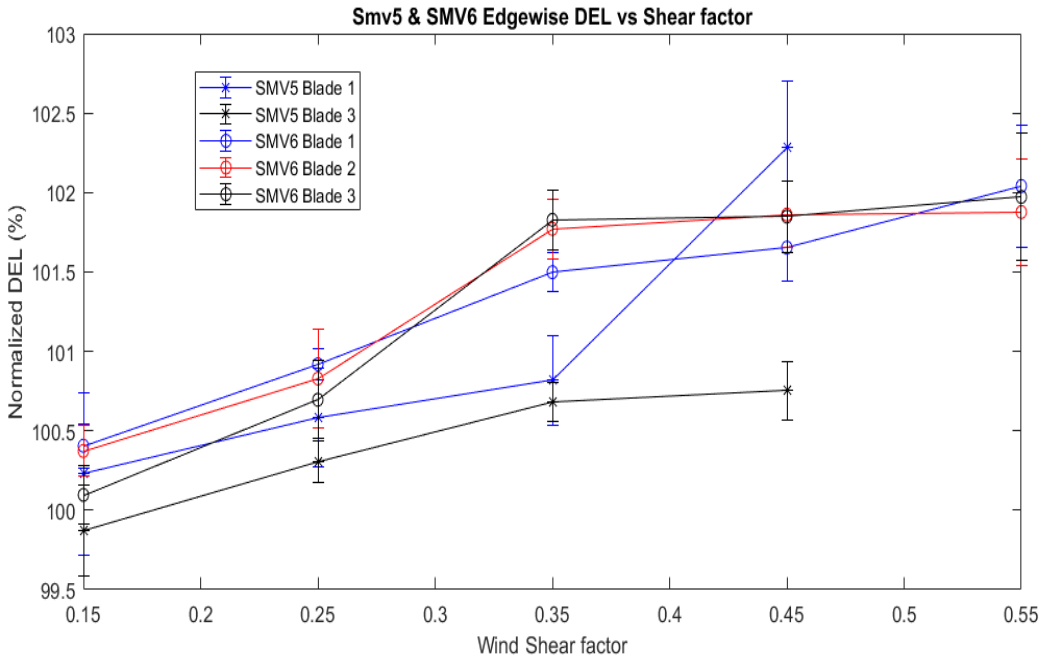

Figure C.1: SMV5 and SMV6 normalized edgewise DEL as a function of shear factor. The error bars represent the 95% confidence interval.

C.0.2 Flapwise DEL vs Turbulence Intensity

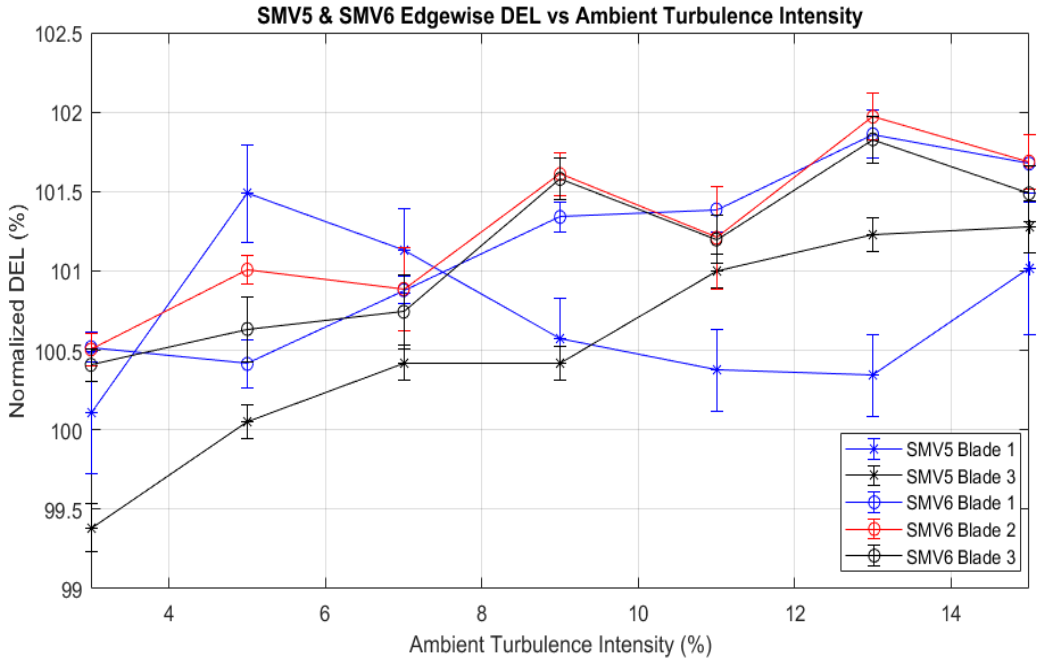

Figure C.2: SMV5 and SMV6 normalized edgewise DEL as a function of turbulence intensity. The error bars represent the 95% confidence interval.

D Yaw-controlled Strategy: Skew Angle Estimation Graphs

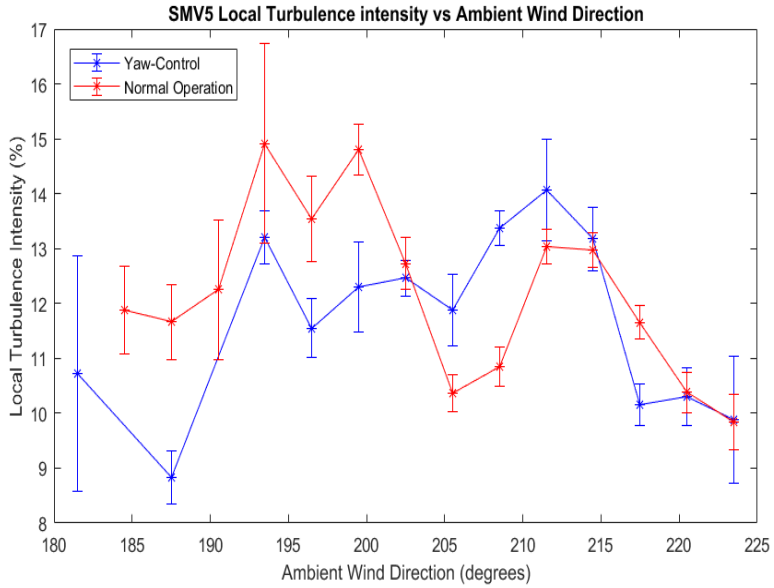

Figure D.1: Local turbulence intensity as a function of ambient wind direction (skew angle estimation). The error bars represent the 95% confidence interval.

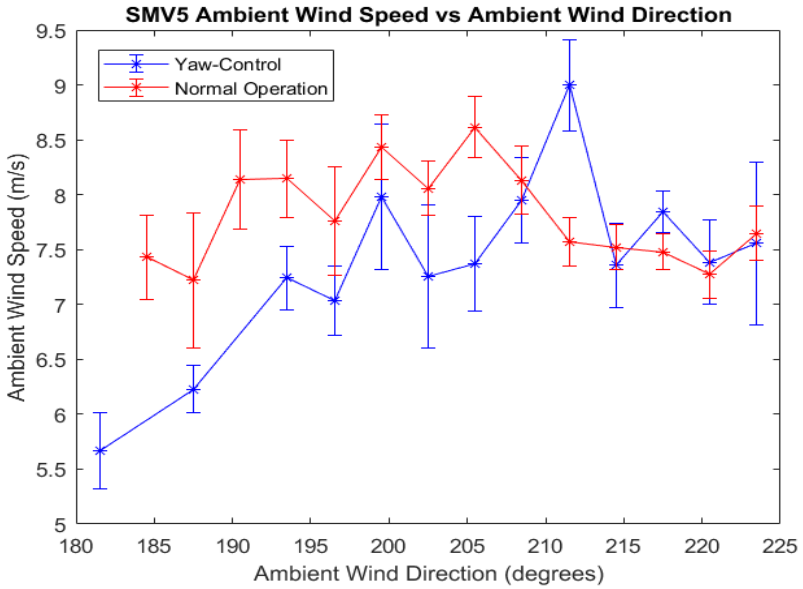

Figure D.2: Ambient Wind Speed as a function of ambient wind direction (skew angle estimation). The power has been normalized with the expected power under normal operation. The error bars represent the 95% confidence interval.

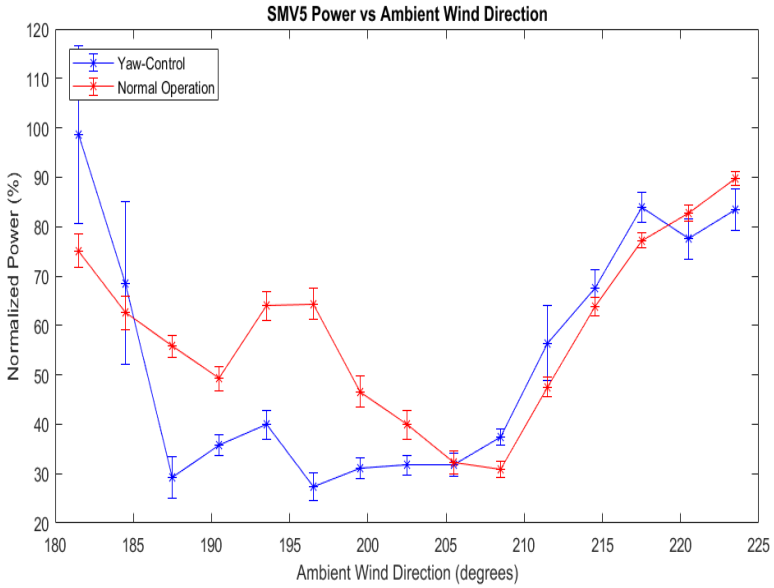

Figure D.3: Power produced as a function of ambient wind direction (full-wake sector). The error bars represent the 95% confidence interval.

The flapwise DEL has been normalized

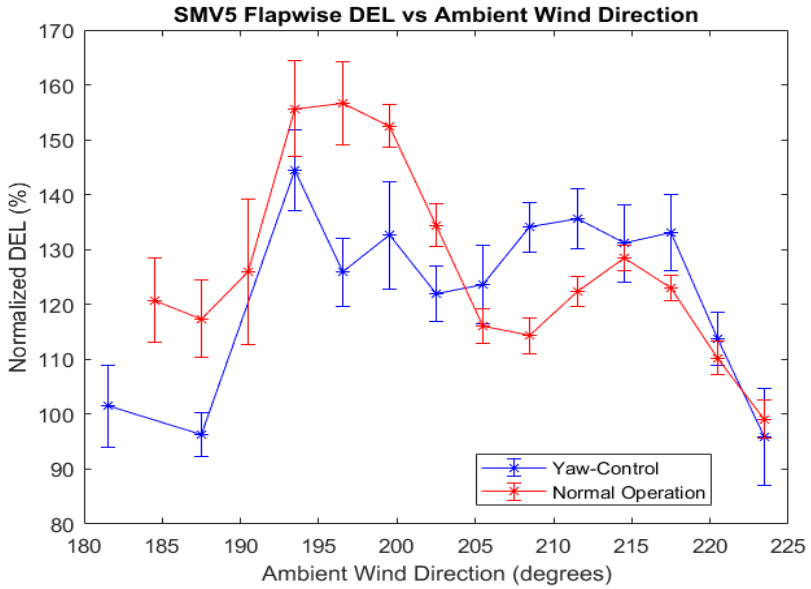

Figure D.4: Flapwise DEL as a function of wind speed (full-wake sector). The flapwise DEL has been normalized with the average no-wake DEL value at their specific wind speed. The error bars represent the 95% confidence interval.